Univerza v Ljubljani
Fakulteta za matematiko in fiziko

Daniel Svenšek

Vpliv hidrodinamičnih tokov na reorientacijsko dinamiko tekočih kristalov

Disertacija

Ljubljana, marec 2003

University of Ljubljana
Faculty of Mathematics and Physics

Daniel Svenšek

Backflow-affected reorientation dynamics in liquid crystals

Thesis

Ljubljana, March 2003

Radovednost je lepa čednost!

Zahvaljujem se prof. Slobodanu Žumru, ki me je tistega davnega poznopomladnega dne, ko sem nenadoma potrkal na vrata njegove sobice, kar hitro sprejel v svojo raziskovalno skupino. Da ta sploh ni majhna, sem spoznal jeseni. Jure B., Primož Z. - Pižo, Anamarija B. B. - Pika, Gregor S. - Gregovec, Andreja Š., Fahimeh K. P. H., Matej B. - Bužec, Boštjan M., prof. Samo K. - Kralj Samo in, seveda, Milan A. - McMillan, hvala! Zelo sem hvaležen tudi prof. Alojzu Kodretu za nasvete, prof. Helmutu Brandu za gostoljubnost, podporo in nasvete ter kritičnim bralcem disertacije v nastajanju. Priznanje ministrstvu MZŠŠ (prej MZT) Republike Slovenije, ki je financiralo raziskovanje. Hvala prijateljem in Brunarci, preka(l)jevalnici idej! Hvala APZ-ju — vse bi bilo drugače, če ne bi naredil avdicije!
Največja hvaležnost pa gre seveda Tanji, staršem in vsem domačim.

Izvleček

V nematskih tekočih kristalih in tankih smektičnih filmih smo z numeričnimi sredstvi raziskovali dinamiko ureditvenega parametra, sklopljeno s hidrodinamiko. Poslužili smo se Ericksen-Lesliejeve teorije nematskega direktorja in raziskali učinke hidrodinamičnega toka, ki spremlja preklopne procese nematika v celicah. Opozorili smo na primere, ko so ti učinki odločilnega pomena. Z upoštevanjem celotnega tenzorskega ureditvenega parametra smo rešili problem anihilacije para topoloških nematskih disklinacijskih linij ter pokazali, da hidrodinamični tok pospeši disklinacijo s pozitivno močjo glede na disklinacijo z negativno močjo, hkrati pa pospeši tudi proces anihilacije v primerjavi z nehidrodinamično obravnavanim primerom. Izkaže se, da je transport s tokom pomemben in je lahko njegov prispevek h gibanju defektov prevladujoč. S posplošitvijo Ericksen-Lesliejeve teorije na celoten vektorski ureditveni parameter smo rešili tudi problem anihilacije para disklinacijskih vrtincev v tankem prostostoječem filmu smektične C-faze, ki je v našem opisu ustrezal XY-modelu. Rezultati se v kvalitativnem pogledu ujemajo s tistimi pri nematikih. Študirali smo še razpad nematske disklinacijske linije z močjo ± 1 na par disklinacij z močjo $\pm 1/2$. V primerjavi z nehidrodinamično obravnavanim problemom tok spet pospeši odbojno gibanje nastalih defektov. Da bi raziskali stabilnost, smo rešili fluktuacijski problem ravne disklinacijske linije s splošno celoštevilčno močjo za celoten tenzorski ureditveni parameter. Našli smo dve vrsti naraščajočih fluktuacij, ki vodijo do razpada oziroma do pobega v tretjo dimenzijo.

Ključne besede: nematski tekoči kristali, smektični tekoči kristali, SmC filmi, ureditveni parameter, nematodinamika, hidrodinamika, Ericksen-Lesliejeva teorija, Freedericksz ov prehod, defekti, disklinacije, vrtinci, parska anihilacija, fluktuacije

PACS: 61.30.Dk, 61.30.Gd, 61.30.Jf, 83.80.Xz, 47.15.Gf, 47.15.Rq, 61.30.Pq, 68.15.+e

Abstract

Dynamics of the order parameter coupled to hydrodynamics is studied numerically in nematic and smectic thin film liquid crystals. The Ericksen-Leslie theory for the nematic director is employed to determine the backflow effects accompanying external field switching processes of nematics confined to cells. It is demonstrated that there are cases where these effects are crucial. Pair-annihilation of topological nematic disclination lines is studied using the full tensor order parameter. It is found that the hydrodynamic flow is responsible for the speed-up of the positive strength disclination relative to the negative one, and for the overall speed-up of the annihilation process as compared to the nonhydrodynamic treatment. Moreover, it is demonstrated that the flow transport is substantial and can dominate the motion of defects. The Ericksen-Leslie theory is generalized to the complete vector order parameter and used to study the pair-annihilation of vortices in a free-standing thin film of the smectic-C liquid crystal as a representative of the XY-model. The results agree qualitatively with those of the nematic. Decay of the nematic strength ± 1 disclination line into a pair of $\pm 1/2$ disclinations is studied. The flow again speeds up the repelling motion of the decay products if compared to the nonhydrodynamic treatment. As a stability analysis, the fluctuation problem of a straight disclination line with a general integer strength is solved for the complete tensor order parameter. Two types of growing fluctuations are found, leading to the decay and to the escape in the third dimension, respectively.

Keywords: nematic liquid crystals, smectic liquid crystals, SmC films, order parameter, nematodynamics, hydrodynamics, backflow, Ericksen-Leslie theory, Freedericksz transition, defects, disclinations, vortices, pair-annihilation, fluctuations

PACS: 61.30.Dk, 61.30.Gd, 61.30.Jf, 83.80.Xz, 47.15.Gf, 47.15.Rq, 61.30.Pq, 68.15.+e

Contents

Razširjeni povzetek

(Abstract in Slovene)

Uvod

Tekoči kristali so bolj urejeni kot tekočine, a manj kot trdne snovi — so nekakšna vmesna faza. Potreben pogoj za obstoj tekočekristalne faze so molekule podolgovate ali ploščate oblike. Pri termotropskih tekočih kristalih je stopnja urejenosti odvisna predvsem od temperature, pri liotropnih pa od koncentracije tekočekristalne komponente v raztopini. Zaradi urejenosti imajo tekoči kristali anizotropne makroskopske lastnosti. Najbližji izotropni tekočini je nematski tekoči kristal ali kratko nematik, ki premore orientacijsko molekulsko urejenost dolgega dosega. Povprečno smer molekul označimo z direktorjem $\mathbf{n}$, ki je del tenzorskega ureditvenega parametra nematika. Bolj urejena je smektična tekočekristalna faza, za katero je poleg orientacijskega reda značilen pozicijski red v eni dimenziji. Ploskvam maksimalne gostote pravimo smektične plasti. V SmA fazi je direktor pravokoten na plasti, v SmC fazi pa je nagnjen.

Modeliranje tekočih kristalov je zaživelo s prihodom dovolj zmogljivih in dostopnih računalnikov. Najprej so obdelali statične probleme, nato so se raziskave usmerile v študij dinamike, ki jo največkrat obravnavajo v okviru direktorskega opisa in brez upoštevanja hidrodinamike. Za opis defektov moramo nujno poseči po tenzorskem opisu ter upoštevati tudi hidrodinamični tok. Predvsem slednje je precej težavno.

V disertaciji se ukvarjamo s simulacijo dinamike v nematskem in SmC tekočem kristalu z upoštevanjem hidrodinamike. V prvem delu obravnavamo relaksacijske procese direktorja pri preklapljanju celice z zunanjim poljem, kjer pokažemo, da vloga hidrodinamskega toka ni omejena zgolj na kvantitativne popravke. V drugem delu se posvetimo glavnemu izzivu — hidrodinamični obravnavi dinamike defektov. Z nadgrajeno metodologijo iz prvega dela uspemo pokazati, da na anihilacijo para nasprotnih defektov kot tudi na odboj para enakih defektov močno vpliva tok, ki pospeši procese in v prvem primeru povzroči asimetrijo pri gibanju defektov.

Teorija

Na kratko bomo predstavili dinamično teorijo kompleksnih disipativnih tekočin, še prej pa bomo uvedli pojem ureditvenega parametra in vpeljali ustrezen termodi-

namični potencial. Teorija se za zdaj še ne bo nanašala na nek izbrani ureditveni parameter, ampak bo splošna, kar bo koristno v nadaljevanju, ko bomo obravnavali sisteme z različnimi ureditvenimi parametri.

Ureditveni parameter in termodinamični potencial

Tekoči kristali so urejeni sistemi. Uredijo se ob faznem prehodu, pri katerem se zlomi simetrija sistema. Za opis urejenosti vpeljemo mezoskopsko količino — ureditveni parameter, ki mora biti ničeln v visokotemperaturni fazi, v urejeni fazi pa od nič različen in odvisen od urejenosti, s simetrijskimi lastnostmi, kot jih ima urejena faza. V splošnem je lahko sistem krajevno nehomogen, tako da je ureditveni parameter polje. Definiramo ga kot povprečje v mezoskopskem volumnu, ki naj bi bil dovolj velik, da je povprečje dobro definirano, hkrati pa dovolj majhen v primerjavi z značilno skalo nehomogenosti, tako da je sistem znotraj njega dovolj homogen. Pri študiju dinamike se zanimamo za neravnovesne lastnosti sistema. Odmike od ravnovesja opišemo z neravnovesnimi vrednostmi ureditvenega parametra. To pomeni, da so neravnovesne lastnosti sistema določene z dinamiko ureditvenega parametra, ko letega izmaknemo iz ravnovesja.

Tekočekristalni termodinamični sistemi v splošnem združujejo termične, električne in magnetne prostostne stopnje, medtem ko delo pri spremembi prostornine zanemarimo. Pri konstantni temperaturi T in konstantnih jakostih zunanjega električnega in magnetnega polja $\mathbf{E}$ in $\mathbf{H}$ je ustrezen termodinamični potencial

$$\mathcal{F} = U - TS - V\mathbf{E}\cdot\mathbf{P} - \mu_0 V\mathbf{H}\cdot\mathbf{M}, \tag{1}$$

$$d\mathcal{F} = -S\,dT - T dS^i - p\,dV - V\mathbf{P}\cdot\mathbf{dE} - \mu_0 V\mathbf{M}\cdot\mathbf{dH} + dA', \tag{2}$$

ki ga imenujemo kar prosta energija; U je notranja energija. Spremembo entropije S smo razdelili na reverzibilni (dQ/T) in ireverzibilni del, $dS^i > 0$. V ravnovesju je prosta energija minimalna. Če sistem pri konstantnih T, $\mathbf{E}$ in $\mathbf{H}$ spravimo iz ravnovesja, je sprememba proste energije enaka minimalnemu delu dA', ki je zato potrebno, t.j. delu pri nadomestni reverzibilni spremembi. Električno in magnetno delo sta že vključeni v (2), tako da je prosta energija sistema v polju $\mathbf{H}$, katerega konfiguracija ustreza ravnovesju pri polju $\mathbf{H}'$, za

$$\Delta\mathcal{F} = -\mu_0 V \int_{\mathbf{H}}^{\mathbf{H}'} dV\,\mathbf{M}(\mathbf{H})\cdot\mathbf{dH} \tag{3}$$

višja od ravnovesne (analogno za električno polje).

Za študij dinamike je torej treba poiskati odvisnost proste energije od ureditvenega parametra $\mathbf{q}$, ki ima v splošnem več komponent q_i. Pri nehomogenih sistemih vpeljemo gostoto proste energije, tako da je prosta energija funkcional,

$$\mathcal{F} = \int dV\, f(\mathbf{q}, \nabla\mathbf{q}). \tag{4}$$

Pri fenomenološkem pristopu gostoto proste energije razvijemo po skalarnih invariantah, ki jih sestavimo iz $\mathbf{q}$, $\nabla\mathbf{q}$ in zunanjih polj. Pri tem nastopa pet kategoričnih

tipov prispevkov: homogeni, elastični, kiralni, prispevki zunanjih polj ter površinski prispevki, ki jih tukaj ne bomo natančneje opisovali.

Ravnovesno konfiguracijo poiščemo tako, da minimiziramo prosto energijo:

$$\delta\mathcal{F} = \int dV \left(\frac{\partial f}{\partial \mathbf{q}} - \nabla \cdot \frac{\partial f}{\partial \nabla \mathbf{q}} \right) \cdot \delta\mathbf{q} + \int \mathbf{dS} \cdot \frac{\partial f}{\partial \nabla \mathbf{q}} \cdot \delta\mathbf{q} = 0, \tag{5}$$

od koder dobimo Euler-Lagrangeve enačbe za volumski in površinski del. Slednjega bomo od zdaj naprej opuščali. Kadar morajo komponente ureditvenega parametra zadoščati vezem, vpeljemo Lagrangeve multiplikatorje kot ponavadi, kar je ekvivalentno projiciranju Euler-Lagrangevih enačb v prostoru ureditvenega parametra na podprostor, pravokoten na tistega, ki ga določajo vezi.

Hidrodinamika ureditvenega parametra

Ko se sistem približuje ravnovesju, se mu prosta energija manjša na račun večanja entropije:

$$T\dot{S}^i = -\dot{\mathcal{F}} = -\int dV \left(\frac{\partial f}{\partial \mathbf{q}} - \nabla \cdot \frac{\partial f}{\partial \nabla \mathbf{q}} \right) \cdot \dot{\mathbf{q}}, \tag{6}$$

kjer pika označuje substancialni odvod. Pri ireverzibilnih pojavih večanje entropije splošno opišemo s tokovi Φ_i in pripadajočimi silami F_i:

$$T\dot{S}^i = \int dV F_i \Phi_i, \tag{7}$$

v režimu šibkih tokov pa predpostavimo še linearno zvezo med silami in tokovi [17]:

$$F_i = \mathsf{K}_{ij}\Phi_j, \quad \mathsf{K}_{ij} = \mathsf{K}_{ji}, \tag{8}$$

kjer je po Onsagerju [18], [19, p. 365] matrika transportnih koeficientov simetrična.

Po enačbi (6) lahko imamo $\dot{\mathbf{q}}$ za tok, izraz v oklepaju (z minusom), ki ga označimo s

$$\mathbf{h} = \nabla \cdot \frac{\partial f}{\partial \nabla \mathbf{q}} - \frac{\partial f}{\partial \mathbf{q}}, \tag{9}$$

pa za silo. Gibanje tekočine opišemo s posplošeno Navier-Stokesovo enačbo

$$\rho\dot{\mathbf{v}} = \nabla \cdot \sigma, \tag{10}$$

pri čemer se vsa kompleksnost skriva v napetostnem tenzorju σ. Poleg tlačnega dela ta vsebuje še elastični del, ki je posledica dejstva, da deformacija sistema spremeni krajevne odvode ureditvenega parametra, torej tudi gostoto proste energije:

$$\sigma^e_{ij} = -\frac{\partial f}{\partial(\partial_i \mathbf{q})} \cdot \partial_j \mathbf{q}. \tag{11}$$

H gostoti proste energije moramo zdaj dodati tudi kinetični prispevek $\frac{1}{2}\rho\mathbf{v}^2$. Entropijski izvir je s tem

$$T\dot{S}^i = \int dV \left[(\sigma_{ij} + p\delta_{ij} - \sigma^e_{ij})\partial_i v_j + \mathbf{h} \cdot \dot{\mathbf{q}} \right]. \tag{12}$$

K naraščanju entropije torej prispevata dva tokova — časovni odvod ureditvenega parametra $\dot{\mathbf{q}}$ in gradient hitrosti $\nabla\mathbf{v}$. Pripadajoči sili sta generalizirana sila na ureditveni parameter $\mathbf{h}$ in viskozni napetostni tenzor $\sigma^v = \sigma + p\,\mathrm{I} - \sigma^e$. Ugodno je, če tenzorje razcepimo na simetrični in antisimetrični del. Gostota entropijskega izvira je potem

$$T\dot{s}^i = \sigma^s_{ij}\mathsf{A}_{ij} + \sigma^a_{ij}\mathsf{W}_{ij} + h_i\dot{q}_i, \tag{13}$$

kjer sta σ^s in σ^a simetrični in antisimetrični del viskoznega napetostnega tenzorja, A in W pa simetrični in antisimetrični del gradienta hitrosti. Splošna linearna zveza (8) med silami in tokovi (enačbe (2.35)-(2.37)) nam določi sile σ^s, σ^a in $\mathbf{h}$ (slednjo imenujemo tudi viskozna generalizirana sila $\mathbf{h}^v$), od koder sledijo gibalne enačbe:

$$-\frac{\delta f}{\delta \mathbf{q}} + \mathbf{h}^v = 0, \tag{14}$$

$$\rho\dot{\mathbf{v}} = -\nabla p + \nabla\cdot(\sigma^v + \sigma^e), \tag{15}$$

$$\nabla\cdot\mathbf{v} = 0. \tag{16}$$

Ureditveni parameter nematika

Za ureditveni parameter nematika izberemo prvi netrivialni neničelni moment porazdelitve smeri molekul $\mathbf{d} = (\sin\theta'\cos\phi', \sin\theta'\sin\phi', \cos\theta')$, to je kvadrupolni moment. Prispevek le-tega k porazdelitveni funkciji g ponavadi zapišemo kartezično:

$$g^{(2)}(\mathbf{e}) = \frac{5}{4\pi}\mathsf{Q}_{ij}\,e_ie_j, \quad \mathsf{Q}_{ij} = \frac{1}{2}(3\langle d_id_j\rangle - \delta_{ij}), \tag{17}$$

pri čemer je $\mathbf{e}$ enotski vektor, ki podaja smer. Vpeljali smo simetrični in brezsledni tenzorski ureditveni parameter nematika Q. V lastnem sistemu ga zapišemo kot

$$\mathsf{Q} = \begin{bmatrix} -\frac{1}{2}(S-P) & & \\ & -\frac{1}{2}(S+P) & \\ & & S \end{bmatrix}, \tag{18}$$

v splošnem pa kot

$$\mathsf{Q}_{ij} = \frac{1}{2}S(3n_in_j - \delta_{ij}) + \frac{1}{2}P(e^1_ie^1_j - e^2_ie^2_j), \tag{19}$$

kjer je

$$S = \frac{3\langle\cos^2\theta'\rangle - 1}{2} \tag{20}$$

skalarni ureditveni parameter,

$$P = \frac{3}{2}\langle\sin^2\theta'\cos 2\phi'\rangle \tag{21}$$

pa stopnja dvoosnosti. V enačbi (19) smo vpeljali trojico ortonormalnih vektorjev $(\mathbf{n}, \mathbf{e}^1, \mathbf{e}^2)$, ki določajo lastni sistem tenzorja Q: $\mathbf{n}$ imenujemo direktor, $\mathbf{e}^1$ pa sekundarni direktor oziroma direktor dvoosnosti.

Dinamika nematskega direktorja

Predstavili bomo Ericksen-Lesliejevo teorijo — hidrodinamično teorijo nematskega direktorja. Numerično bomo obdelali proces preklapljanja/relaksacije direktorja v magnetnem polju. Ogledali si bomo osnovne mehanizme nastanka toka zaradi vrtenja direktorja in njegovega povratnega vpliva na direktor. Relaksacijo s tokom bomo primerjali s poenostavljenim primerom brez toka.

Ericksen-Lesliejeva teorija

Gre za posebni primer splošnih enačb (14) in (15), ko je ureditveni parameter direktor $\mathbf{n}$ — enotski vektor s simetrijo $\mathbf{n} = -\mathbf{n}$.

Gostoto proste energije v zunanjem magnetnem polju zapišemo po Franku kot [46–48], [49, pp. 102, 119]

$$f = \frac{1}{2}K_{11}(\nabla\cdot\mathbf{n})^2 + \frac{1}{2}K_{22}\left[\mathbf{n}\cdot(\nabla\times\mathbf{n})\right]^2 + \frac{1}{2}K_{33}\left[\mathbf{n}\times(\nabla\times\mathbf{n})\right]^2 - \frac{1}{2}\chi_a\mu_0(\mathbf{n}\cdot\mathbf{H})^2, \quad (22)$$

kjer so K_{11}, K_{22} in K_{33} temperaturno odvisne elastične konstante za pahljačno, zvojno in upogibno deformacijo direktorja, $\mathbf{H}$ je jakost magnetnega polja, χ_a pa razlika med magnetnima susceptibilnostma v smereh vzporedno in pravokotno na direktor. V približku ene elastične konstante, tudi enokonstantnem približku, se izraz poenostavi v

$$f^{one} = \frac{1}{2}K(\nabla\mathbf{n})^2, \quad (23)$$

pri čemer se nismo menili za površinske prispevke.

Generalizirano elastično in magnetno silo na direktor dobimo z (9),

$$h_i^{em} = -\frac{\partial f}{\partial n_i} + \partial_j\left(\frac{\partial f}{\partial(\partial_j n_i)}\right). \quad (24)$$

Viskozna generalizirana sila sledi iz splošne linearne zveze (2.37) med silami in tokovi [50, p. 142]:

$$-\mathbf{h}^v = \gamma_1\mathbf{N} + \gamma_2\mathsf{A}\cdot\mathbf{n}, \quad (25)$$

kjer je $\gamma_1 = \alpha_3 - \alpha_2$ rotacijska viskoznost, $\gamma_2 = \alpha_3 + \alpha_2 = \alpha_6 - \alpha_5$, α_i pa so Lesliejevi viskoznostni koeficienti [49, p. 206]. $\mathbf{N}$ je relativni substancialni časovni odvod direktorja glede na vrtenje tekočine, en. (4.7). Zaradi vezi $\mathbf{n}^2 = 1$ je treba obe sili projicirati pravokotno na direktor, tako da je na kratko zapisana enačba gibanja

$$\left\{\mathbf{h}^{em} + \mathbf{h}^v\right\}_{\perp\mathbf{n}} = 0. \quad (26)$$

Posplošena Navier-Stokesova enačba,

$$\rho\left[\frac{\partial\mathbf{v}}{\partial t} + (\mathbf{v}\cdot\nabla)\mathbf{v}\right] = -\nabla p + \nabla\cdot(\sigma^v + \sigma^e), \quad (27)$$

kjer je ρ gostota in p tlak, vsebuje dva prispevka k napetostnemu tenzorju. Viskozni sledi po enačbah (2.35) in (2.36), [50, p. 142]:

$$\begin{aligned}\sigma^v &= \alpha_1 \mathbf{n}\otimes\mathbf{n}(\mathbf{n}\cdot\mathsf{A}\cdot\mathbf{n}) + \alpha_2\mathbf{n}\otimes\mathbf{N} + \alpha_3\mathbf{N}\otimes\mathbf{n} + \\ &\quad \alpha_4\mathsf{A} + \alpha_5\mathbf{n}\otimes(\mathsf{A}\cdot\mathbf{n}) + \alpha_6(\mathsf{A}\cdot\mathbf{n})\otimes\mathbf{n},\end{aligned} \tag{28}$$

elastični pa po enačbi (11), [49, p. 152]:

$$\sigma^e_{ij} = -\frac{\partial f}{\partial(\partial_i n_k)}\partial_j n_k. \tag{29}$$

Tlak v enačbi (27) določimo tako, da zadostimo pogoju nestisljivosti (16).

Značilni krajevni skali problema sta velikost celice L in magnetna koherenčna dolžina [49, p. 123]

$$\xi_m = \frac{1}{H}\sqrt{\frac{K_{11}}{\mu_0|\chi_a|}}, \tag{30}$$

značilna časa pa sta relaksacijski čas direktorskega polja

$$\tau = \frac{\gamma_1\xi_m^2}{K_{11}} \tag{31}$$

in relaksacijski čas hitrostnega polja

$$\tau_0 = \frac{\rho L^2}{\alpha_4}, \tag{32}$$

za katera velja ocena (parameter nestacionarnosti toka)

$$\tau_0/\tau = \frac{L^2}{\xi_m^2}\frac{\rho K_{11}}{\gamma_1^2} \approx L^2/\xi_m^2\cdot 10^{-6}. \tag{33}$$

Adiabatna aproksimacija za hitrostno polje, kjer zanemarimo časovni odvod v enačbi (27), je torej upravičena. Ocena za Reynoldsovo število je

$$Re = \frac{L}{\xi_m}\frac{\rho K_{11}}{\gamma_1^2} \approx L/\xi_m\cdot 10^{-6}, \tag{34}$$

torej lahko zavržemo tudi nelinearni advekcijski člen v en. (27).

Obstaja še tretji značilni čas, to je relaksacijski čas temperaturnega polja

$$\tau_Q = \frac{\rho c_p l^2}{\lambda}, \tag{35}$$

kjer je l značilna dolžina temperaturnih nehomogenosti, c_p specifična toplotna kapaciteta, λ pa toplotna prevodnost. Primerjava časov da

$$\tau_Q/\tau = \frac{K\rho c_p}{\gamma_1\lambda}, \tag{36}$$

kar je reda velikosti $5\cdot 10^{-4}$. Ocena je splošna in velja tudi, ko imamo opravka z defekti. Torej lahko res vedno privzamemo, da je temperatura konstantna.

Obdelani primeri

Prvi obdelani primer je dvodimenzionalen (slika 4.1). Magnetno polje leži v y-smeri. Privzamemo močno sidranje, s smermi razvidnimi s slike 4.1.

Oglejmo si mehanizme nastanka toka. Direktor parametrizirajmo s kotom $\mathbf{n} = (\cos\varphi, \sin\varphi, 0)$. Pri okvirni obravnavi je potrebno upoštevati samo viskozno silo, ki jo podaja člen s koeficientom α_2. Prispevek tega člena lahko razdelimo na dva dela — silo, ki je odvisna od gradienta kotne hitrosti ω vrtenja direktorja, in silo, ki zavisi od gradienta direktorskega polja. Prvo najlepše vidimo pri $\varphi = 0$:

$$\mathbf{f}_1 = \alpha_2 \left(0\ ,\ \frac{\partial\omega}{\partial x}\right). \tag{37}$$

Ta sila je torej pravokotna na direktor, njena velikost pa je sorazmerna z odvodom ω v smeri direktorja, $\mathbf{n}\cdot\nabla\omega$. Drugo silo poglejmo v primeru $\nabla\varphi = (\varphi_x\,,\,0)$:

$$\mathbf{f}_2 = -\alpha_2\omega\varphi_x\,(\cos 2\varphi\,,\,\sin 2\varphi)\,. \tag{38}$$

Velikost te sile je odvisna le od $\omega|\nabla\varphi|$, njena smer pa je taka, da z gradientom $\nabla\varphi$ oklepa dvakrat večji kot kot direktor. Paziti je potrebno na negativni predznak parametra α_2 in na to, da je smer sil odvisna od predznaka ω.

Sedaj si oglejmo še, kakšen je vpliv toka na direktor. Tokovno polje, ki ustreza homogenemu vrtenju ($\mathsf{W} \neq 0$, $\mathsf{A} = 0$), povzroči, da se tudi direktor vrti enako, seveda če nanj ne delujejo druge sile. Tokovno polje, ki ustreza čistemu deformacijskemu toku ($\mathsf{W} = 0$, $\mathsf{A} \neq 0$), pa skuša poravnati direktor v tisti lastni smeri A, ki ustreza raztegu. V primeru strižnega toka, ki je vsota obeh pravkar omenjenih tokov, enačba (26) da

$$\dot{\varphi} = -\frac{1}{2}\eta\left(\frac{\gamma_2}{\gamma_1}\cos 2\varphi + 1\right), \tag{39}$$

kjer je η velikost strižne hitrosti, kot φ pa je merjen glede na smer hitrosti, slika 4.2. Stacionarna rešitev obstaja le, če je $|\gamma_2/\gamma_1| > 1$, torej če je $\alpha_3 < 0$, in se glasi

$$|\varphi_0| \ll 1, \tag{40}$$

saj je $\gamma_2/\gamma_1 \approx -1$. To pomeni, da se v strižnem toku direktor približno poravna s smerjo hitrosti. Rešitev s $\varphi_0 > 0$ je stabilna, tista s $\varphi_0 < 0$ pa nestabilna. Za nematik MBBA kot φ_0 znaša približno $\varphi_0 \approx 7°$. Opozoriti je treba na to, da se direktor k temu kotu vrti v nasprotni smeri urinega kazalca le za $|\varphi| < |\varphi_0|$, pri vseh drugih kotih pa se vrti v smeri urinega kazalca.

Z mehanizmi, ki smo jih pravkar spoznali, je mogoče približno predvideti, kakšen bo potek relaksacije direktorskega polja ob vklopu ali izklopu zunanjega polja, ne da bi bilo treba narediti numerični izračun (razdelek 4.5.2). Glavna ugotovitev je, da lahko relaksacija zaradi hidrodinamičnega toka poteka v dveh dobro definiranih korakih, ki se med seboj ločita po smeri glavnega tokovnega vrtinca in celo po smeri vrtenja direktorja, slike 4.3, 4.5, 4.9 in 4.10. Tako se direktor nekaj časa vrti v napačni smeri, kar je znano kot *kickback* pojav [55, p. 167], ki ga je moč opaziti v celicah tekočekristalnih zaslonov kot migotanje.

Če popolno hidrodinamično relaksacijo primerjamo s poenostavljenim modelom brez toka, največkrat velja, da je dinamika s tokom nekoliko hitrejša, slika 4.11. Ta trditev pa ne velja splošno, enega od protiprimerov prikazuje slika 4.12. Večje razlike med obravnavama se pokažejo, če primerjamo vrtenje direktorja v določenem delu celice, kar je lepo razvidno z grafov krajevnih Fourierovih komponent (slike 4.12-4.14).

Z željo, da bi se bolj približali situacijam, ki jih lahko uresničijo v poskusih, smo simulirali še dva primera, kjer smo dovolili vrtenje direktorja iz xy-ravnine, prav tako pa smo dopustili tudi tok v z-smeri, v kateri sicer ni bilo nobenih gradientov. Geometrija tokrat ustreza kapilari s kvadratnim presekom, slika 4.18. Sidranje je spet močno, a tokrat vzporedno z osjo kapilare. Obakrat je bil vzorec na začetku poravnan z magnetnim poljem v smeri osi x. Potem smo polje nenadoma preklopili pravokotno glede na začetno smer, v prvem primeru v z-smer, v drugem pa je končno polje ležalo v ravnini yz in z osjo z oklepalo kot $70°$. V obeh primerih zaradi hidrodnamičnega toka proces preklapljanja poteka zelo nenavadno, sliki 4.19 in 4.20. H končnemu stanju prispemo v dveh izrazitih korakih: najprej zaradi vpliva toka hitro nastane domenska stena, nato pa se notranja domena zaradi ukrivljenosti domenske stene počasi manjša [56, p. 213] in končno izgine. Tudi tukaj se da potek (nastanek domene) približno zaslutiti z zgornjimi mehanizmi.

Ves čas smo računali v limiti neskončno močnega sidranja. Če je sidranje končno, $\xi > 0$, a še vedno močno, $\xi/\xi_m \ll 1$, velja ocena, da se hitrost hidrodinamičnega toka zmanjšuje kot $1 - 3\xi/\xi_m$, s tem pa tudi navor toka na direktor.

Z dodatnimi numeričnimi računi smo ugotovili, da oblika celice nima odločilnega vpliva na dinamiko, če je le velikost celice v posameznih smereh približno enaka. Če torej kvadrat nadomestimo s krogom, ne bo velikih sprememb, čisto drugače pa je, če celico, znatno raztegnjeno v x-smeri, nadomestimo s tako, ki je raztegnjena v y-smeri.

Dinamika vektorskega ureditvenega parametra

Izpeljali bomo dinamične enačbe za vektorski ureditveni parameter $\mathbf{c}$. Gre za posplošitev Ericksen-Lesliejeve teorije z dodatkom nehidrodinamične prostostne stopnje — dolžine vektorja. Opozoriti je treba, da je Ericksen-Lesliejeva teorija vektorska teorija, zato jo lahko konsistentno posplošimo le na popoln vektorski ureditveni parameter in ne na tenzorskega. Obravnavali bomo splošen tridimenzionalni primer, dvodimenzionalna različica pa bo prišla prav pri opisu tankega filma smektika-C.

Gostota proste energije

Osredotočili se bomo na homogeni in elastični del gostote proste energije $f(\mathbf{c}, \nabla\mathbf{c})$:

$$f = \frac{1}{2}A\,c^2 + \frac{1}{4}C\,c^4 + \frac{1}{2}L_{ijkl}\,(\partial_i c_j)(\partial_k c_l). \tag{41}$$

Homogena člena, kjer velja $A = A'(T - T^0)$, $A' > 0$, $C > 0$, opisujeta fazni prehod in določata ravnovesno velikost vektorja $\mathbf{c}$, $c_0 = \sqrt{-A/C}$. V elastični del vključimo

samo člene, kvadratne v prvih odvodih, ne pa členov z drugimi odvodi $L_{ijk}\,\partial_i\partial_j c_k$, ki prinesejo samo dodatne površinske prispevke.

Poiskati je torej treba matriko L_{ijkl}. Zahtevali bomo, da je prosta energija invariantna na inverzijo ($\mathbf{r} \to -\mathbf{r}$, $\mathbf{c} \to -\mathbf{c}$), kar pomeni, da mora biti L_{ijkl} posebej invariantna na to operacijo. Poleg tega mora zadoščati permutacijski simetriji $L_{ijkl} = L_{klij}$. Matriko L_{ijkl} smemo sestaviti le iz komponent vektorja $\mathbf{c}$ ter matrik δ_{ik} in ϵ_{ijk}. Posamezni prispevki so zbrani v tabeli 5.1. Vpeljali smo fundamentalne elastične konstante L_i, ki so neodvisne od dolžine vektorja $\mathbf{c}$.

Člen z L_1 je izotropen in vse deformacije polja $\mathbf{c}$ obravnava enako. Členi z L_2, L_4 in L_9 ustrezajo pahljačni, zvojni, oziroma upogibni deformaciji, člen z L_3 pa je površinski. Ostali prispevki so neničelni le, če se spreminja velikost vektorja $\mathbf{c}$. Posebej zanimiva sta člena z L_6 in L_7, ki ustrezata sklopitvi med spreminjanjem velikosti $\mathbf{c}$ in pahljačno oziroma upogibno deformacijo, slika 5.1. Primerjava z izrazom (22) poveže Frankove elastične konstante s fundamentalnimi konstantami L_i:

$$\begin{aligned} K_{11} &= c^2 L_1 + c^2 L_2, && (42)\\ K_{22} &= c^2 L_1 + c^4 L_9, && (43)\\ K_{33} &= c^2 L_1 + c^4 L_4, && (44) \end{aligned}$$

pri čemer smo določili tudi odvisnost Frankovih konstant od velikosti vektorja $\mathbf{c}$ v najnižjem redu.

Sklopitev s tokom

Najti moramo izraz za viskozni napetostni tenzor in viskozno generalizirano silo na vektor $\mathbf{c}$, kar pomeni, da moramo določiti matrike S, M, R, C, D in B v enačbah (2.35)-(2.37) z lastnostmi (2.39). Tudi tukaj zahtevamo, da je gostota entropijskega izvira invariantna na inverzijo, torej morajo biti matrike S, M, R in B sode v $\mathbf{c}$, C in D pa lihi. Matrike smemo sestaviti le iz komponent vektorja $\mathbf{c}$ ter matrik δ_{ik} in ϵ_{ijk}. Prispevki, ki podajajo disipacijo v izotropni tekočini, so zbrani v tabeli 5.2, ostali pa v tabeli 5.3. Vpeljali smo fundamentalne viskozne parametre η_i, ki so spet neodvisni od velikosti vektorja $\mathbf{c}$.

Zahtevati moramo, da pri togi rotaciji sistema ni disipacije (2.38) in sil (2.35)-(2.37). Simetrični in antisimetrični del viskoznega napetostnega tenzorja sta tako

$$\begin{aligned} \sigma^s_{ij} &= \eta_0 \mathsf{A}_{ij} + \tfrac{1}{2}\eta_1(\mathsf{A}_{ik}c_k c_j + \mathsf{A}_{jk}c_k c_i) + \eta_2 \mathsf{A}_{kl}c_k c_l c_i c_j + \\ &\quad \tfrac{1}{2}\eta_4(N_i c_j + N_j c_i) + \eta_6 c_k \dot{c}_k c_i c_j, \\ \sigma^a_{ij} &= \tfrac{1}{2}\eta_3(N_i c_j - N_j c_i) + \tfrac{1}{2}\eta_4(\mathsf{A}_{ik}c_k c_j - \mathsf{A}_{jk}c_k c_i), \end{aligned} \qquad (45)$$

viskozna generalizirana sila na vektor $\mathbf{c}$ pa

$$-h^v_i = \eta_3 N_i + \eta_4 \mathsf{A}_{ij}c_j + \eta_6 \mathsf{A}_{jk}c_j c_k c_i + \eta_9 c_j \dot{c}_j c_i, \qquad (46)$$

kjer je

$$N_i = \dot{c}_i + \mathsf{W}_{ij}c_j \qquad (47)$$

relativni substancialni časovni odvod vektorja $\mathbf{c}$ glede na vrtenje tekočine.

Primerjava z izrazi Ericksen-Lesliejeve teorije (4.13) in (4.6) poveže Lesliejeve viskoznostne koeficiente α_i s fundamentalnimi koeficienti η_i:

$$\begin{aligned} \alpha_4 &= \eta_0, \\ \alpha_5 + \alpha_6 &= c^2\eta_1, \\ \alpha_1 &= c^4\eta_2, \\ \gamma_1 &= c^2\eta_3, \\ \gamma_2 &= c^2\eta_4, \end{aligned} \tag{48}$$

kjer je $\gamma_1 = \alpha_3 - \alpha_2$ in $\gamma_2 = \alpha_3 + \alpha_2$ kot običajno. Določili smo odvisnost Lesliejevih koeficientov od velikosti vektorja $\mathbf{c}$ v najnižjem redu.

V splošnem vektorskem primeru viskozne sile določata dva parametra več, η_6 in η_9, ki sta povezana z disipacijo, kadar je $\dot{\mathbf{c}}$ vzporeden s $\mathbf{c}$. Prav tako prispevek člena z η_4 h generalizirani sili zdaj ni več omejen na smer, pravokotno na $\mathbf{c}$.

Defekti

Na kratko bomo spregovorili o točkovnih defektih vektorja/direktorja v dvodimenzionalnem sistemu in o linijskih defektih direktorja v nematiku. Poenostavljeno lahko rečemo, da je defekt nezveznost ali nedefiniranost ureditvenega parametra na neki množici točk v prostoru — točki, krivulji ali ploskvi. Seveda pa v fizičnem sistemu nikoli ne srečamo nezveznosti. V nematiku, na primer, imamo opravka z nezveznostjo le, dokler vztrajamo pri direktorskem opisu, kakor hitro pa uporabimo celoten tenzorski ureditveni parameter, dobimo zvezne rešitve [61–63]. Ne glede na to pa je pojem defekta še vedno smiseln, ker ima le-ta daljnosežne posledice za polje ureditvenega parametra — defekt lahko dobro definiramo, četudi sploh ne poznamo strukture njegovega jedra. V ta namen si zamislimo zanko, ki jo sklenemo okrog središča defekta, tako da poteka po območju, kjer velja direktorski opis (slika 6.1). Ko se po njej enkrat sprehodimo, direktor opiše kot θ, ki mora biti zaradi zveznosti direktorskega polja in simetrije $\mathbf{n} = -\mathbf{n}$ večkratnik π, $\theta = 2\pi n$. Pravkar smo definirali ovojno število ali moč defekta n, ki s topološkega vidika defekt popolnoma določa,

$$n = 0, \pm\tfrac{1}{2}, \pm 1, \pm\tfrac{3}{2}, \ldots \tag{49}$$

Pri tem je šlo za točkovni defekt v namišljenem dvodimenzionalnem nematiku ali pa za pravi linijski defekt v treh dimenzijah.

Defekti, ki jih lahko z zvezno transformacijo pretvorimo eden v drugega, so v topološkem smislu ekvivalentni. Torej taki, ki jih lahko zvezno transformiramo v brezdefektno strukturo, sploh niso defekti. V dvodimenzionalnem primeru, ko je direktor definiran na ravnini, vsa ovojna števila (49) označujejo različne defekte, saj zvezne transformacije med njimi ne obstajajo. Če bi bil ureditveni parameter vektor z $\mathbf{n} \neq -\mathbf{n}$, bi bile dovoljene le celoštevilske moči. Drugače je v treh dimenzijah. Tam lahko vse celoštevilske defekte s takoimenovanim pobegom v tretjo dimenzijo [68,69] pretvorimo v brezdefektno strukturo. Velja še več: vsakemu defektu lahko z zvezno transformacijo moč spremenimo za celo število. To pomeni, da v nematiku obstaja le en topološki defekt, to je defekt z močjo 1/2.

Točkovni defekti v 2D primeru

Ogledali si bomo konfiguracijo in prosto energijo točkovnih defektov dvodimenzionalnega direktorja v enokonstantnem približku, en. (23). Vsi izrazi veljajo tudi za ravne linijske defekte; tiste, ki podajajo prosto energijo, v tem primeru pač razumemo kot dolžinsko gostoto proste energije. Ob parametrizaciji $\mathbf{n} = (\cos\theta, \sin\theta)$ se ravnovesni pogoj za defekt s središčem v izhodišču glasi

$$\nabla^2\theta = 0. \tag{50}$$

Rešitev sme biti odvisna le od polarnega kota ϕ:

$$\theta = n\phi + \theta_0 = n\,\mathrm{arctg}\frac{y}{x} + \theta_0, \quad n = 0, \pm\tfrac{1}{2}, \pm 1, \pm\tfrac{3}{2}, ..., \tag{51}$$

kjer je θ_0 prosti parameter. Polcelo število n je moč defekta. Deformacijska prosta energija te strukture je

$$\mathcal{F}_d = \frac{K}{2}\int_{r_0}^{R} rdr \int_0^{2\pi} d\phi \left[\left(\frac{\partial\theta}{\partial x}\right)^2 + \left(\frac{\partial\theta}{\partial y}\right)^2\right] = \pi K n^2 \ln\frac{R}{r_0}, \tag{52}$$

kjer je R velikost vzorca, r_0 pa mikroskopska dolžina, pri kateri preneha veljati direktorski opis. V prvem približku vpeljemo izotropno jedro z radijem r_0, ki se takoj nato nadaljuje z direktorskim poljem in ravnovesno vrednostjo skalarnega ureditvenega parametra. Prosta energija je izotropnega jedra je tako

$$\mathcal{F}_c = \pi r_0^2 \Delta f, \tag{53}$$

kjer je Δf razlika gostot proste energije izotropne in urejene faze. Z minimizacijo celotne proste energije $\mathcal{F}_d + \mathcal{F}_c$ določimo radij jedra,

$$r_0 = \sqrt{\frac{Kn^2}{2\Delta f}}, \tag{54}$$

ki je tako sorazmeren z močjo defekta in je velikostnega reda nematske korelacijske dolžine (7.18). Celotna prosta energija defekta je končno

$$\mathcal{F} = \mathcal{F}_c + \mathcal{F}_d = \pi n^2 K\left(\frac{1}{2} + \ln\frac{R}{r_0}\right). \tag{55}$$

Če imamo opravka z večimi defekti, dobimo rešitev zaradi linearnosti ravnovesne enačbe (50) kar s seštevanjem posameznih rešitev (51):

$$\theta = \sum_i (n_i\phi_i + \theta_{0i}) = \sum_i n_i\,\mathrm{arctg}\frac{y - y_i}{x - x_i} + \theta_0'. \tag{56}$$

Prosta energija dveh defektov na razdalji r je [65, p. 529]

$$\mathcal{F} = \mathcal{F}_1 + \mathcal{F}_2 + 2\pi K n_1 n_2 \ln\frac{R}{r}. \tag{57}$$

Prva člena sta prosti energiji (55) posameznih defektov, tretji pa predstavlja interakcijsko prosto energijo. Vidimo, da se defekta z močmi istega predznaka odbijata, defekta z močmi nasprotnih predznakov pa privlačita. V posebnem primeru $n_2 = -n_1$ je prosta energija

$$\mathcal{F} = 2\pi n^2 K \left(\frac{1}{2} + \ln\frac{r}{r_0}\right), \quad n = |n_1|, \quad r_1 = r_2 = r_0, \tag{58}$$

tako da se znebimo logaritemske divergence v odvisnosti od velikosti vzorca. V splošnem se bodo defekti z močmi nasprotnih predznakov (ne nujno enakimi po absolutni vrednosti) združevali, saj bo na ta način prosta energija manjša. Nasprotno pa je ugodno, če defekt z veliko močjo razpade na več manjših, tako da se ti potem oddaljijo drug od drugega in zmanjšajo prosto energijo.

Anihilacija disklinacijskih linij v nematiku

Če želimo študirati statiko ali dinamiko defektov v nematiku, se moramo poslužiti popolnega tenzorskega opisa nematske faze. Za vključitev hidrodinamike, ki jo v direktorskem opisu obravnavamo v okviru Ericksen-Lesliejeve teorije, potrebujemo tenzorsko različico te teorije [89,90,92].

Rešili bomo problem anihilacije ravnih disklinacijskih linij moči $\pm 1/2$ v nematiku, pri čemer bomo izhajali iz tenzorske teorije [92]. Vključili bomo samo tiste disipacijske člene, ki v direktorskem opisu s konstantno stopnjo ureditve preidejo v Lesliejeve člene. Tako bo viskoznih parametrov toliko kot pri Leslieju, z njimi pa bodo preprosto linearno povezani.

Dinamične enačbe

Gostoto proste energije v odvisnosti od Q zapišemo v približku ene elastične konstante [10, p. 156]:

$$f = \frac{1}{2}A\,\mathsf{Q}_{ij}\mathsf{Q}_{ji} + \frac{1}{3}B\,\mathsf{Q}_{ij}\mathsf{Q}_{jk}\mathsf{Q}_{ki} + \frac{1}{4}C\,(\mathsf{Q}_{ij}\mathsf{Q}_{ji})^2 + \frac{1}{2}L\,(\partial_i\mathsf{Q}_{jk})(\partial_i\mathsf{Q}_{jk}). \tag{59}$$

Da bi ločili med pahljačno in upogibno deformacijo, bi morali vključiti tudi elastične člene, kubične v Q [99]. Euler-Lagrangeva enačba za funkcional proste energije

$$\mathcal{F} = \int dV\,\left[f(\mathsf{Q}, \nabla\mathsf{Q}) - \lambda\mathsf{Q}_{ii} - \lambda_i\epsilon_{ijk}\mathsf{Q}_{jk}\right], \tag{60}$$

pri čemer smo zahtevali simetričnost in brezslednost Q, nam da homogeni in elastični del generalizirane sile na ureditveni parameter Q:

$$\mathsf{h}^{he}_{ij} = L\,\partial_k^2\mathsf{Q}_{ij} - \frac{\partial\phi}{\partial\mathsf{Q}_{ij}} + \lambda\delta_{ij} + \lambda_k\epsilon_{kij}. \tag{61}$$

Lagrangeovih multiplikatorjev se znebimo, če enačbo (61) projiciramo na simetrični in brezsledni podprostor (odštejemo njen simetrični in izotropni del). Elastični

napetostni tenzor je po enačbi (11)

$$\sigma^e_{ij} = -\frac{\partial f}{\partial(\partial_i \mathsf{Q}_{kl})}\partial_j \mathsf{Q}_{kl}. \tag{62}$$

Viskozni napetostni tenzor in viskozna generalizirana sila na tenzor Q sta [92]

$$\sigma^v_{ij} = \beta_1 \mathsf{Q}_{ij}\mathsf{Q}_{kl}\mathsf{A}_{kl} + \beta_4 \mathsf{A}_{ij} + \beta_5 \mathsf{Q}_{ik}\mathsf{A}_{kj} + \beta_6 \mathsf{Q}_{jk}\mathsf{A}_{ki} + \frac{1}{2}\mu_2 \mathsf{N}_{ij} - \mu_1 \mathsf{Q}_{ik}\mathsf{N}_{kj} + \mu_1 \mathsf{Q}_{jk}\mathsf{N}_{ki}, \tag{63}$$

$$-\mathsf{h}^v_{ij} = \frac{1}{2}\mu_2 \mathsf{A}_{ij} + \mu_1 \mathsf{N}_{ij}, \tag{64}$$

kjer je

$$\mathsf{N}_{ij} = \dot{\mathsf{Q}}_{ij} + \mathsf{W}_{ik}\mathsf{Q}_{kj} - \mathsf{Q}_{ik}\mathsf{W}_{kj}, \tag{65}$$

$\dot{\mathsf{Q}}_{ij} = \partial \mathsf{Q}_{ij}/\partial t + (\mathbf{v}\cdot\nabla)\mathsf{Q}_{ij}$ pa je substancialni odvod. A in W sta simetrični in antisimetrični del gradienta hitrosti. Med viskoznimi koeficienti v (63) in (64) velja zveza $\mu_2 = \beta_6 - \beta_5$.

Gibalna enačba za ureditveni parameter Q je ravnovesje brezslednega simetričnega dela ($\perp$) generaliziranih sil,

$$\left\{\mathsf{h}^{he} + \mathsf{h}^v\right\}_\perp = 0, \tag{66}$$

z vezmi

$$\mathsf{Q}_{ii} = 0, \quad \epsilon_{ijk}\mathsf{Q}_{jk} = 0. \tag{67}$$

Hitrostno polje je določeno s posplošeno Navier-Stokesovo enačbo (15) in pogojem nestisljivosti (16), pri čemer je napetostni tenzor podan z enačbama (62) in (63).

Značilna krajevna skala problema je nematska korelacijska dolžina (tipično znaša nekaj nanometrov)

$$\xi = \sqrt{\frac{3}{2}\frac{L}{f''|_{S_0}}}, \tag{68}$$

kjer je $f''|_{S_0}$ vrednost drugega odvoda gostote proste energije po skalarnem ureditvenem parametru pri ravnovesni vrednosti le-tega. Značilni čas, ki ima pomen relaksacijskega časa ureditvenega parametra na krajevni skali ξ in znaša tipično nekaj deset nanosekund, pa je

$$\tau = \gamma_1 \xi^2/K = \mu_1 \xi^2/L, \tag{69}$$

kjer je γ_1 direktorska rotacijska viskoznost, K pa direktorska elastična konstanta.

Rezultati

Slika 7.2 kaže, da zaradi hidrodinamičnega toka anihilacija poteka hitreje in asimetrično, pri čemer je defekt s pozitivno močjo hitrejši od defekta z negativno močjo. Na sliki 7.3 pa vidimo, da tok vpliva predvsem na defekt s pozitivno močjo, medtem ko hitrost negativnega ni tako močno spremenjena. Izkaže se, da tok na defekte v največji meri vpliva prek advekcije. Rezultate je moč kvalitativno pojasniti z upoštevanjem poglavitnih prispevkov k napetostnemu tenzorju, ki ženejo tok: to

so električni napetostni tenzor in členi z μ_1 in μ_2 v viskoznem napetostnem tenzorju. S simetrijskimi argumenti lahko pokažemo, da je tok, ki ga poganja električni tenzor, simetričen za oba defekta in ju seveda žene skupaj, medtem ko je tok, ki ga poganja μ_1 člen, točno antisimetričen, njegova smer pa je od pozitivnega defekta k negativnemu, slika 7.6. K pospešitvi anihilacije torej najbolj prispevajo električne sile, k asimetriji pa viskozni člen z μ_1. Še več, prispevka se za pozitivni defekt konstruktivno seštejeta, medtem ko se za negativnega odštejeta, s čimer pojasnimo močnejši tok na mestu prvega.

Primerjava slik 7.4 in 7.5 pokaže, da sta advekcijski prispevek k hitrosti defekta in prispevek zaradi reorientacije ureditvenega parametra enakih velikostnih redov. Pri majhnih meddefektnih razdaljah (nekaj korelacijskih dolžin) prevlada drugi, pri večjih pa je advekcija pomembnejša (slika 9.10).

Člen v viskoznem napetostnem tenzorju z μ_2 nima posebne simetrije glede spremembe predznaka defektov, razlikuje pa tudi med konfiguracijami, ki se ločijo po homogeni rotaciji direktorskega polja, slika 7.1 (električni in μ_1 členi so na to neobčutljivi). V enokonstantnem približku brez toka se takšne konfiguracije obnašajo enako, s tokom pa ne, slika 7.2, za kar je najprej odgovoren μ_2 člen.

Zaključimo lahko, da je za asimetrijo in pospešitev anihilacije pomembno razmerje μ_1/β_4, in sicer z večanjem razmerja hidrodinamični učinki naraščajo. Razlika v dinamiki konfiguracij, ki se razlikujejo po homogeni rotaciji direktorja, pa narašča z večanjem razmerja μ_2/μ_1. Pasivni viskozni členi z β_1, β_5 in β_6 v kvalitativnem pogledu niso pomembni. Če spremenimo električno konstanto, se to pozna samo pri značilnem času procesa, tako da z reskaliranjem časovne dimenzije anihilacija poteka enako.

Anihilacija defektov v filmih SmC

Ureditveni parameter SmC faze

V SmA fazi je direktor, ki podaja povprečno smer molekul, pravokoten na smektične plasti, v SmC fazi pa je nagnjen. Z eksperimentalnega vidika je zelo pripraven sistem za opazovanje dinamike defektov prostostoječi film SmC, debel le nekaj smektičnih plasti. Projekcija direktorja na smektično ravnino je dvodimenzionalni vektor, takoimenovani c-direktor, ki je primeren ureditveni parameter SmC faze. Takoj je treba opozoriti, da je c-direktor imenu navkljub v resnici vektor, $\mathbf{c} \neq -\mathbf{c}$. Njegova velikost (nagib, amplituda) kondenzira in postane od nič različna ob prehodu iz SmA v SmC fazo, medtem ko je smer (faza) hidrodinamična količina z Goldstoneovo ekscitacijo.

Topološki defekti c-direktorja so disklinacijske linije s celimi ovojnimi števili — vrtinci. Da se izognemo singularnosti v središču defekta, moramo dovoliti, da se spreminja velikost $\mathbf{c}$, tako da se sistem lahko zateče k SmA fazi.

Poudariti je potrebno, da sta ureditvena parametra SmC in nematske faze v osnovi različna in da lahko SmC sistem — s spodnjimi omejitvami — prevedemo na XY-model, nematika pa ne. Zatorej se zdi, da ima dinamika vrtincev v SmC sistemu zelo splošno veljavo. Opozoriti moramo še na to, da so disklinacije s celimi močmi

v nematiku nestabilne in razpadejo na vsaksebi bežeče $\pm 1/2$ disklinacije. Če želimo študirati dinamiko vrtincev, se moramo nujno zateči k vektorskemu ureditvenemu parametru.

Dinamične enačbe

Izhajamo iz hidrodinamične teorije Carlssona, Leslieja, Stewarta in Clarka za SmC tekočekristalno fazo [108,109], ki privzame smektične plasti s konstantno debelino ter konstanten povprečni nagib molekul. Za opis defektov je treba dovoliti vsaj spreminjanje nagiba, torej moramo teorijo nekoliko posplošiti. Po drugi strani pa jo bomo bistveno poenostavili, saj bomo obravnavali sistem z variacijami v samo dveh dimenzijah in z ravnimi smektičnimi plastmi. Tako iz sistema dinamičnih količin izločimo normalo na smektične ravnine, ki naj bo kar $\hat{\mathbf{e}}_z$. Ker imamo opravka s prostostoječim tankim filmom, vpeljemo dve neodvisni krajevni spremenljivki x in y, z $\nabla = \hat{\mathbf{e}}_x\partial_x + \hat{\mathbf{e}}_y\partial_y$, prav tako pa tudi tok omejimo na ravnino, $\mathbf{v} = v_x\hat{\mathbf{e}}_x + v_y\hat{\mathbf{e}}_y$. S tem smo naš sistem prevedli na XY-model. Izkaže se, da se v tem primeru teorija [108,109] prevede na Ericksen-Lesliejevo teorijo za nematski tekoči kristal. Dodatno bomo morali poskrbeti še za spreminjanje nagiba molekul. Tako smo prispeli natančno do dvodimenzionalne različice dinamike vektorskega ureditvenega parametra. V dveh dimenzijah se, razen odsotnosti zvojne deformacije, ne spremeni nič drugega.

Površinske elastične člene bomo spustili, prav tako pa tudi večino prispevkov iz tabele 5.1, saj zanje ne poznamo elastičnih konstant. Razlikovati želimo le med pahljačno in upogibno deformacijo, ker sta lahko zaradi spontane polarizacije v SmC energijsko zelo različni [110–112]. Gostoto proste energije tako zapišemo kot

$$f = \frac{1}{2}A\,c^2 + \frac{1}{4}C\,c^4 + \frac{1}{2}B_1(\nabla\times\mathbf{c})^2 + \frac{1}{2}B_2(\nabla\cdot\mathbf{c})^2. \tag{70}$$

Primerjava z elastičnimi členi iz tabele 5.1 pokaže, da, ne meneč se za površinske prispevke, velja

$$B_1 = L_1, \quad B_2 = L_1 + L_2, \tag{71}$$

kar pomeni, da smo člene z L_4-L_8 spustili konsistentno. Opozoriti želimo, da sta elastični konstanti B_1 in B_2 neodvisni od nagiba. Euler-Lagrangeova enačba za funkcional proste energije $\mathcal{F} = \int dV f(\mathbf{c}, \nabla\mathbf{c})$ da homogeni in elastični del generalizirane sile na vektor $\mathbf{c}$:

$$h_i = -(A + Cc^2)c_i + B_1\,\partial_j^2 c_i + (B_2 - B_1)\,\partial_i\partial_j c_j. \tag{72}$$

Elastični napetostni tenzor dobimo po enačbi (2.26) iz (70):

$$\sigma_{ij}^e = -\frac{\partial f}{\partial(\partial_i c_k)}\partial_j c_k. \tag{73}$$

Neokrnjena teorija [109] zajema 20 viskoznih členov, od katerih pa v primeru ravnih smektičnih plasti, ravninskega toka in odsotnosti gradientov v smeri normale na plasti ostanejo zgolj Lesliejevi. Če upoštevamo še spreminjanje dolžine $\mathbf{c}$,

nam prav enačbe (45) in (46) podajajo točen opis disipativnih sil. Kljub temu se bomo omejili samo na standardne Lesliejeve prispevke, katerih viskozne parametre poznamo, in spustili člene s parametroma η_6 in η_9. Viskozni napetostni tenzor je tako

$$\begin{aligned}\sigma^v_{ij} &= \eta_0\,\mathsf{A}_{ij} + \eta_2\,c_k c_l \mathsf{A}_{kl} c_i c_j + \tfrac{1}{2}\eta_3\,(N_i c_j - c_i N_j) + \\ &\quad \tfrac{1}{2}\eta_4\,(N_i c_j + c_i N_j) + \tfrac{1}{2}(\eta_1 - \eta_4)\,c_i \mathsf{A}_{jk} c_k + \tfrac{1}{2}(\eta_1 + \eta_4)\,\mathsf{A}_{ik} c_k c_j, \end{aligned} \tag{74}$$

viskozna generalizirana sila na vektor $\mathbf{c}$ pa

$$-h^v_i = \eta_3\,N_i + \eta_4\,\mathsf{A}_{ij} c_j, \quad N_i = \dot{c}_i + \mathsf{W}_{ij} c_j, \tag{75}$$

kjer je $\dot{\mathbf{c}} = \partial\mathbf{c}/\partial t + (\mathbf{v}\cdot\nabla)\mathbf{c}$ substancialni časovni odvod vektorja $\mathbf{c}$ glede na vrtenje tekočine, A in W pa sta simetrični oziroma antisimetrični del gradienta hitrosti. Četudi sta enačbi (74) in (75) natančno taki, kot v Ericksen-Lesliejevi teoriji, je pomembna razlika ta, da tukaj viskozni parametri niso odvisni od kondenzirane količine — velikosti vektorja $\mathbf{c}$, medtem ko Lesliejevi so, en. (48).

Zavedati se moramo, da smo s spreminjanjem velikosti $\mathbf{c}$ naravno posplošili Ericksen-Lesliejevo teorijo za primer neenotskega vektorja, s čimer smo tudi avtomatsko določili pravilne odvisnosti sil od nagiba molekul. Nasprotno za nematike šele tenzorska teorija da prave odvisnosti sil od skalarnega ureditvenega parametra in stopnje biaksialnosti. Našli smo torej sistem, za katerega Ericksen-Lesliejeva teorija točno velja.

Gibalna enačba za vektor $\mathbf{c}$ je na kratko

$$\mathbf{h} + \mathbf{h}^v = 0 \tag{76}$$

in skupaj s posplošeno Navier-Stokesovo enačbo (15) in pogojem nestisljivosti (16) predstavlja sistem treh parcialnih diferencialnih enačb, ki opisujejo dinamiko modeliranega SmC sistema. Spet vpeljemo značilno dolžino, ki je tokrat korelacijska dolžina nagiba molekul,

$$\xi = \sqrt{\frac{B_0}{(A + 3C c_0^2)}}, \tag{77}$$

tipično nekaj nanometrov, in karakteristični čas

$$\tau = \frac{\eta_3 \xi^2}{B_0}, \tag{78}$$

kjer je $B_0 = (B_1 + B_2)/2$. Čas τ je relaksacijski čas deformacij vektorja $\mathbf{c}$ na dolžinski skali ξ, ali ekvivalentno, čas prilagajanja velikosti vektorja $\mathbf{c}$, tipično nekaj deset nanosekund.

Rezultati

Najprej poglejmo primer z izotropno elastičnostjo, $B_1 = B_2$. Anihilacija poteka kvalitativno enako kot pri nematskih defektih s polovično močjo, slika 8.3. Hidrodinamični tok (slika 8.2) spet pospeši proces in povzroči asimetrijo v gibanju defektov. Tok, ki ga poganjajo elastične sile, daje glavni prispevek k pospešitvi, tok, ki ga

poganja vrtenje ureditvenega parametra (natančneje člen z η_3 v viskoznem napetostnem tenzorju), pa k asimetriji (slika 8.5). Tok je močan ob pozitivnem defektu in šibak ob negativnem, ker se omenjena tokovna prispevka enkrat konstruktivno, drugič destruktivno sestavita. Hitrost obeh prispevkov glede na hitrost gibanja defekta samo zaradi reorientacije c-direktorja je sorazmerna z η_3/η_0. Asimetrijo med konfiguracijami, ki se razlikujejo za homogeno rotacijo vektorskega polja $\mathbf{c}$, spet prinaša v glavnem viskozni prispevek člena z η_4, tako da se ta asimetrija veča z večanjem razmerja η_4/η_0. Ostali (pasivni) viskozni členi kvalitativno niso pomembni. Reskaliranje elastičnih konstant glede na viskoznosti spet spremeni samo značilni čas procesa. V manjši meri k asimetriji prispeva tudi elastična anizotropija, kot pokaže slika 8.6.

Razpad defektov s celimi močmi

Brez upoštevanja hidrodinamike bomo rešili splošen problem stabilnosti neskončnih, ravnih disklinacijskih linij s celimi močmi v nematiku, tako da bomo poiskali lastne rešitve perturbacij okrog teh struktur. V nelinearnem režimu bomo preučili vplih hidrodinamike na razpad disklinacije z močjo ± 1 ter odbojno gibanje nastalega para enakih defektov moči $\pm 1/2$.

Linearizirani problem

Poslužimo se cilindričnih koordinat (r, ϕ, z) s pripadajočimi baznimi vektorji $(\hat{\mathbf{e}}_r, \hat{\mathbf{e}}_\phi, \hat{\mathbf{e}}_z)$, pri čemer disklinacijska linija leži na osi z. V enokonstantnem približku (59) je prosta energija invariantna na homogeno rotacijo tenzorja Q. To pomeni, da se lastni sistem tenzorja vrti kot $\psi = \psi_0 + (s-1)\phi$, ko gremo okrog defekta z močjo s v izhodišču, pri čemer je ψ_0 prosti parameter defektne strukture in predstavlja kot med direktorjem pri $\phi = 0$ in osjo x (za radialni defekt je $\psi_0 = 0$, za tangencialnega pa $\psi_0 = \pi/2$). Od kota ϕ je odvisna samo orientacija lastnega sistema, skalarne invariante tenzorja Q pa ne. Zaradi te posplošene cilindrične simetrije je problem lastnih rešitev moč dovolj enostavno rešiti.

Definirajmo še eno ortonormalno trojico vektorjev $(\hat{\mathbf{e}}_1, \hat{\mathbf{e}}_2, \hat{\mathbf{e}}_z)$,

$$\begin{bmatrix} \hat{\mathbf{e}}_1 \\ \hat{\mathbf{e}}_2 \end{bmatrix} = \begin{bmatrix} \cos\psi & \sin\psi \\ -\sin\psi & \cos\psi \end{bmatrix} \begin{bmatrix} \hat{\mathbf{e}}_r \\ \hat{\mathbf{e}}_\phi \end{bmatrix}, \tag{79}$$

tako da pri neperturbirani rešitvi (imenujmo jo osnovno stanje) lastni sistem tenzorja Q povsod sovpada s to trojico. Vpeljemo še pet ortonormalnih baznih tenzorjev T_i, en. (9.2), in zapišemo

$$\mathsf{Q}(\mathbf{r}, t) = a_i(\mathbf{r}, t)\mathsf{T}_i(\mathbf{r}), \quad i = -2, -1, 0, 1, 2. \tag{80}$$

Osnovno stanje zaradi simetrije vsebuje le komponenti a_0 in a_1, perturbacije pa so splošne:

$$a_i(\mathbf{r}, t) = \begin{cases} q_i(\mathbf{r}) + x_i(\mathbf{r}, t) & ; \quad i = 0, 1 \\ x_i(\mathbf{r}, t) & ; \quad i = -1, 2, -2 \end{cases}, \tag{81}$$

$q_{0,1}$ sta komponenti osnovnega stanja, x_i pa so komponente perturbacij, $x_i \ll q_{0,1}$. Komponenti osnovnega stanja zadoščata enačbam (9.6) in (9.7) in ju dobimo iz numerične rešitve. Iz enačb moramo izluščiti le njun potek v bližini $r = 0$. Linearizirane enačbe za perturbacije pa tvorijo dva sistema:

$$\dot{x}_0 = \nabla^2 x_0 - f_0(r)\, x_0 + f_{01}(r)\, x_1, \tag{82}$$

$$\dot{x}_1 = \nabla^2 x_1 - \frac{4s^2}{r^2} x_1 - \frac{4s}{r^2}\frac{\partial x_{-1}}{\partial \phi} - f_1(r)\, x_1 + f_{01}(r)\, x_0, \tag{83}$$

$$\dot{x}_{-1} = \nabla^2 x_{-1} - \frac{4s^2}{r^2} x_{-1} + \frac{4s}{r^2}\frac{\partial x_1}{\partial \phi} - f_{-1}(r)\, x_{-1} \tag{84}$$

in

$$\dot{x}_2 = \nabla^2 x_2 - \frac{s^2}{r^2} x_2 - 2s\frac{\partial x_{-2}}{\partial \phi} - f_2(r)\, x_2, \tag{85}$$

$$\dot{x}_{-2} = \nabla^2 x_{-2} - \frac{s^2}{r^2} x_{-2} + 2s\frac{\partial x_2}{\partial \phi} - f_{-2}(r)\, x_{-2}, \tag{86}$$

kjer je ∇^2 Laplaceov operator v cilindričnih koordinatah, $f_i(r)$ pa so polinomi druge stopnje v komponentah q_0 in q_1, en. (9.15). Sicer preprosta odvisnost od koordinate z nas zaenkrat ne bo zanimala. Poudarimo še to, da za defekta z močema s in $-s$ dobimo identične enačbe, če ustrezno popravimo bazne tenzorje: $s \to -s$ in $\mathsf{T}_{-1,-2} \to -\mathsf{T}_{-1,-2}$ ne spremeni enačb.

Lastne rešitve sistemov (82)-(84) in (85)-(86) iščemo z nastavkom

$$\begin{Bmatrix} x_0 \\ x_1 \\ x_{-1} \end{Bmatrix} = \begin{Bmatrix} R_0(r)\cos(m\phi) \\ R_1(r)\cos(m\phi) \\ R_{-1}(r)\sin(m\phi) \end{Bmatrix} \exp(-\lambda t), \tag{87}$$

$$\begin{Bmatrix} x_2 \\ x_{-2} \end{Bmatrix} = \begin{Bmatrix} R_2(r)\cos(m\phi) \\ R_{-2}(r)\sin(m\phi) \end{Bmatrix} \exp(-\lambda t), \tag{88}$$

kjer je m celo število. Zaradi preglednosti smo izpustili prosto fazo v kotnem delu. Preostaneta lastna sistema za radialne funkcije $R_i(r)$ z lastno vrednostjo λ:

$$\nabla^2 R_0 + \left(\lambda - f_0(r) - \frac{m^2}{r^2}\right) R_0 + f_{01}(r)\, R_1 = 0, \tag{89}$$

$$\nabla^2 R_1 + \left(\lambda - f_1(r) - \frac{m^2{+}4s^2}{r^2}\right) R_1 - \frac{4sm}{r^2}\, R_{-1} + f_{01}(r)\, R_0 = 0, \tag{90}$$

$$\nabla^2 R_{-1} + \left(\lambda - f_{-1}(r) - \frac{m^2{+}4s^2}{r^2}\right) R_{-1} - \frac{4sm}{r^2}\, R_1 = 0 \tag{91}$$

in

$$\nabla^2 R_2 + \left(\lambda - f_2(r) - \frac{m^2{+}s^2}{r^2}\right) R_2 - \frac{2sm}{r^2}\, R_{-2} = 0, \tag{92}$$

$$\nabla^2 R_{-2} + \left(\lambda - f_{-2}(r) - \frac{m^2{+}s^2}{r^2}\right) R_{-2} - \frac{2sm}{r^2}\, R_2 = 0. \tag{93}$$

Rešimo ju z metodo streljanja [54, p. 582].

Razpad defekta

Lastne ekscitacije, ki vodijo do razpada defekta, zaradi simetrije vsebujejo le komponente x_0, x_1 in x_{-1}. Za defekt z močjo 1 najdemo eno samo naraščajočo lastno rešitev ($\lambda < 0$), in sicer pri $m = 2$, kar ustreza razpadu na dva defekta z močjo 1/2, sliki 9.2 in 9.3. Vpliv hidrodinamičnega toka na časovno konstanto naraščajoče ekscitacije je pričakovano majhen (manjši od 5%) in pospeši naraščanje. Izjava ni čisto trdna, saj nismo upoštevali vseh viskoznih prispevkov, poleg tega je sam koncept hidrodinamike pri teh dolžinskih in časovnih skalah (1 nm, 10 ns) precej vprašljiv.

Pri defektih z večjimi celoštevilskimi močmi najdemo več naraščajočih ekscitacij. Ekscitacije z $\lambda < 0$ imajo diskreten spekter in so lokalizirane, spekter onih z $\lambda > 0$ pa je zvezen. Tako lahko naraščajoče rešitve preštevamo. Izkaže se, da za vsak topološko dovoljen razpad obstaja vsaj ena naraščajoča rešitev, če le nobena od moči nastalih defektov ni prevelika. Rešitve imajo značilno kotno simetrijo, določeno z m. V splošnem defekt z močjo s razpade na m defektov z močmi $\pm 1/2$, simetrično razporejenih okrog defekta z močjo $\pm s \mp m/2$, slika 9.4. Vse razpadne možnosti defektov z $s = 2$ in $s = 3$ so zbrane v tabelah 9.1 in 9.2. Razpad samo na $\pm 1/2$ defekte je vedno najhitrejši.

Pobeg defekta

V neomejenem sredstvu lahko celoštevilski defekti pobegnejo v nedeformirano strukturo, katere deformacijska energija je ničelna. Poglejmo torej, kako je s stabilnostjo na majhne perturbacije. Tokrat nastopata le komponenti x_2 in x_{-2}, pri čemer pričakujemo, da bo za pobeg pomembna komponenta x_2, ki ustreza vrtenju direktorja iz ravnine. Pri $m = 0$ se enačbi (92) in (93) res razklopita in ugotovimo, da so vse ekscitacije x_2 naraščajoče, hkrati pa tudi lokalizirane in z diskretnim spektrom. Rešitve x_{-2} pri $m = 0$ in vse ostale rešitve pri $m \neq 0$ so pojemajoče. Izkaže se, da so naraščajoče ekscitacije, ki vodijo do pobega, veliko razsežnejše in s tem počasnejše od onih, ki privedejo do razpada. Za defekt z močjo 1 je razmerje časovnih konstant okrog 53. Torej bo defekt razpadel, preden mu bo uspelo pobegniti.

Vpliv hidrodinamičnega toka

Oglejmo si še vpliv hidrodinamike na defekta z močjo $\pm 1/2$, ki nastaneta z razpadom ± 1 defekta. Tokrat asimetrije pri gibanju seveda ni, zato pa ima tok toliko večji vpliv na hitrost defektov (slika 9.7), saj oba prispevka, elastični in viskozni (člen z μ_1), poganjata tok v isti smeri. Vpliv hidrodinamike je večji pri večjih razmerjih μ_1/β_4, kar je lepo vidno tudi na sliki 9.8.

Ker v tem primeru ni težav z začetnim pogojem (tukaj je to končno stanje) kot pri anihilaciji, lahko zvemo več o tem, kaj se dogaja s hitrostjo defektov pri velikih meddefektnih razdaljah. Posebej zanimiv je graf 9.10, ki prikazuje, kako se razmerje med advekcijsko hitrostjo (transport s tokom) in celotno hitrostjo defekta spreminja z razdaljo med defektoma. Razmerje z razdaljo narašča in znatno preseže polovico. Hidrodinamičnega toka torej ne gre zanemarjati, še posebej, če upoštevamo dejstvo,

da s simulacijami zaenkrat dosežemo le majhne meddefektne razdalje — na grafu 9.10 okrog 80ξ ali 0.17 μm.

Zaključek

V disertaciji sem predstavil nekaj problemov dinamike tekočih kristalov z upoštevanjem hidrodinamike, ki smo jih izbrali z vidika eksperimentalne in teoretične relevantnosti, nenazadnje pa seveda tudi z vidika rešljivosti.

Relaksacijske probleme smo v 4. poglavju obravnavali z uveljavljeno Ericksen-Lesliejevo teorijo nematskega direktorja. Služili so predvsem kot priprava za kasnejše težje podvige. Z izbiro dovolj kompleksne geometrije smo vseeno uspeli opozoriti na primere, ko hidrodinamični tok povsem spremeni časovni razvoj sistema.

Dinamične enačbe za vektorski ureditveni parameter, izpeljane v 5. poglavju, potrebujemo za opis defektov v sistemu s tem ureditvenim parametrom, v našem primeru je bil to film SmC faze. Z izpeljavo smo hkrati pokazali, da je Ericksen-Lesliejeva teorija natančno teorija za enotski vektorski ureditveni parameter in ni v nikakršni zvezi z nematskim ureditvenim tenzorjem.

Za študij dinamike defektov v nematiku je tako treba začeti znova in izdelati tenzorsko teorijo. Le-to je potem moč poenostaviti do direktorske. Obratna pot, kjer bi Ericksen-Lesliejevo teorijo, v kateri direktor nastopa linearno, razširili s tem, da bi dovolili variacijo skalarnega ureditvenega parametra, se ne obnese. V 7. poglavju smo z okrnjeno tenzorsko teorijo rešili hidrodinamični problem anihilacije para ravnih nematskih disklinacijskih linij. Pokazali smo, da je za asimetrijo pri gibanju defektov odgovoren predvsem tok nematske tekočine.

Kljub eksperimentalni pripravnosti v literaturi nismo zasledili nobenih numeričnih študij dinamike defektov v SmC filmih. Eden od možnih razlogov je zapletenost enačb z velimi številom snovnih parametrov, povečini neizmerjenih. Pri tem bi morali upoštevati še spreminjanje dolžine c-direktorja. V 8. poglavju smo se večini težav izognili, s tem da smo ob dodatnih predpostavkah dinamično teorijo SmC faze poenostavili do Ericksen-Lesliejeve teorije, sistem SmC filma pa prevedli na XY-model, katerega dinamiko opisujejo vektorske enačbe iz 5. poglavja. Pokazali smo, da je vpliv toka na anihilacijo para disklinacij z močjo ± 1 kvalitativno enak kot pri nematiku.

V nematiku je disklinacija z močjo ± 1 nestabilna in spontano razpade na par enakih $\pm 1/2$ disklinacij. Da bi raziskali začetni stadij razpada, smo v 9. poglavju študirali dinamiko perturbacij ravnih nematskih dikslinacijskih linij s celimi močmi. V približku ene elastične konstante smo uspeli rešiti tenzorski fluktuacijski problem ravnih dikslinacijskih linij splošnih celoštevilskih moči. Našli smo dve vrsti naraščajočih fluktuacij, odgovornih za razpad na disklinacije z manjšimi močmi oziroma pobeg v tretjo dimenzijo. V obeh primerih je spekter diskreten, fluktuacije pa lokalizirane. Časovna konstanta prvih je za več kot red velikosti manjša, torej disklinacije z velikimi močmi razpadejo, še preden jim uspe pobegniti. Preverili smo tudi vpliv hidrodinamike na odbojno gibanje dveh enakih $\pm 1/2$ disklinacij, nastalih po razpadu, ki je zaradi toka veliko hitrejše.

Če bi si od predstavljenega morali zapomniti le eno stvar, naj bo to pomembnost hidrodinamičnega toka pri dinamiki defektov v tekočih kristalih. Pokazali smo, da je prispevek advekcije (transporta s tokom) h gibanju defekta povsem primerljiv s prispevkom zaradi reorientacije ureditvenega parametra. V primeru izbire viskoznih parametrov, ki ustrezajo nematiku MBBA, je pri relevantnih meddefektnih razdaljah advekcija celo pomembnejša.

1

Introduction

Liquid crystals are *mesophases* between the liquid and solid phases, in the sense that they are more ordered than liquids, yet less ordered than solids. There exist many liquid-crystalline phases as there are many steps in which the translational and rotational symmetry of the liquid can be reduced to that of the solid. Microscopically, the required condition for a material to exhibit a liquid-crystalline phase is that it consists of elongated or disc-like molecules/particles. In *thermotropic* liquid crystals the order is controlled by the temperature, whereas in *lyotropic* liquid crystals it is controlled by the concentration of the liquid-crystalline material in a solution. Due to the ordering, liquid crystals exhibit anisotropic properties on the macroscopic level.

The least ordered among liquid crystals is the nematic [1], which possesses a long-range orientational order of the molecules, Fig. 1.1. The average orientation of the molecules is specified by the director $\mathbf{n}$, which is a part of the nematic tensor order parameter. The name "nematic" was invented by Friedel [2] in the early twentieth century. It originates from the Greek word for a thread, many of which can be observed between crossed polarizers due to line defects in the nematic.

A more ordered phase is the smectic phase [3], which, if present, occurs at a lower temperature than the nematic phase. The name is again due to Friedel and comes from the Greek word for soap (smectics can form thin films). Besides orientational order, the smectic possesses also an one-dimensional long-range translational order in the cast of a density wave. The surfaces of maximum density are called smectic layers or planes. In the smectic-A (SmA) phase the director $\mathbf{n}$ is normal to the layers, while in the smectic-C (SmC) phase occurring at a yet lower temperature the director is tilted with respect to the layer normal. One must point out that the notion of the translational ordering is different than in solid crystals, where the molecules/atoms are actually bound to crystal sites and can merely oscillate around them. In smectics, the molecules are not bound to the layers.

Owing to the optical anisotropy, thermotropic liquid crystals are used in applications related to optics — liquid crystal displays (LCD's), optical switches, shutters, polarization rotators, tunable color filters, etc. On the other hand, lyotropic liquid crystals are widely used in chemical and food industry.

The modelling of liquid crystal systems has come to life with powerful enough

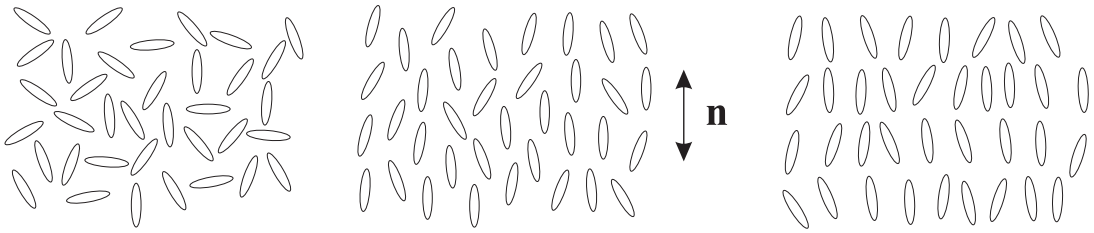

(a) isotropic (b) nematic (c) smectic

Figure 1.1 Schematic representation of (b) the nematic and (c) smectic phases. The average orientation of the molecules is specified by the director **n**, Eq. (3.10). The smectic phase is characterized by an one-dimensional periodic density modulation.

computers. Static structures of confined liquid crystals have been studied thoroughly in the last two decades; the same can be said for the structures of the defect cores. Dynamic studies have followed next, either as simulations of applied or applicable set-ups, or arising from the sheer theoretical interest in dynamic processes. Most frequently, the dynamics of the nematic liquid crystals, including that of the defects, has been studied in the director description, neglecting the hydrodynamic flow entirely. While the director description is efficient and perfectly adequate for the problems not involving any defects, the neglect of the flow is always questionable. Hence, in a proper treatment of defect dynamics, one must both use the complete tensor order parameter as well as take into account the hydrodynamic part of the problem. The use of the tensor order parameter does not bring any significant complications — it only yields richer structures. The drawback is that it introduces a microscopic length scale, which sets an upper limit to the (possibly macroscopic) length scales that can be reached in a simulation. On the other hand, the inclusion of the hydrodynamics makes the treatment difficult, both conceptually and computationally. The problems are particularly demanding if they involve more than just one spatial coordinate, because in this case the incompressibility of the fluid must be ensured by finding the proper pressure distribution.

In the Thesis, we study the dynamics of nematic and SmC liquid crystals. In particular, we focus on the hydrodynamic phenomena accompanying the time evolution of the order parameter. More precisely, we are interested in the so-called backflow effects — the generation of the fluid flow by motion of the order parameter (e.g., by the director reorientation) and conversely, the influence of the generated flow to the motion of the order parameter. In the first part of the Thesis we study director relaxation processes in liquid crystal cells triggered by external field switching [4,5]. One-dimensional problems of this kind were studied in the 1970s (see the Introduction to Chapter 4 for a more detailed review). Our geometry is more confined leading to the dependence on two spatial coordinates. This makes the problems much harder to solve requiring involved computation approaches. We show that the backflow can be more than just quantitatively important — it can cause the

switching to occur in two characteristic steps rather than just in one.

The second part is devoted to the dynamics of defects, which has been the primary challenge to us. For the motivation and a short review of the preceding research see also the Introduction to Chapter 7. Our ambition has been to solve a full hydrodynamic annihilation problem of a defect-antidefect pair. For this purpose we make use of the numerical method developed with the switching problems, properly modified in order to be able to describe the defects. The dependence on two spatial coordinates is a minimum for these problems. We study two liquid crystal systems, the nematic and the SmC free-standing thin film, showing that both the annihilation [6,7] and repulsion of defects are always subject to strong backflow, which speeds up the processes remarkably. In the case of the annihilation, it introduces also an asymmetry in defect motion, i.e., it makes one defect move faster than the other.

The structure of the Thesis is as follows. In Chapter 2 the dynamic theory coupling the order parameter dynamics and the hydrodynamics is reviewed. The theory is kept general in this Chapter, not assuming any specific form of the order parameter. Chapter 3 defines the nematic order parameter in a rigorous manner, illuminating it from the physical and mathematical viewpoints. In Chapter 4 the Ericksen-Leslie theory — the dynamic theory of the nematic director — is presented and applied to the switching phenomena. In Chapter 5 the dynamic theory for a vector order parameter representing a generalization of the Ericksen-Leslie theory is derived. The starting point of the derivation is the general theory of Chapter 2. Chapter 6 provides the basics on disclination defects in liquid crystals, needed to understand the forthcoming Chapters. In Chapter 7 the tensorial dynamic theory is presented and applied to the pair-annihilation of disclination lines in nematics. In Chapter 8 the vectorial theory of Chapter 5 is used to study the pair-annihilation of vortices in a modelled SmC thin film system belonging to the class of the XY-model. Finally, Chapter 9 is devoted to the (in)stability and decay of disclinations with integer winding numbers in nematics.

2

Theory

In this section, an outline of the dynamic theory of dissipative complex fluids will be presented after an introductory discussion on the order parameter and the thermodynamic potential. At this stage the theory will be kept general, not depending on the specific choice of the order parameter. This will appear convenient later on as diverse systems with different order parameters will be studied.

2.1 Order parameter and thermodynamic potential

Liquid crystals are ordered systems, the order of which emerges at a symmetry breaking phase transition. To describe the ordering, a mesoscopic quantity — the order parameter — is introduced, which must vanish in the high temperature phase and be nonzero in the ordered phase, depending on the ordering and reflecting its symmetry properties. As the system may be spatially inhomogeneous in general, the order parameter is a field quantity. It is defined as an average over the mesoscopic volume of the sample, which, ideally, is large enough to serve a well-defined average, and small enough compared with the inhomogeneities to contain essentially a homogeneous portion of the sample. In dynamic studies, one is interested in nonequilibrium properties of the system. Departures from equilibrium are described by the order parameter taking a different value than the equilibrium one. Thus, the nonequilibrium properties of the system are to be related to the dynamics of the order parameter when out of equilibrium.

Thermodynamic systems to be considered will generally involve thermal, electric, and magnetic degrees of freedom. The total differential of the internal energy, $d\mathcal{U} = dQ + dA$, where

$$TdS = dQ + TdS^i, \tag{2.1}$$

is thus

$$d\mathcal{U} = T(dS - dS^i) - p\,dV + V\mathbf{E}\cdot d\mathbf{P} + \mu_0 V\mathbf{H}\cdot d\mathbf{M} + dA'. \tag{2.2}$$

In Eq. (2.1) the entropy change has been split into reversible (dQ/T) and irreversible parts, $dS^i > 0$. The last term in Eq. (2.2) represents the work of any contingent

forces not accounted for explicitly. At constant temperature T and constant electric and magnetic field strengths $\mathbf{E}$ and $\mathbf{H}$, the proper thermodynamic potential — the free energy $\mathcal{F}$ — is obtained by a Legendre transformation:

$$\mathcal{F} = U - TS - V\mathbf{E}\cdot\mathbf{P} - \mu_0 V\mathbf{H}\cdot\mathbf{M}, \tag{2.3}$$

$$d\mathcal{F} = -S\,dT - T dS^i - p\,dV - V\mathbf{P}\cdot d\mathbf{E} - \mu_0 V\mathbf{M}\cdot d\mathbf{H} + dA'. \tag{2.4}$$

Changes in the volume are normally neglected in liquid crystal systems. At constant T, $\mathbf{E}$, and $\mathbf{H}$, the free energy is decreasing when the system is approaching equilibrium, where it reaches its minimum value. It is the order parameter dependence of the free energy that describes this behavior. Before finding it, let us alert to how the free energy of nonequilibrium states can be calculated. Being a thermodynamic variable, it depends on the state of the system and not on the particular path leading to it. Hence, we are allowed to choose a different — reversible — path running only through equilibrium states, for which dS^i vanishes in Eq. (2.4) enabling us to perform the integration. The free energy change is thus equal to the minimal work dA' required to put the system into the final state at constant temperature and external fields. Let us consider an isothermal system of dipoles below the phase transition as an example. Clearly, the equilibrium state is homogeneous with all dipoles pointing in the same direction on average. Now think of a spatially modulated configuration — a nonequilibrium state with a higher free energy. To determine the free energy increase, one can imagine applying some forces that convey the system from the homogeneous to the modulated state via an equilibrium path. The increase of the free energy is equal to the work dA' of these forces. Similarly, if the sample is subject to an external field $\mathbf{H}$, with a configuration corresponding to equilibrium at a different field $\mathbf{H}'$, the free energy cost of this nonequilibrium state is given by

$$\Delta\mathcal{F} = -\mu_0 V \int_{\mathbf{H}}^{\mathbf{H}'} dV\,\mathbf{M}(\mathbf{H})\cdot d\mathbf{H}. \tag{2.5}$$

where the integration is performed over the equilibrium path $\mathbf{M}(\mathbf{H})$. For the electric field the situation is analogous.

2.2 Free energy functional

In this Section, the standard Landau phenomenological approach [8] will be taken to derive the equation of motion for a general order parameter (the application of the Landau theory to the nematic phase is due to de Gennes [9]). Let the order parameter $\mathbf{q}$ be multicomponent, with the components denoted q_i. As learned in the previous Section, the free energy dependence on the order parameter must be obtained in order to study nonequilibrium dynamics. It will be established in the form of an expansion around the equilibrium state. The free energy density $f(\mathbf{q}, \nabla\mathbf{q})$ is introduced as a function of the order parameter field and its spatial derivatives. A consistent derivation of this concept on the thermodynamic basis is given in [10, pp. 143-153]. Hence, the free energy is a functional,

$$\mathcal{F} = \int dV\, f(\mathbf{q}, \nabla\mathbf{q}). \tag{2.6}$$

In the phenomenological spirit, the free energy density functional is constructed from scalar invariants formed with $\mathbf{q}$, $\nabla\mathbf{q}$, and any external fields. There are five classifiable types of contributions.

1. Homogeneous terms. These are the standard Landau terms describing the phase transition and consist of scalar invariants of $\mathbf{q}$, which are the condensed quantities exhibiting a soft mode, i.e., they spontaneously become nonzero at the phase transition. Schematically,

$$f^{hom} = \frac{1}{2}A\,\mathbf{q}^2 + \frac{1}{3}B\,\mathbf{q}^3 + \frac{1}{4}C\,\mathbf{q}^4. \tag{2.7}$$

   The linear term is absent due to the requirement that $\mathcal{F}$ and so does f be a minimum at equilibrium. The quadratic term models the transition — at the supercooling temperature T^* it changes sign, $A = A'(T - T^*)$. The third order term is present only in the case $\mathbf{q} \neq -\mathbf{q}$, otherwise B is zero by symmetry. It is this term that gives a discontinuous phase transition. The fourth order term is necessary to provide the existence of a global minimum. The constants A', B, and C are temperature-independent.

2. Elastic terms. They give the free energy density cost of spatial inhomogeneities. In the original spirit they relate to the Goldstone degrees of freedom [11], but have been generalized to apply to the complete order parameter. This terms are invariant to inversion and always give positive contributions. Schematically,

$$f^{elast} = \frac{1}{2}L\,(\nabla\mathbf{q})^2, \tag{2.8}$$

   where L is a temperature-independent elastic constant. Depending on the complexity of the order parameter, there can exist many scalar invariants formed with ∇ and $\mathbf{q}$ and thus many elastic terms, each with its own elastic constant L_i. The most general expression, second-order in the derivative, is

$$f^{elast} = \frac{1}{2}L_{ijkl}\,(\partial_i q_j)(\partial_k q_l), \tag{2.9}$$

   where the fourth-rank tensor of elastic constants must reflect the symmetry of the system and thus can be composed only of the identity matrix δ_{ij}, the Levi-Civita antisymmetric matrix ϵ_{ijk}, and the order parameter q_i. Furthermore, the permutation symmetry

$$L_{ijkl} = L_{klij} \tag{2.10}$$

   must be obeyed on the basis of the definition (2.9). Hence, the matrix L_{ijkl} can be diagonalized in the sense that L_{ijkl} vanishes unless $i = k$ and $j = l$, i.e., the quadratic form (2.9) can be written as a sum of square terms only. The elastic coefficients of the diagonalized form must be all positive to yield a positive definite free energy density. In principle, one can include also higher order derivatives or terms of higher order in $\mathbf{q}$.

3. Chiral (Lifshitz) terms. These are pseudoscalars of the form

$$f^{chir} = L_c\, \epsilon_{ijk} q_i \partial_j q_k. \tag{2.11}$$

As they change sign upon inversion they are allowed only in chiral systems — systems lacking the inversion symmetry.

4. External field terms. They couple the order parameter to external fields (electric, magnetic, elastic deformation, etc.). In liquid crystals, the average density of permanent electric or magnetic moments is usually zero, which implies the coupling to be quadratic in the fields, schematically:

$$f^{em} = -\frac{1}{2}\varepsilon_0 X_e\, \mathbf{E}\cdot\mathbf{q}\cdot\mathbf{E} - \frac{1}{2}\mu_0 X_m\, \mathbf{H}\cdot\mathbf{q}\cdot\mathbf{H}. \tag{2.12}$$

The actual way of contraction depends on the order parameter. The constants X_e and X_m are microscopic parameters related to molecular susceptibilities. Forming scalars with $\mathbf{E}$ and $\nabla\mathbf{q}$ results in the so-called flexoelectric terms of the form $\nabla\mathbf{q}\cdot\mathbf{E}$, [12,13]. In flexoelectric phenomena, the inhomogeneity of the order parameter produces a polarization, which couples to the external field, or vice versa.

5. Surface terms. Some of the elastic terms can be written as a divergence, and therefore converted to a surface integral when performing (2.6). Physically, they appear on account of the reduced symmetry due to the presence of the surface, where there is another vector — the surface normal — that can take part in the scalar contraction.

Another type of surface terms is delivered by the anchoring, which represents a contribution to the free energy of the sample due to the interaction with the walls as well as due to the confinement-reduced phase space. Commonly, the anchoring is modelled by the surface favoring a certain value of the order parameter $\mathbf{q}_0$ [14–16], schematically:

$$f^{anch} = \frac{1}{2} W\,(\mathbf{q}-\mathbf{q}_0)^2. \tag{2.13}$$

If the order parameter is fixed at the surface or if there is no surface, the surface terms can be ignored when determining the configuration.

To find the equilibrium configuration, the free energy as a functional of the order parameter has to be minimized:

$$\delta\mathcal{F} = \int dV \left(\frac{\partial f}{\partial \mathbf{q}} - \nabla\cdot\frac{\partial f}{\partial\nabla\mathbf{q}}\right)\cdot\delta\mathbf{q} + \int \mathbf{dS}\cdot\frac{\partial f}{\partial\nabla\mathbf{q}}\cdot\delta\mathbf{q} = 0, \tag{2.14}$$

which yields the Euler-Lagrange equations for the bulk and the surface. In the following, the surface contributions will be omitted for brevity. In case the order parameter is subject to any constraints, Lagrange multipliers are introduced in a standard manner, which is equivalent to projecting Eq. (2.14) in the order parameter space to the subspace normal to the one defined by the constraints. The latter notion is quite convenient and will be used in the numerics.

2.3 Dynamic equation for the order parameter

Out of equilibrium, the free energy density fails to satisfy (2.14). When the system is approaching equilibrium, the free energy is decreasing on account of the increasing entropy:

$$T\dot{S}^i = -\dot{\mathcal{F}} = -\int dV \left(\frac{\partial f}{\partial \mathbf{q}} - \nabla \cdot \frac{\partial f}{\partial \nabla \mathbf{q}} \right) \cdot \dot{\mathbf{q}}, \tag{2.15}$$

where the dot stands for the material time derivative and the surface contributions have been omitted.

In general irreversible processes, the entropy production is expressed in terms of fluxes Φ_i and forces F_i:

$$T\dot{S}^i = \int dV F_i \Phi_i. \tag{2.16}$$

In the limit of weak fluxes the forces depend linearly on the fluxes [17]:

$$F_i = \mathsf{K}_{ij} \Phi_j, \quad \mathsf{K}_{ij} = \mathsf{K}_{ji}, \tag{2.17}$$

where the matrix of transport coefficients is symmetric according to Onsager's reciprocity principle [18], [19, p. 365]. Combining Eqs. (2.16) and (2.17), a quadratic form results for the entropy production:

$$T\dot{S}^i = \int dV \, 2D = \int dV \, \mathsf{K}_{ij} \Phi_i \Phi_j, \tag{2.18}$$

where we have defined the dissipation function D [19, p. 368]. The forces can be obtained, but need not (Eq. (2.17) is just as good), directly from the dissipation function as

$$F_i = \frac{\partial D}{\partial \Phi_i}. \tag{2.19}$$

The symmetric matrix K_{ij} can be diagonalized, i.e., such linear combinations of the fluxes can be found that the dissipation is expressed as a sum of squares of the fluxes.

According to Eq. (2.15), we can identify $\dot{\mathbf{q}}$ as the flux. The simplest (the lowest order in $\mathbf{q}$) choice for the coefficient matrix is $\mathsf{K}_{ij} = \gamma \delta_{ij}$, where γ is a material parameter with the dimension of the viscosity. Now, comparing Eqs. (2.15) and (2.18) the equation of motion for the order parameter is obtained [20]:

$$\nabla \cdot \frac{\partial f}{\partial \nabla \mathbf{q}} - \frac{\partial f}{\partial \mathbf{q}} = \gamma \dot{\mathbf{q}}. \tag{2.20}$$

Frequently, Eq. (2.20) is interpreted as a balance of two generalized forces, $\mathbf{h} + \mathbf{h}^v = 0$, where $\mathbf{h}$ is the driving force, to be denoted briefly

$$\mathbf{h} = \nabla \cdot \frac{\partial f}{\partial \nabla \mathbf{q}} - \frac{\partial f}{\partial \mathbf{q}} \equiv -\frac{\delta f}{\delta \mathbf{q}}, \tag{2.21}$$

and $\mathbf{h}^v = -\gamma \dot{\mathbf{q}}$ is the opposing or "viscous" force.

2.4 Coupling to the flow

In general, the order parameter dynamics is coupled to the fluid flow, which means that either can generate the other. The fluid flow is governed by a generalized Navier-Stokes equation

$$\rho\dot{\mathbf{v}} = \nabla \cdot \sigma, \tag{2.22}$$

where σ is the stress tensor to be determined. Besides the pressure, if the free energy density contains gradient terms, there is an elastic contribution to the stress tensor. It arises because a change in the deformation of the system $\delta\mathbf{u}$ (while keeping $\delta\mathbf{q} = 0$) changes the gradient of $\mathbf{q}$,

$$\delta\frac{\partial\mathbf{q}}{\partial x_i} = -\frac{\partial\mathbf{q}}{\partial x_j}\,\delta\frac{\partial u_j}{\partial x_i}, \tag{2.23}$$

and thus the free energy density:

$$\delta f = \frac{\partial f}{\partial(\partial_i\mathbf{q})}\cdot\delta\partial_i\mathbf{q} = -\frac{\partial f}{\partial(\partial_i\mathbf{q})}\cdot\partial_j\mathbf{q}\;\delta\frac{\partial u_j}{\partial x_i}. \tag{2.24}$$

Comparing Eq. (2.24) with the constitutive relation

$$\delta f = \sigma_{ij}\;\delta\frac{\partial u_j}{\partial x_i}, \tag{2.25}$$

the elastic contribution to the stress tensor follows:

$$\sigma^e_{ij} = -\frac{\partial f}{\partial(\partial_i\mathbf{q})}\cdot\partial_j\mathbf{q}. \tag{2.26}$$

Let us inspect the equilibrium condition $\delta\mathcal{F} = 0$, allowing also a deformation $\delta\mathbf{u}$ of the system (omitting the surface terms everywhere):

$$0 = \delta\mathcal{F} = \int dV\left[\sigma_{ij}\,\delta(\partial_i u_j) + \frac{\delta f}{\delta\mathbf{q}}\cdot\delta\mathbf{q}\right]. \tag{2.27}$$

Putting $\sigma_{ij} = \sigma^e_{ij} - p\delta_{ij}$, where p is the pressure, and inserting Eq. (2.26), we get

$$0 = \delta\mathcal{F} = \int dV\left\{\left[\partial_i\frac{\partial f}{\partial(\partial_i\mathbf{q})}\cdot\partial_j\mathbf{q} + \frac{\partial f}{\partial(\partial_i\mathbf{q})}\cdot\partial_j\partial_i\mathbf{q} + \partial_j p\right]\delta u_j + \frac{\delta f}{\delta\mathbf{q}}\cdot\delta\mathbf{q}\right\}. \tag{2.28}$$

Expressing the first term by the equilibrium condition for the order parameter, $\delta f/\delta\mathbf{q} = 0$, the expression in the bracket — the body force — simplifies to

$$0 = \int dV\left[\frac{\partial f}{\partial\mathbf{q}}\cdot\partial_j\mathbf{q} + \frac{\partial f}{\partial(\partial_i\mathbf{q})}\cdot\partial_j\partial_i\mathbf{q} + \partial_j p\right]\delta u_j = \int dV\,\partial_j(f+p)\delta u_j, \tag{2.29}$$

i.e., in equilibrium the pressure is such that $f + p$ is constant.

Out of equilibrium, in presence of the fluid flow the density of the kinetic energy $\frac{1}{2}\rho\mathbf{v}^2$ must be added to the free energy density; now the entropy production is

$$T\dot{S}^i = -\frac{d}{dt}\int dV \left(\frac{1}{2}\rho\mathbf{v}^2 + f(\mathbf{q},\nabla\mathbf{q})\right). \tag{2.30}$$

Inserting Eq. (2.22) and dropping surface terms, we get

$$T\dot{S}^i = \int dV \left[\sigma_{ij}\partial_i v_j - \frac{\delta f}{\delta \mathbf{q}}\cdot\dot{\mathbf{q}} - \frac{\delta f}{\delta(\partial_i u_j)}\partial_i v_j\right], \tag{2.31}$$

where the first factor of the last term is recognized as $\sigma^e_{ij} - p\delta_{ij}$. The entropy production is

$$T\dot{S}^i = \int dV \left[(\sigma_{ij} + p\delta_{ij} - \sigma^e_{ij})\partial_i v_j - \frac{\delta f}{\delta \mathbf{q}}\cdot\dot{\mathbf{q}}\right], \tag{2.32}$$

recall that $\dot{\mathbf{q}}$ is the material time derivative: $\dot{\mathbf{q}} = \partial\mathbf{q}/\partial t + (\mathbf{v}\cdot\nabla)\mathbf{q}$. Thus, there are two fluxes that raise the entropy in the flow-coupled system — the time derivative of the order parameter $\dot{\mathbf{q}}$ and the velocity gradient $\nabla\mathbf{v}$. The force conjugated to the latter is the difference between the total stress tensor without the pressure contribution and the elastic stress tensor and will be called the viscous stress tensor $\sigma^v = \sigma + p\,\mathrm{I} - \sigma^e$. Conveniently, the entropy source density $\dot{s}^i$ is expressed by splitting the tensors into symmetric and antisymmetric parts:

$$T\dot{s}^i = \sigma^s_{ij}\mathsf{A}_{ij} + \sigma^a_{ij}\mathsf{W}_{ij} + h_i\dot{q}_i, \tag{2.33}$$

where σ^s and σ^a are the symmetric and antisymmetric viscous stress tensor parts, while A and W are the symmetric and antisymmetric parts of the velocity gradient:

$$\mathsf{A}_{ij} = \frac{1}{2}(\partial_i v_j + \partial_j v_i), \quad \mathsf{W}_{ij} = \frac{1}{2}(\partial_i v_j - \partial_j v_i). \tag{2.34}$$

The forces read

$$\begin{aligned}
\sigma^s_{ij} &= \mathsf{S}_{ijkl}\mathsf{A}_{kl} + \mathsf{M}_{ijkl}\mathsf{W}_{kl} + \mathsf{C}_{ijk}\dot{q}_k, &(2.35)\\
\sigma^a_{ij} &= \mathsf{M}_{klij}\mathsf{A}_{kl} + \mathsf{R}_{ijkl}\mathsf{W}_{kl} + \mathsf{D}_{ijk}\dot{q}_k, &(2.36)\\
-h^v_i \equiv h_i &= \mathsf{C}_{kli}\mathsf{A}_{kl} + \mathsf{D}_{kli}\mathsf{W}_{kl} + \mathsf{B}_{ij}\dot{q}_j, &(2.37)
\end{aligned}$$

and the entropy source density is

$$\begin{aligned}
T\dot{s}^i = {} & \mathsf{S}_{ijkl}\mathsf{A}_{kl}\mathsf{A}_{ij} + \mathsf{M}_{ijkl}\mathsf{W}_{kl}\mathsf{A}_{ij} + \mathsf{C}_{ijk}\dot{q}_k\mathsf{A}_{ij} + \\
& \mathsf{M}_{klij}\mathsf{A}_{kl}\mathsf{W}_{ij} + \mathsf{R}_{ijkl}\mathsf{W}_{kl}\mathsf{W}_{ij} + \mathsf{D}_{ijk}\dot{q}_k\mathsf{W}_{ij} + \\
& \mathsf{C}_{kli}\mathsf{A}_{kl}\dot{q}_i + \mathsf{D}_{kli}\mathsf{W}_{kl}\dot{q}_i + \mathsf{B}_{ij}\dot{q}_j\dot{q}_i.
\end{aligned} \tag{2.38}$$

The coefficient matrices obey the following properties regarding the permutation of indices:

$$\begin{aligned}
&\mathsf{S}_{ijkl} = \mathsf{S}_{klij}, \quad \mathsf{S}_{ijkl} = \mathsf{S}_{jikl},\\
&\mathsf{R}_{ijkl} = \mathsf{R}_{klij}, \quad \mathsf{R}_{ijkl} = -\mathsf{R}_{jikl},\\
&\mathsf{M}_{ijkl} = \mathsf{M}_{jikl}, \quad \mathsf{M}_{ijkl} = -\mathsf{M}_{ijlk},\\
&\mathsf{C}_{ijk} = \mathsf{C}_{jik}, \quad \mathsf{D}_{ijk} = -\mathsf{D}_{jik},\\
&\mathsf{B}_{ij} = \mathsf{B}_{ji}.
\end{aligned} \tag{2.39}$$

Recall that the quadratic (2.38) can be diagonalized. Furthermore, the entropy production must be invariant under the symmetry operations of the system. As a consequence, the coefficient matrices can consist only of quantities characterizing the system — the order parameter $\mathbf{q}$, the identity matrix δ_{ij}, and the Levi-Civita antisymmetric matrix ϵ_{ijk}. Each term comes with its own material parameter. One can verify that the entropy production is also invariant to time reversal. Finally, there must be no entropy production (2.38) and no forces (2.35)-(2.37) for a homogeneous rotation of the sample, which imposes essential relations on the material parameters, reducing the number of independent constants.

To summarize, in a brief form the dynamic equations for the order parameter coupled to the incompressible fluid flow read:

$$-\frac{\delta f}{\delta \mathbf{q}} + \mathbf{h}^v = 0, \tag{2.40}$$

$$\rho \dot{\mathbf{v}} = -\nabla p + \nabla \cdot (\sigma^v + \sigma^e), \tag{2.41}$$

$$\nabla \cdot \mathbf{v} = 0, \tag{2.42}$$

where the forces σ^v and $\mathbf{h}^v$ are given by Eqs. (2.35)-(2.37), σ^e is given by Eq. (2.26), and the functional derivative in (2.40) has been defined in Eq. (2.21). A detailed derivation of the equations for a vectorial order parameter coupled to the hydrodynamic flow is carried out in Chapter 5.

3

Nematic order parameter

In this Chapter we will define the order parameter of the nematic liquid crystal. Nematic substances consist of molecules with an elongated or a disc-like shape, which are effectively cylindrical objects due to their rotation. Let us assign a unit vector $\mathbf{d} = (\sin\theta'\cos\phi', \sin\theta'\sin\phi', \cos\theta')$ to the long axis of the liquid crystal molecule. In case of disc-like molecules $\mathbf{d}$ is the normal of the disc. The distribution of molecular orientations, i.e., the distribution of vectors $\mathbf{d}$, defined in the mesoscopic volume, is naturally specified by an angular probability distribution function

$$g(\mathbf{e}) = g(\theta, \phi), \tag{3.1}$$

where $\mathbf{e}$ is a unit vector $\mathbf{e} = (x, y, z) = (\sin\theta\cos\phi, \sin\theta\sin\phi, \cos\theta)$. In nematics, we find empirically that $g(\mathbf{e}) = g(-\mathbf{e})$, or

$$g(\theta, \phi) = g(\pi - \theta, \phi + \pi), \tag{3.2}$$

i.e., there is no polar ordering. The distribution function g carries to much information on the ordering — it cannot be determined experimentally, neither is it convenient for analytical work. Therefore, the lowest nontrivial moment of g is chosen to serve as the order parameter. The probability density g can be expanded in spherical harmonics [21, p. 338]:

$$g(\theta, \phi) = \sum_l g^{(l)}(\theta, \phi) = \sum_{l,m} g_{l,m} Y^{\mathcal{R}}_{l,m}(\theta, \phi), \quad g_{l,m} = \int d\Omega\, Y^{\mathcal{R}}_{l,m}(\theta, \phi) g(\theta, \phi), \tag{3.3}$$

where real combinations of the spheric functions $Y_{l,m}$ have been used:

$$Y^{\mathcal{R}}_{l,m} = \begin{cases} Y_{l,m} & ; \quad m = 0 \\ \frac{1}{\sqrt{2}}(Y_{l,m} + (-1)^m Y_{l,-m}) & ; \quad m > 0 \\ \frac{1}{\sqrt{2}i}(Y_{l,m} - (-1)^m Y_{l,-m}) & ; \quad m < 0 \end{cases} . \tag{3.4}$$

Due to (3.2) $g_{l,m}$ is zero for l odd. Thus, the lowest nontrivial moment is the quadrupole, $l = 2$, and the set of 5 quantities $q_{2,m}$ represents the nematic order parameter. In the isotropic phase, where $g = g^{(0)} = 1/4\pi$, the order parameter is zero as required. In the ordered phase, the quadrupole moment is nonzero, and

$g^{(2)}$ corresponds to the deviation (up to the quadrupole moment) of the probability distribution g from the isotropic distribution. It is customary to use the Cartesian notation

$$g^{(2)} = \sum_{m=-2}^{2} g_{2,m} Y^{\mathcal{R}}_{2,m} = \sqrt{\tfrac{5}{4\pi}}\, g_{2,0}\, \frac{3z^2-1}{2} + \sqrt{\tfrac{15}{16\pi}} \left[g_{2,1}\, 2zx + g_{2,-1}\, 2zy + g_{2,2}\,(x^2-y^2) + g_{2,-2}\, 2xy \right] \equiv \frac{5}{4\pi} \mathsf{Q}_{ij}\, e_i e_j. \tag{3.5}$$

Recalling that $\mathbf{e}^2 = x^2 + y^2 + z^2 = 1$, we have defined the nematic tensor order parameter Q. Being symmetric by definition, the quadratic form can be diagonalized for briefness:

$$g^{(2)} = \frac{5}{4\pi} \left(\mathsf{Q}_{zz}\, z^2 + \mathsf{Q}_{xx}\, x^2 + \mathsf{Q}_{yy}\, y^2 \right), \tag{3.6}$$

where

$$\mathsf{Q}_{zz} = \sqrt{\tfrac{4\pi}{5}}\, g_{2,0} = \frac{3\langle \cos^2\theta' \rangle - 1}{2}, \tag{3.7}$$

$$\mathsf{Q}_{xx} = \sqrt{\tfrac{3\pi}{5}}\, g_{2,2} - \tfrac{1}{2}\sqrt{\tfrac{4\pi}{5}}\, g_{2,0} = \frac{3}{4}\langle \sin^2\theta' \cos 2\phi' \rangle - \frac{1}{2}\frac{3\langle \cos^2\theta' \rangle - 1}{2}, \tag{3.8}$$

$$\mathsf{Q}_{yy} = -\sqrt{\tfrac{3\pi}{5}}\, g_{2,2} - \tfrac{1}{2}\sqrt{\tfrac{4\pi}{5}}\, g_{2,0} = -\frac{3}{4}\langle \sin^2\theta' \cos 2\phi' \rangle - \frac{1}{2}\frac{3\langle \cos^2\theta' \rangle - 1}{2}. \tag{3.9}$$

Note that Q is traceless. Briefly,

$$\mathsf{Q} = \begin{bmatrix} -\frac{1}{2}(S-P) & & \\ & -\frac{1}{2}(S+P) & \\ & & S \end{bmatrix}, \tag{3.10}$$

which can be expressed also in a general coordinate system as

$$\mathsf{Q}_{ij} = \frac{1}{2} S (3 n_i n_j - \delta_{ij}) + \frac{1}{2} P (e^1_i e^1_j - e^2_i e^2_j), \tag{3.11}$$

where

$$S = \frac{3\langle \cos^2\theta' \rangle - 1}{2} \tag{3.12}$$

is the scalar order parameter, also called the degree of order, and

$$P = \frac{3}{2}\langle \sin^2\theta' \cos 2\phi' \rangle \tag{3.13}$$

is the biaxiality. In Eq. (3.11) we have introduced an orthonormal triad $(\mathbf{n}, \mathbf{e}^1, \mathbf{e}^2)$ specifying the Q-tensor eigensystem: $\mathbf{n}$ is the director, and $\mathbf{e}^1$ is the secondary director. Usually, the director $\mathbf{n}$ represents the eigenvector with the largest in absolute eigenvalue, but not necessarily (as in Chapter 9). In a general coordinate system, it follows from Eq. (3.5) that

$$g^{(2)}(\mathbf{e}) = \frac{5}{4\pi} \mathsf{Q}_{ij}\, e_i e_j, \quad \mathsf{Q}_{ij} = \frac{1}{2}(3\langle d_i d_j \rangle - \delta_{ij}), \tag{3.14}$$

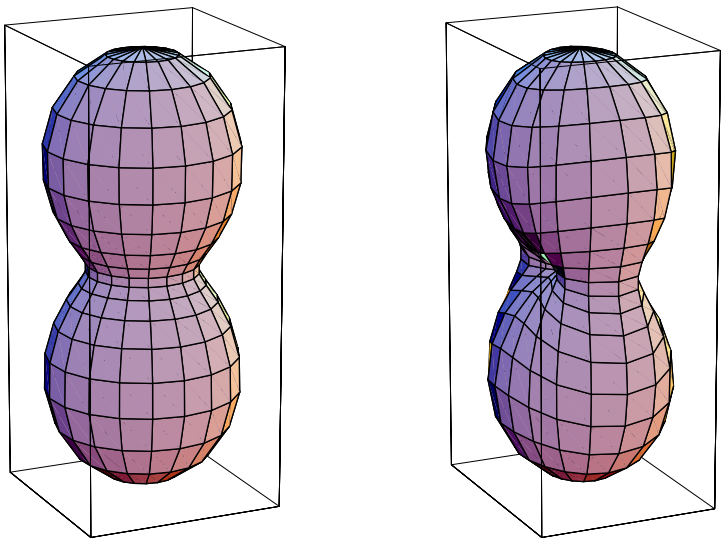

(a) uniaxial, $P = 0$ (b) biaxial, $P \neq 0$

Figure 3.1 The quadrupole contribution to the probability distribution function, $g^{(2)}$, in the case of (a) uniaxial and (b) biaxial ordering. In Cartesian coordinates, $g^{(2)}$ is given by the quadratic form $g^{(2)}(\mathbf{e}) = \frac{5}{4\pi}\mathsf{Q}_{ij}\, e_i e_j$, where $\mathbf{e}$ is a unit vector.

and

$$g^{(2)}(\mathbf{e}) = \frac{5}{8\pi}\left(3\langle(\mathbf{d}\cdot\mathbf{e})^2\rangle - 1\right). \tag{3.15}$$

4

Director dynamics in nematics

The aim of this Chapter presenting the early stages of our research is to provide the machinery for the hydrodynamic description of liquid crystal dynamics and to get acquainted with the basic principles of flow generation and its influence on the nematic director. Moreover, we present numeric solutions to two-dimensional and quasi-three-dimensional switching processes, which are scarce in literature. We demonstrate that in confined systems the backflow can lead to drastic effects far from mere perturbations, for which it is usually recognized.

4.1 Introduction

Problems involving hydrodynamic motion of the nematic liquid crystal due to the director reorientation have been studied mainly in terms of the Ericksen-Leslie continuum theory of the nematic liquid crystal [22–24]. For one-dimensional geometry, Clark and Leslie [25] have given a thorough approximative analysis of nematic relaxation upon removal of electric or magnetic field; a complete numerical treatment of the problem has been contributed by van Doorn [26]. One-dimensional backflow dynamics in the twist cell has been studied by Berreman [27,28]. Recently, an optical observation of the backflow in the twist cell was reported [29]. Pieranski, Brochard and Guyon [30,31] have studied, both theoretically and experimentally, one-dimensional dynamic behavior in magnetic field for three geometries (twisted, planar to homeotropic, homeotropic to planar), limited to small deformations (applying near-critical fields). They give the distortion wave vector and effective viscosity dependence on the magnetic field strength. The instability against periodic distortion in the case of the Freedericksz transition (first observed by Carr [32]) has been studied by Guyon *et al.* [33] for the two-dimensional case, and by Hurd *et al.* [34] for three dimensions. The pattern formation in a rotating magnetic field has been observed experimentally and accounted for by a numerical study based on the Ericksen-Leslie equations [35,36]. An experiment measuring the rotational viscosity is presented by Bajc *et al.* [37], together with a full hydrodynamic numerical treatment in cylindrical geometry (one-dimension), yielding an exact expression for the effective viscosity, depending on the director field configuration. Lately, the interest in hydrodynamic description of pattern formation in fluids has been increasing,

amongst others involving also nematic and nematic polymer fluids [38–44].

In this Chapter a full two-dimensional hydrodynamic study of a nematic sample in magnetic field is presented, producing nontrivial backflow fields even in the simplest geometries like a square or a rectangle. First a short review of nematodynamic equations is given, followed by an introduction of characteristic scales of the problem. In the second part the flow fields are tentatively interpreted by strict analytic as well as less strict arguments. Also, the influence of the backflow on the director reorientation is discussed. The idea pursued throughout the Chapter is to give enough qualitative physical understanding of the backflow generation and its effect on the director field to be able to explain or even foresee the global time path of relaxation processes [45]. The relaxation with the backflow is then compared to the simplified case where backflow is not taken into account. The issues in question here are the change in the switching time of the cell caused by the backflow, and the local departure of director orientation from the orientation in the simple case, pursued along the whole path of relaxation. The drastic backflow effect as the consequence of a special magnetic field switching is demonstrated in the 2D and quasi-3D examples. The 3D geometry is closer to a possible experiment.

4.2 Ericksen-Leslie theory

Here we are going to present the Ericksen-Leslie theory [22,23], which is the dynamic theory for the nematic director coupled to hydrodynamic flow. It can be derived following the theoretical basis set in Chapter 2. At this point, we will skip the derivation and invite the reader to visit Chapter 5, where the Ericksen-Leslie theory in a generalized form is derived thoroughly.

Three basic equations are involved in the problem of nematodynamics; these are the equation of motion of the director field (2.40), the generalized Navier-Stokes equation (2.41), and the equation of continuity. The latter is simply reduced to the equation of incompressibility (2.42), whereas the former two are relatively extensive due to the (uniaxial) anisotropy of the nematic fluid as well as to the coupling between the director reorientation and flow.

The time evolution equation for the director field is a balance between generalized elastic, electric, magnetic, and viscous forces. In principle, both electric and magnetic fields can be used to manipulate the nematic director. However, the use of the electric field, though more efficient due to larger susceptibility anisotropies, brings about some difficulties to deal with, i.e., the dielectric problem has to be solved exactly, and the convection of ions should be taken into account. As a result of this, the theoretical study to be presented in this Chapter uses a magnetic field.

To obtain the elastic and magnetic part, the Frank elastic free energy density [46–48], [49, pp. 102, 119] is used:

$$f = \frac{1}{2}K_{11}(\nabla\cdot\mathbf{n})^2+\frac{1}{2}K_{22}\left[\mathbf{n}\cdot(\nabla\times\mathbf{n})\right]^2+\frac{1}{2}K_{33}\left[\mathbf{n}\times(\nabla\times\mathbf{n})\right]^2-\frac{1}{2}\chi_a\mu_0(\mathbf{n}\cdot\mathbf{H})^2, \quad (4.1)$$

where $\mathbf{n}$ is a unit vector representing the director, K_{11}, K_{22}, and K_{33} are the splay, twist, and bend elastic constants, respectively, $\mathbf{H}$ is the magnetic field, and χ_a is the

magnetic susceptibility anisotropy, i.e., the difference between the susceptibilities parallel and perpendicular to the director. The case of $\chi_a > 0$ will be considered here, as this is the situation present in most nematic substances. In the one elastic constant approximation, the elastic part of Eq. (4.1) reduces to

$$f^{one} = \frac{1}{2}K(\nabla \mathbf{n})^2. \tag{4.2}$$

The surface terms have been dropped in Eqs. (4.1) and (4.2) on account of fixed boundary conditions, corresponding to infinitely strong anchoring.

The Euler-Lagrange equations for the free energy functional

$$\mathcal{F} = \int dV \, \left(f(\mathbf{n}, \nabla \mathbf{n}) - \lambda(\mathbf{r})\mathbf{n}^2 \right) \tag{4.3}$$

with the constraint $\mathbf{n}^2 = 1$ and f given by (4.1), give the generalized elastic and magnetic force:

$$h_i^{em} = -\frac{\partial f}{\partial n_i} + \partial_j \left(\frac{\partial f}{\partial(\partial_j n_i)} \right). \tag{4.4}$$

The equilibrium condition reads

$$\mathbf{h}^{em} = -\lambda(\mathbf{r})\mathbf{n}, \tag{4.5}$$

where λ is the Lagrange multiplier, i.e., the force $\mathbf{h}^{em}$ must be parallel to $\mathbf{n}$ everywhere. One gets rid of the redundant director degree of freedom and the multiplier by projecting Eq. (4.5) onto the plane perpendicular to the director.

The generalized viscous force is obtained from the dissipation function, Eq. (2.19) containing scalar invariants formed with $\mathbf{n}$, $\dot{\mathbf{n}}$, and $\nabla \mathbf{v}$, being bilinear in the latter two [50, p. 142]:

$$-\mathbf{h}^v = \gamma_1 \mathbf{N} + \gamma_2 \mathsf{A} \cdot \mathbf{n}, \tag{4.6}$$

where the rotational viscosity γ_1 and γ_2 are expressed in terms of the Leslie viscosity coefficients α_i [49, p. 206], $\gamma_1 = \alpha_3 - \alpha_2$, $\gamma_2 = \alpha_3 + \alpha_2$. With $\dot{\mathbf{n}}$ being the material time derivative of the director,

$$\mathbf{N} = \dot{\mathbf{n}} - \frac{1}{2}(\nabla \times \mathbf{v}) \times \mathbf{n} = \dot{\mathbf{n}} + \mathsf{W} \cdot \mathbf{n} \tag{4.7}$$

is the vector of the relative director rotation with respect to the rotation of the fluid. The symmetric and antisymmetric parts of the velocity gradient, A_{ij} and W_{ij}, have been defined in Eq. (2.34). The viscous force $\mathbf{h}^v$ also needs to be projected to the plane perpendicular to the director. The equation of motion of the director reads briefly

$$\left\{ \mathbf{h}^{em} + \mathbf{h}^v \right\}_{\perp \mathbf{n}} = 0, \tag{4.8}$$

or in more detail

$$\gamma_1 \frac{\partial \mathbf{n}}{\partial t} = \left\{ \mathbf{h}^{em} - \gamma_2 \mathsf{A} \cdot \mathbf{n} - \gamma_1 \left[\mathsf{W} \cdot \mathbf{n} + (\mathbf{v} \cdot \nabla)\mathbf{n} \right] \right\}_{\perp \mathbf{n}}. \tag{4.9}$$

The generalized Navier-Stokes equation,

$$\rho\left[\frac{\partial \mathbf{v}}{\partial t}+(\mathbf{v}\cdot\nabla)\mathbf{v}\right]=-\nabla p+\nabla\cdot(\sigma^{v}+\sigma^{e}), \tag{4.10}$$

where ρ is the density, p is the pressure, and the divergence of a tensor defined as $(\nabla\cdot\sigma)_i=\partial_j\sigma_{ji}$, involves two stress tensor contributions. The viscous part is obtained from the same dissipation function as the generalized force (4.6) [50, p. 142]:

$$\begin{aligned}\sigma^{v} &= \alpha_1\mathbf{n}\otimes\mathbf{n}(\mathbf{n}\cdot\mathsf{A}\cdot\mathbf{n})+\alpha_2\mathbf{n}\otimes\mathbf{N}+\alpha_3\mathbf{N}\otimes\mathbf{n}+\\ &\quad \alpha_4\mathsf{A}+\alpha_5\mathbf{n}\otimes(\mathsf{A}\cdot\mathbf{n})+\alpha_6(\mathsf{A}\cdot\mathbf{n})\otimes\mathbf{n},\end{aligned} \tag{4.11}$$

with the Leslie coefficients obeying the Parodi relation [51]

$$\alpha_6-\alpha_5=\alpha_3+\alpha_2 \tag{4.12}$$

due to the Onsager's reciprocity principle. For future purposes, let us split the viscous stress tensor into the symmetric and antisymmetric parts:

$$\begin{aligned}\sigma^{s} &= \alpha_1\mathbf{n}\otimes\mathbf{n}(\mathbf{n}\cdot\mathsf{A}\cdot\mathbf{n})+\alpha_4\mathsf{A}+\\ &\quad \frac{1}{2}\gamma_2(\mathbf{N}\otimes\mathbf{n}+\mathbf{n}\otimes\mathbf{N})+\frac{1}{2}(\alpha_5+\alpha_6)\left[(\mathsf{A}\cdot\mathbf{n})\otimes\mathbf{n}+\mathbf{n}\otimes(\mathsf{A}\cdot\mathbf{n})\right],\\ \sigma^{a} &= \frac{1}{2}\gamma_1(\mathbf{N}\otimes\mathbf{n}-\mathbf{n}\otimes\mathbf{N})+\frac{1}{2}\gamma_2\left[(\mathsf{A}\cdot\mathbf{n})\otimes\mathbf{n}-\mathbf{n}\otimes(\mathsf{A}\cdot\mathbf{n})\right].\end{aligned} \tag{4.13}$$

The elastic part of the stress tensor (Eq. (2.26)) is a consequence of deformations changing the director field gradients, Eq. (2.26), [49, p. 152]:

$$\sigma^{e}_{ij}=-\frac{\partial f}{\partial(\partial_i n_k)}\partial_j n_k. \tag{4.14}$$

The pressure field in Eq. (4.10) is set by the incompressibility condition (2.42), i.e., it has to be determined in such a way that Eq. (2.42) is satisfied.

4.3 Characteristic scales

The problems to be addressed in this Chapter involve two length scales: the container size or the thickness of the capillary L and the magnetic coherence length [49, p. 123]

$$\xi_m=\frac{1}{H}\sqrt{\frac{K_{11}}{\mu_0|\chi_a|}}. \tag{4.15}$$

In order that field effects be prominent, ξ_m must be small compared with L. Therefore, ξ_m is the length relevant for the dynamics of the system.

The director equation of motion (4.9) and the generalized Navier-Stokes equation (4.10) introduce a characteristic time scale each. Typical relaxation time of the director field is

$$\tau=\frac{\gamma_1\xi_m^2}{K_{11}}, \tag{4.16}$$

if ξ_m is the characteristic length of the director variation. Since the dynamics is governed by the director field relaxation, τ is the characteristic time of the switching process.

The other time scale is given by a typical transition time during which the velocity field is equilibrated to its stationary value due to viscous forces,

$$\tau_0 = \frac{\rho L^2}{\alpha_4}. \tag{4.17}$$

The isotropic viscosity coefficient α_4 (see Eq. (4.11)) is of the same order of magnitude as the rotational viscosity γ_1, so it is convenient to use the latter in the estimate (4.18). Typically, the ratio of the two time scales — the unsteadiness parameter — is of the order of

$$\tau_0/\tau = \frac{L^2}{\xi_m^2}\,\frac{\rho K_{11}}{\gamma_1^2} \approx L^2/\xi_m^2 \cdot 10^{-6}. \tag{4.18}$$

This means that unless the container size L is much larger than the coherence length, the velocity field is adapted quickly to a given director field and its time derivative, so that during the reorientation process it behaves quasi-stationary — the partial time derivative in (4.10) can be dropped.

The characteristic magnitude of the velocity can be estimated by equating the viscous force (the α_4 term in (4.11)) and the viscous force exerted by the director rotation, which drives the flow (the α_2 and α_3 terms in (4.11)), yielding

$$v_0 = \frac{K_{11}}{\gamma_1 \xi_m} = \xi_m/\tau. \tag{4.19}$$

As indicated in (4.19), the same estimate can be obtained in a simpler fashion, although it might not seem as lucid. Again it was assumed that $\alpha_4 \approx \alpha_2 \approx \gamma_1$. The characteristic length of the velocity variation is estimated to L. To be more precise, both length scales, L and ξ_m, are intertwined here, but L is used in order to overestimate the Reynolds number:

$$Re = \frac{L}{\xi_m}\,\frac{\rho K_{11}}{\gamma_1^2} \approx L/\xi_m \cdot 10^{-6}. \tag{4.20}$$

Unless the magnetic coherence length is tiny in comparison with L, the Reynolds number is much smaller than unity, and the nonlinear advective derivative term in (4.10) can be dropped. In addition, if the ratio (4.18) is small as well, also the partial time derivative in (4.10) can be omitted, as mentioned above. The reader should note that usually the Reynolds number is more than an order of magnitude smaller than the unsteadiness parameter. The final equation to solve is thus

$$0 = -\nabla p + \nabla \cdot (\sigma^v + \sigma^e). \tag{4.21}$$

Material parameters such as the viscosity and the elastic coefficients will correspond to those for MBBA, listed in [49, pp. 105, 231]. It is convenient to give some typical magnitudes. A magnetic field with strength 0.1 T gives a coherence length of about 10 μm and the characteristic time (4.16) of around 2 s. Extrapolation lengths [49, p. 113] as small as 100 nm or even smaller are readily observed, so that the strong anchoring limit is realistic.

4.3.1 Comment on heat diffusion

Throughout the Thesis we assume that the temperature is constant. One should not proceed further without having justified this limit. In particular, the dynamics of defects studied in Chapters 7 and 8 might be affected by temperature gradients, since the motion of defect cores — regions of high free energy density — is generally accompanied by a transport of heat. The heat diffusion equation

$$\frac{\partial T}{\partial t} - \frac{1}{\rho c_p} \nabla \cdot (\underline{\lambda} \cdot \nabla T) = 0 \tag{4.22}$$

introduces yet another time scale,

$$\tau_Q = \frac{\rho c_p l^2}{\lambda}, \tag{4.23}$$

where l is the characteristic length of the temperature variation, c_p is the specific heat capacity, and λ is a typical component of the heat conductivity tensor. Comparing τ_Q and the characteristic dynamic time of the order parameter (4.16), both at the same length l, one gets

$$\tau_Q / \tau = \frac{K \rho c_p}{\gamma_1 \lambda}, \tag{4.24}$$

which is of the order of $5 \cdot 10^{-4}$ for typical material parameters of liquid crystals. The ratio (4.24) is the same also if defects are present (Eq. (7.19)). This means that the heat diffusion is fast compared to the order parameter diffusion, so that there cannot exist any substantial inhomogeneities in temperature induced by the order parameter dynamics. The constant temperature limit is realistic in fact.

4.4 Description of the problem and numerical implementation

The relaxation of a confined nematic sample upon switching a magnetic field will be studied. A container of square or rectangular cross section (the xy plane) is adopted, extending to infinity in the z direction. Infinitely strong anchoring is assumed, which fixes the director field at the boundaries. In practice, this means that the extrapolation length [49, p. 113], ξ, must be much smaller compared both with the sample size and the magnetic coherence length, i.e., $\xi \ll L$ and $\xi \ll \xi_m$. Standard no-slip boundary conditions are prescribed for the flow, setting the velocity to zero at the boundaries.

The partial differential equations (4.9) and (4.10) are cast in dimensionless form using characteristic scales introduced above. They are solved using finite difference discretisation. The outline of the method is as follows. At a given director field and its time derivative, the generalized Navier-Stokes equation (4.10) without the advective derivative term is explicitly iterated in time. After that, knowing the velocity field, the director equation (4.9) is explicitly iterated in time to yield the new director field. Then the velocity is updated again, and so forth. According to

the big difference in characteristic time scales (4.17) and (4.16), one makes many iterations of Eq. (4.10) before updating the director field. For a generic set of material parameters the unsteadiness parameter (4.18) is small enough, so one could drop the time derivative term in (4.10) in the first place. However, with the explicit iterative numerical scheme described above, this has little sense. On the other hand, Eq. (4.10) without the nonlinear term and Eq. (2.42) together result in a large set of linear equations for the discretized velocity and pressure variables, which can be solved directly for the stationary velocity field. In practice it turned out that the iterative method is far more efficient. The velocity and pressure variables are discretized on a staggered grid [52, p. 331] in order to prevent the occurrence of the well-known oscillatory pressure solution [53]. The incompressibility condition is satisfied in a standard way by solving a Poisson equation for pressure corrections at every velocity iteration step [52, p. 340] using the SOR method [54, p. 655]. At the boundaries, normal pressure correction derivatives are specified in order to meet the incompressibility condition there. The calculations were typically done on a square mesh of size 60x60.

4.5 2D problem

The first problem considered is fully two-dimensional (Fig. 4.1): the quantities involved depend on x and y, while the director and the flow velocity are lying in the xy plane. The orienting magnetic field points along the y axis. To avoid any frustration, the alignment dictated by the strong anchoring is parallel for horizontal sides, while for vertical ones it is homeotropic. Where convenient, the angle parametrization of the director and the angle-conjugated generalized force (the torque) h will used:

$$\mathbf{n} = (\cos\varphi, \sin\varphi, 0), \tag{4.25}$$

$$\mathbf{h} = (0, 0, h) \times \mathbf{n}. \tag{4.26}$$

Throughout the Section 4.5, the following dimensionless quantities for length, time, velocity, and magnetic field will be used:

$$r \leftarrow r/L, \quad t \leftarrow t/\tau_L, \quad v \leftarrow v\tau_L/L, \quad H \leftarrow H/H_0, \tag{4.27}$$

where

$$\tau_L = \frac{\gamma_1 L^2}{K_{11}} = \frac{L^2}{\xi_m^2}\tau \tag{4.28}$$

is the characteristic relaxation time for the director field deformation on the scale of the container size L and

$$H_0 = \frac{1}{L}\sqrt{\frac{K_{11}}{\mu_0|\chi_a|}} \tag{4.29}$$

is the magnetic field with the coherence length of L.

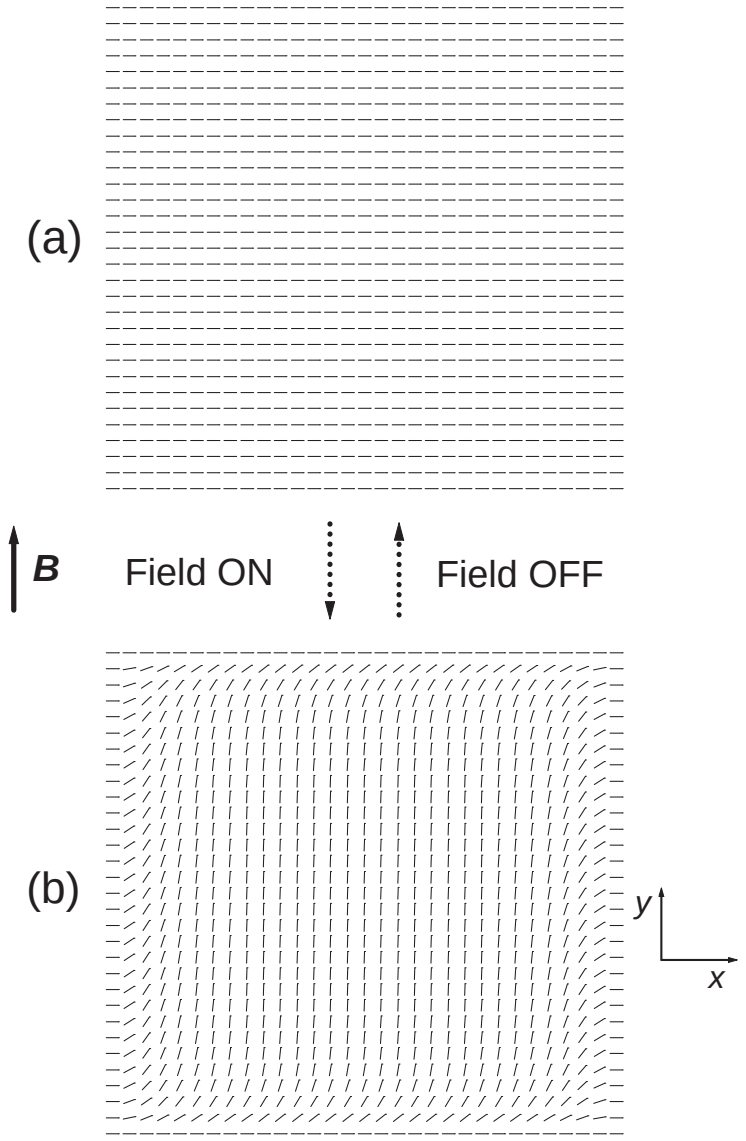

Figure 4.1 The calculations are performed in a square or rectangular geometry. Two types of relaxation are studied: (a) starting with a uniform director field, the magnetic field is switched on, or (b) the magnetic field is switched off to disorient a field-aligned sample. The director is fixed at the boundaries as shown.

4.5.1 Mechanisms governing the problem

Backflow generation

As indicated by calculations, the elastic stress tensor contribution (4.14) alters the velocity field by up to 10%. Thus, while it is of some importance when studying the flow fields, in first approximation it can be neglected when the influence of the backflow on the director field is in question, this influence itself also being small.

Our interpretation of the velocity fields will be based solely on the viscous coupling given by Eq. (4.11). What is more, it turns out that the anisotropy of the fluid viscosity, described by the α_1, α_5, and α_6 terms in (4.11) has no qualitative importance. The driving force of all the interesting flow phenomena observed is the anisotropy of the coupling to the director rotation given by the α_2 and α_3 terms in (4.11). Since $\alpha_2/\alpha_3 \approx 70$, only the α_2 term needs to be taken into account when trying to interpret the results. There are two contributions to the force exerted on the fluid described by this term, one depending on the gradient of director rotation, and the other on the director field gradient. Putting $\dot{\varphi} = \omega$ and $\varphi = 0$ one obtains

$$\mathbf{f}_1 = \alpha_2 \left(0 \, , \, \frac{\partial \omega}{\partial x} \right) \tag{4.30}$$

for the rotation gradient dependent force. Generally, this force is always perpendicular to the director, while its magnitude depends on the ω derivative along the director, $\mathbf{n} \cdot \nabla\omega$. The second contribution is best seen if we put $\nabla\varphi = (\varphi_x \, , \, 0)$:

$$\mathbf{f}_2 = -\alpha_2 \omega \varphi_x \left(\cos 2\varphi \, , \, \sin 2\varphi \right) . \tag{4.31}$$

Thus, the magnitude of this force depends only on $\omega|\nabla\varphi|$, whereas its direction is such that it makes twice the angle with $\nabla\varphi$ as the director. The reader should bear in mind that α_2 is negative and that the direction of the force just described depends on the sign of ω.

Influence of backflow on the director rotation

Let us discuss the torque on the director exerted by the flow. A flow field corresponding to a pure rotation ($\mathsf{W} \neq 0$, $\mathsf{A} = 0$) imposes the same rotation on the director, as Eq. (4.9) suggests putting $\mathbf{h}^{em}$ to zero. Conversely, pure extensional flow ($\mathsf{W} = 0$, $\mathsf{A} \neq 0$) aligns the director along the axis of extension. For shear flow, which is a sum of the flows just mentioned, Eq. (4.9) gives

$$\dot{\varphi} = -\frac{1}{2}\eta \left(\frac{\gamma_2}{\gamma_1} \cos 2\varphi + 1 \right) , \tag{4.32}$$

where φ measures the angle relative to the velocity direction and η is the shear rate (see Fig. 4.2 for the sign convention). Equation (4.32) has a stationary solution only if $|\gamma_2/\gamma_1| > 1$, i.e., if $\alpha_3 < 0$, which is the condition for the flow-aligning nematic, as opposed to the flow-tumbling nematic, where $\alpha_3 > 0$ (see the end of Section 4.5.2 for

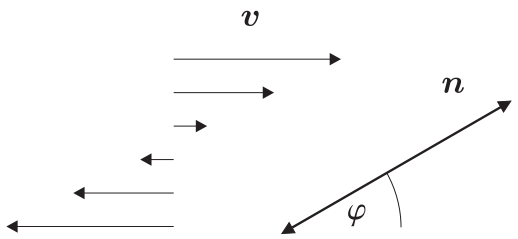

Figure 4.2 The director angle φ in Eq. (4.32), is measured relative to the shear as shown.

a short discussion on the backflow effect in flow-tumbling nematics). The stationary solution of (4.32) gives

$$|\varphi_0| \ll 1, \tag{4.33}$$

since $\gamma_2/\gamma_1 \approx -1$. The director is thus rotated towards the velocity direction. The solution with $\varphi_0 > 0$ is stable, whereas that with $\varphi_0 < 0$ is not. For MBBA the alignment angle is approximately $\varphi_0 \approx 7°$. Note that when out of equilibrium, the director is rotated anticlockwise only for $|\varphi| < |\varphi_0|$, whereas for any other orientation the stationary state is approached by a clockwise rotation (for the situation as depicted in Fig. 4.2).

4.5.2 Results and interpretation

Field-off relaxation

In this example the sample is initially aligned with a magnetic field. The field is then switched off instantaneously, and the system relaxes back to the undeformed configuration. In the square cell, the early stages of this relaxation show an anticlockwise central vortex, accompanied by two clockwise eddies at the bottom and top, whereas there are no eddies near the vertical boundaries (Fig. 4.3(a)). Equations (4.30) and (4.31) can explain this asymmetry, for both force contributions depend on the relative orientation of the director with respect to $\nabla\omega$ and $\nabla\varphi$, respectively, which is different for the horizontal as it is for the vertical boundaries. The size of the eddies is of the order of the magnetic coherence length. Their centers are located near the region in which director field curvature is a maximum ($\varphi = \pi/4$). In the course of time, the maximum curvature region moves to the middle of the cell, and so do the clockwise eddies (Fig. 4.3(b)). Finally, the central anticlockwise current is completely eliminated. Figure 4.4 shows the total deformation of the fluid due to the backflow after the relaxation process has stopped.

Let us now take a qualitative look at the forces near the boundaries, considering regions in the middle of the edges where lateral derivatives can be neglected to a first approximation. Only the components parallel to the boundaries are considered, since this must be the direction of the velocity there. One has to realize that the initial relaxation rate $|\omega|$ has a maximum at $\varphi = \pi/4$, since the magnetic force is the strongest there, implying a maximum elastic force to be balanced with. Note that ω is negative. For outermost parts of the sample, where $\varphi < \pi/4$, $|\omega|$ increases

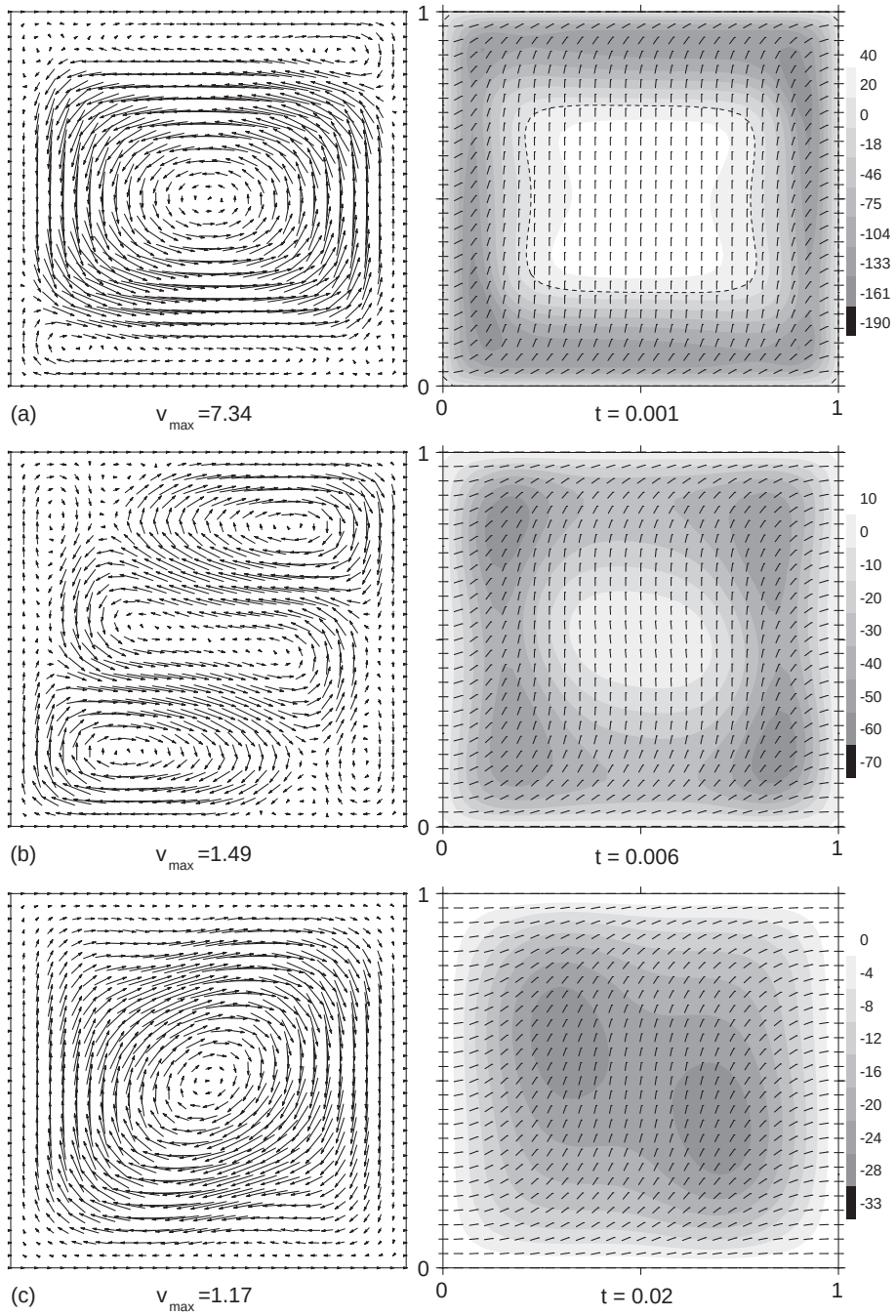

Figure 4.3 Field off in the square cell: subsequent snapshots of the velocity fields (left column), director fields and director angular velocity fields (represented by levels of gray) show a typical two-step relaxation. (a) In the beginning, three vortices are present, while the director in the middle rotates in the opposite sense; the line of the stationary director field is indicated by the dashed contour. (b) Clockwise vortices are becoming dominant, note the reverse director deformation at the center. (c) The clockwise vortices have joined to form a single vortex, the sense of rotation now being opposite to that at the beginning. The interior starts rotating in the right sense at a high rate (compare with the rotation in (a)).

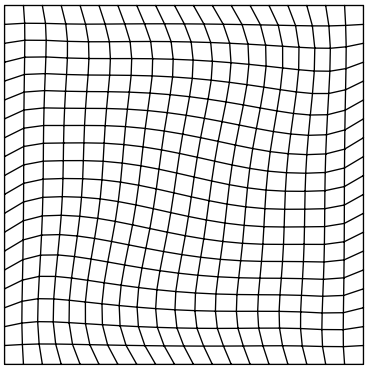

Figure 4.4 The total deformation of the fluid after the field-off relaxation in the square cell. In the field-on case, the deformation is similar (though not the same) but opposite.

on moving away from the boundary. Hence, Eq. (4.30) gives forces trying to start a clockwise current round the cell. However, the forces described by Eq. (4.31) oppose the first ones for the vertical boundaries, whereas those for the horizontal boundaries add constructively. This is one of the reasons for the missing eddies near the vertical boundaries. Moving further away from the boundaries, φ becomes essentially $\pi/2$ and there are no forces parallel to the boundaries given by Eq. (4.31). On the other hand, Eq. (4.30) does yield forces for the horizontal boundaries (and none for the vertical ones), starting an anticlockwise current.

Of course, the situation is too complicated for the square cell to be interpreted completely due to the fact that the corners play an important role, the problem there being fully two-dimensional. Therefore we aim to make a more exact analysis for one-dimensional cases, obtained by extending either the horizontal or the vertical boundaries to infinity. In this way we arrive at the systems studied by Pieranski, Brochard and Guyon [30,31] in the limit of weak deformations. Figure 4.5 (and Figure 4.10 in next section) representing a cell with a 5:1 side ratio, should serve as an illustration for the one-dimensional cases.

Calculations for $L_x \gg L_y$ clearly give three vortices (Fig. 4.5(a)), whereas those for $L_y \gg L_x$ result in a single vortex only (L_x and L_y are dimensions of the cell in x and y direction, respectively). Being able to explain this on the basis of Eqs. (4.30) and (4.31) would yield evidence for the nontrivial flow fields being a consequence of the α_2 term in (4.11). In the one elastic constant approximation (4.2),

$$h^{em} = \nabla^2\varphi + \frac{1}{2}H^2 \sin 2\varphi, \tag{4.34}$$

the initial director configuration for large enough fields is

$$\varphi = 2\arctan\left(e^{Hr}\right) - \frac{\pi}{2}, \tag{4.35}$$

where H is the magnetic field used to align the sample (always lying in the vertical direction), and r is the distance from the boundary. This solution is obtained

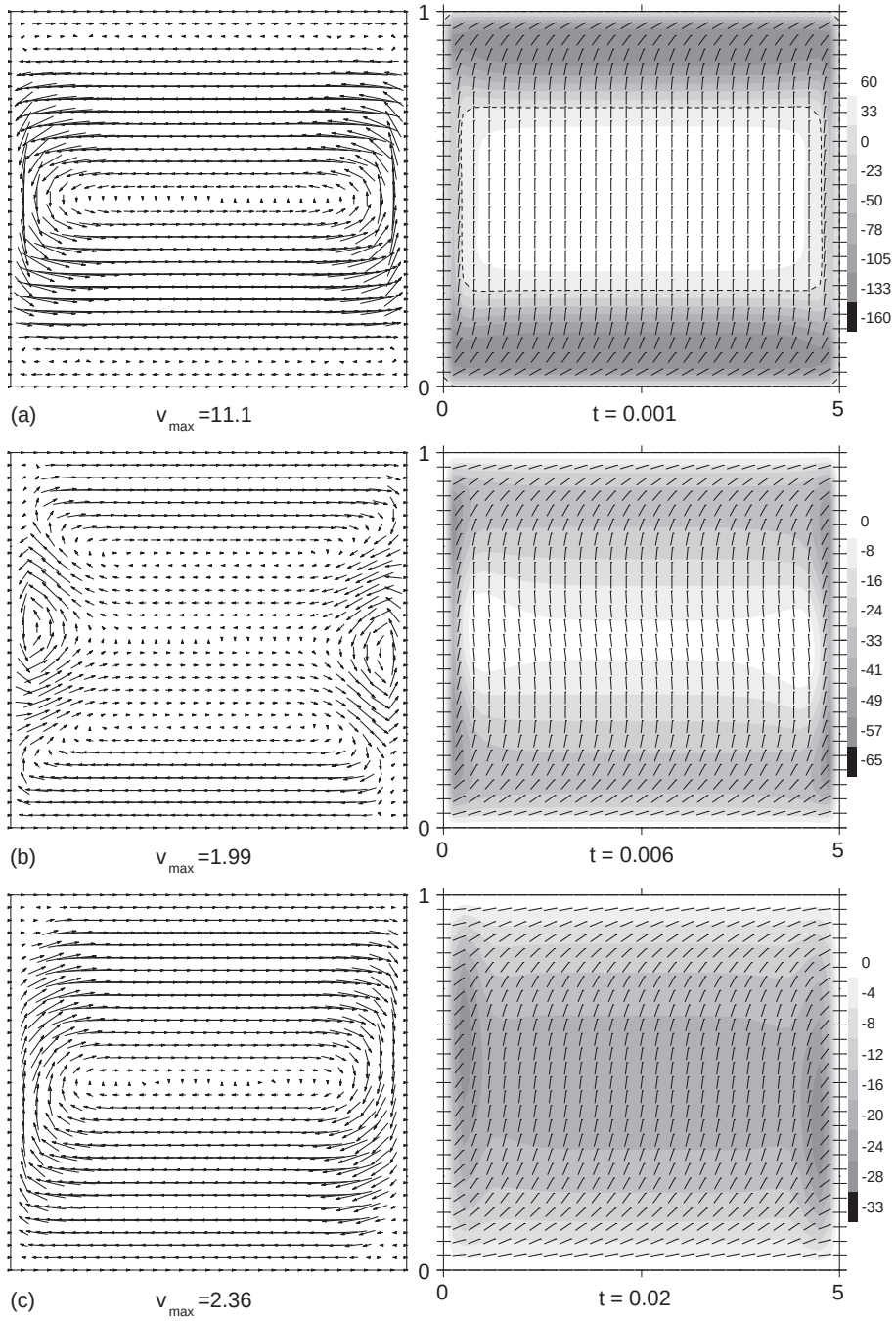

Figure 4.5 Field off in a horizontal cell with $L_x/L_y = 5$ (note the scale): two-step relaxation. See Fig. 4.3 for the key to the figures. (a) In the beginning three vortices are formed (Fig. 4.7), the director field undergoes a reverse rotation in the middle (note the zero rotation contour, shown dashed). (b) At the moment of flow reversal, note the deformation of the central director field. (c) A clockwise current results, while the director in the center is rotating in the right sense at maximum rate (compare with the rotation in (a)).

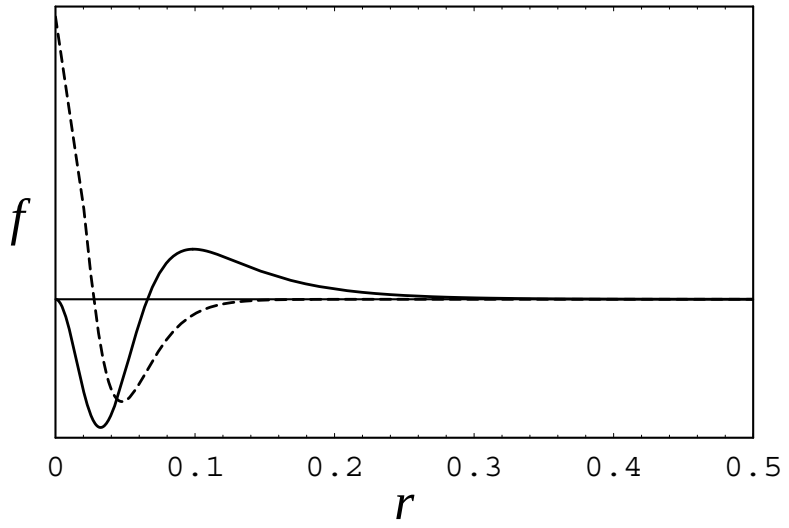

Figure 4.6 Total initial forces (sum of (4.30), (4.31)) for the horizontal and vertical (dashed) cell as functions of the distance from the boundary ($r = 0.5$ in the center).

by using the boundary condition $\varphi' = 0$ for $\varphi = \pi/2$, where the prime denotes differentiation with respect to r. The correct condition requires $\varphi' = 0$ for $r = 1/2$ (center of the cell), which, however, introduces elliptic integrals. Thus, solution (4.35) is valid if the field is large enough such that for $r = 1/2$ the director is well aligned ($\varphi \approx \pi/2$).

Putting $\omega = \varphi''$ and $\omega' = \varphi'''$, with φ given by the solution (4.35), one obtains the forces (4.30) and (4.31). The components parallel to the boundary are shown in Fig. 4.6. They behave as expected from the preceding discussion.

Now let us calculate approximate initial velocity profiles for both the horizontal and the vertical one-dimensional cell. In one dimension the pressure term and the elastic stress term in Eq. (4.21) can be dropped since they can only yield transversal forces. The remaining equation

$$\nabla \cdot \sigma^v = 0 \tag{4.36}$$

is solved easily when retaining only the α_2 and α_4 terms in σ^v (Eq. (4.11)). Together with Eq. (4.35) the solution reads

$$v(r) = -H^2 \frac{\alpha_2}{\alpha_4} \left[\left\{ \begin{array}{c} -3/2 \\ -1/2 \end{array} \right\} \cos\varphi \pm \frac{1}{6} \cos 3\varphi + C \ln\left(\cos^{-1}\varphi + \tan\varphi \right) + D \right],$$

with the constants

$$C = \frac{1}{\ln\left(\cos^{-1}\varphi_0 + \tan\varphi_0\right)} \left[\left\{ \begin{array}{c} 3/2 \\ 1/2 \end{array} \right\} \cos\varphi_0 \pm \frac{1}{6} \cos 3\varphi_0 - \left\{ \begin{array}{c} 4/3 \\ 2/3 \end{array} \right\} \right],$$

$$D = \left\{ \begin{array}{c} 4/3 \\ 2/3 \end{array} \right\},$$

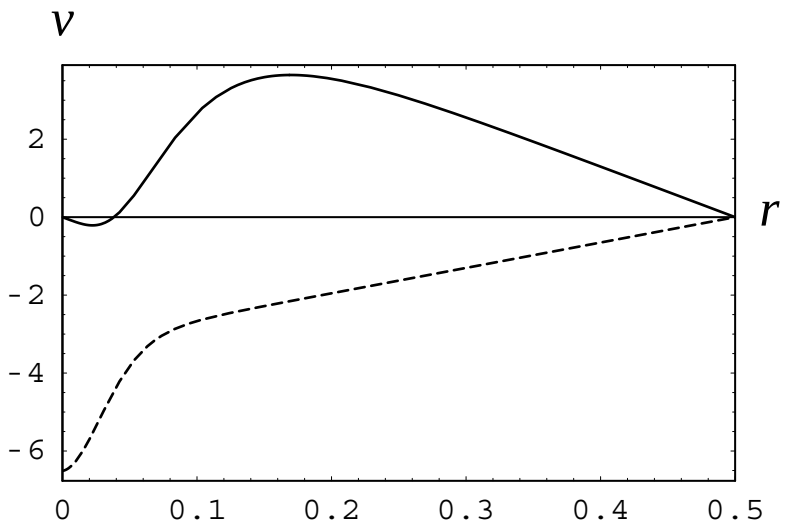

Figure 4.7 Initial velocity profile (Eq. (4.36)) for the horizontal and the vertical (dashed) cell ($H = 20$). In the horizontal case, two opposing currents are predicted. The width of the counter-current near the boundary is of the order of the magnetic coherence length. On the other hand, the vertical cell gives a single current only, although the net force changes sign near the boundary (Fig. 4.6). Both analytical predictions based on the simplified viscous stress tensor are consistent with numerical results.

where φ_0 represents the director angle in the middle of the cell. The upper expressions stand for the horizontal cell, the lower ones for the vertical cell. The solutions are plotted in Fig. 4.7, where the difference between the horizontal and vertical cases is clearly seen. It is worth pointing out again that, qualitatively, it is also possible to use these results for the regions close to the middle of the boundaries of the square cell, where the situation resembles the one-dimensional case (compare Figs. 4.3(a) and 4.5(a)).

So far, only the generation of the backflow has been studied. We now consider the inverse phenomenon of how the backflow influences the director rotation. In both one-dimensional cases we are confronted with pure shear flow, the effects of which are described by Eq. (4.32). The situation is now completely different for the horizontal and vertical cases. In the horizontal case, the shearing backflow slows down the director rotation in the middle of the cell (Fig. 4.5(a)), and is moreover actually able to reverse the direction of rotation due to weak elastic forces there (Figs. 4.5(b) and 4.8). This phenomenon is known as the *kickback* effect [55, p. 167]. Near the boundaries, however, the shear is opposite, thus accelerating the relaxation. As a result, the gradient of ω becomes larger, which induces an even stronger backflow (a positive feedback effect). One has to keep in mind that the backflow effect is only a perturbation to the relaxation which, in this case, is governed by elastic forces. Thus, when talking about the positive feedback, one must remember that this is only a small contribution to the director and flow fields, whereas global behavior is still set by the elasticity. Eventually, elastic forces become dominant even in the

middle of the cell (Fig. 4.8), reversing the rotation of the inner part and accelerating it, while slowing the rotation of the outer part. We are then left with the center reorienting faster than the edges (Figs. 4.5(c) and 4.8), a situation opposite to the initial one. As a result, the backflow also changes direction, transforming from the anticlockwise central current with two opposite eddies at the top and bottom to a single clockwise current. The latter is then stable; accelerating the relaxation in the middle of the cell it grows stronger initially (a positive feedback again), then slowly fades as the elastic forces vanish. This type of process where, in a region of the sample, the director is rotated backwards for some period of time and then the flow direction is suddenly reversed, will be referred to as a two-step relaxation. One can notice that in the square cell the relaxation path is quite similar. The kickback effect is observed (Fig. 4.3(a), (b)), as well as the reversal of the flow (Fig. 4.3(c)).

For the vertical case, however, in the middle of the cell the director is not rotated backwards by the backflow, but merely held in the field-aligned orientation. By contrast, near the boundaries the reorientation is accelerated by the backflow as for the horizontal case. As a result, the relaxation proceeds from the edges and then gradually bites to the center, much like the case of a simple relaxation without taking into account the backflow (Fig. 4.8, lower diagram). This conserves the direction of the current. One can call a process like this a one-step relaxation. Eventually, we end up with a reverse current in this case also, but this happens much later and when the sample has almost relaxed. Besides, the reversal of the current proceeds very slowly and steadily from the outside; it does not happen suddenly in the whole cell as in the horizontal case.

Field-on relaxation

Now we consider the case in which the initial director field is undeformed, and a vertical magnetic field is applied at a small angle (2°) off the normal to the director, which does not significantly alter the critical behavior of the transition [55, p. 105]. Due to the increasing rate of rotation ω toward the center, an anticlockwise current is predicted by Eq. (4.30), whereas the force (4.31) is initially unimportant, since the director is uniform. Calculations for the square cell show that in the course of time the current is split into two vortices, while in between these two clockwise vortices are also formed, and we finish with 4 major vortices (Fig. 4.9(b)).

Again it is useful if one first focuses on the one-dimensional cases. For the horizontal cell initially there is no current, because the director is perpendicular to the gradient of ω (Eq. 4.30). If the cell is not infinite, but just extended in the horizontal direction, the flow is limited to the short boundaries, where $\nabla\omega$ points along the director. For a long cell, however, this is unimportant. When the director turns a little, the force (4.30) becomes larger initiating the anticlockwise current. With the deformed director field the force (4.31) also starts contributing to the anticlockwise current. After the director has reached the angle of instability (4.33) in the center, the reorientation is accelerated by the current, resulting in a positive feedback strengthening the backflow. The positive feedback is greatly amplified by the magnetic torque, which in this case is the driving force of the relaxation.

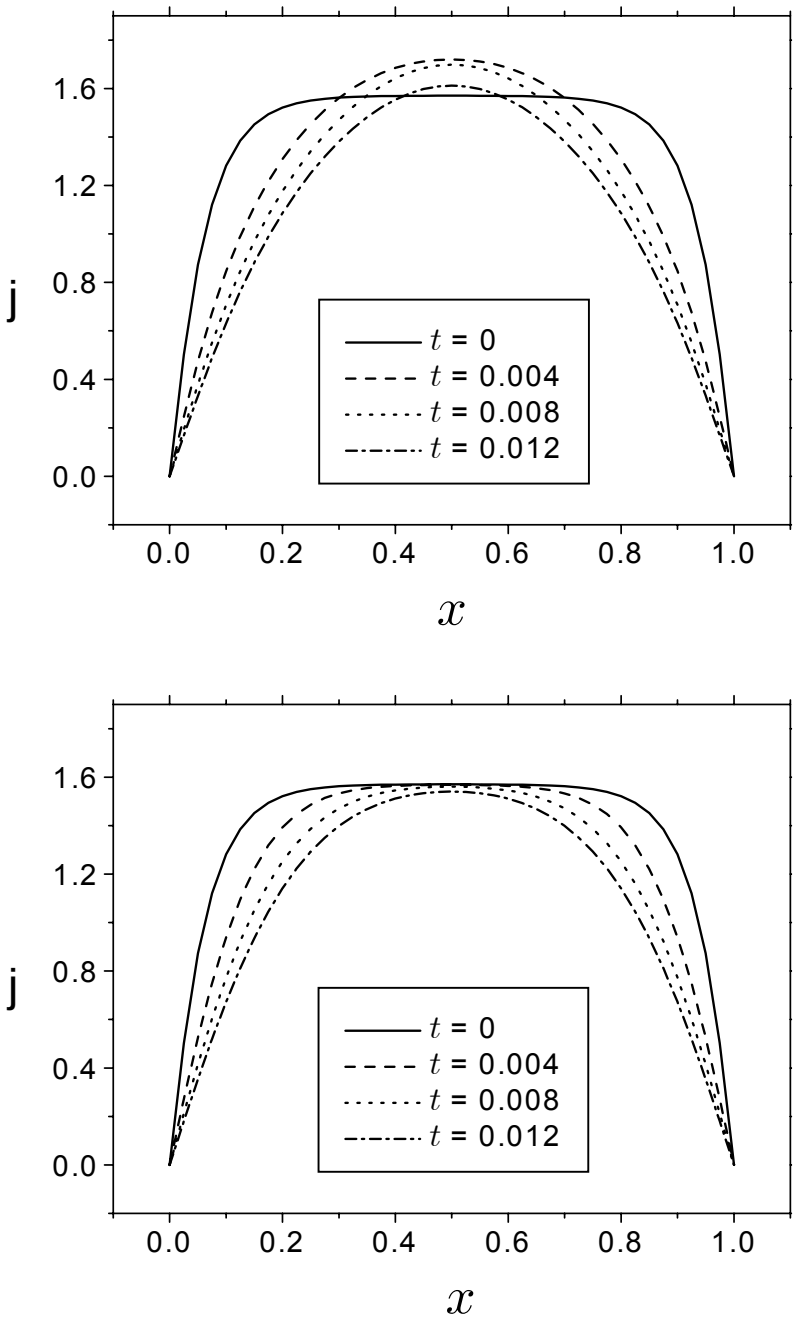

Figure 4.8 Vertical cross-sections through the center of the horizontal cell (field-off): director angle as a function of transverse coordinate is shown for subsequent moments in time (early stage only). The backflow alters the process in the center (above), compared with the simple relaxation without the flow (below).

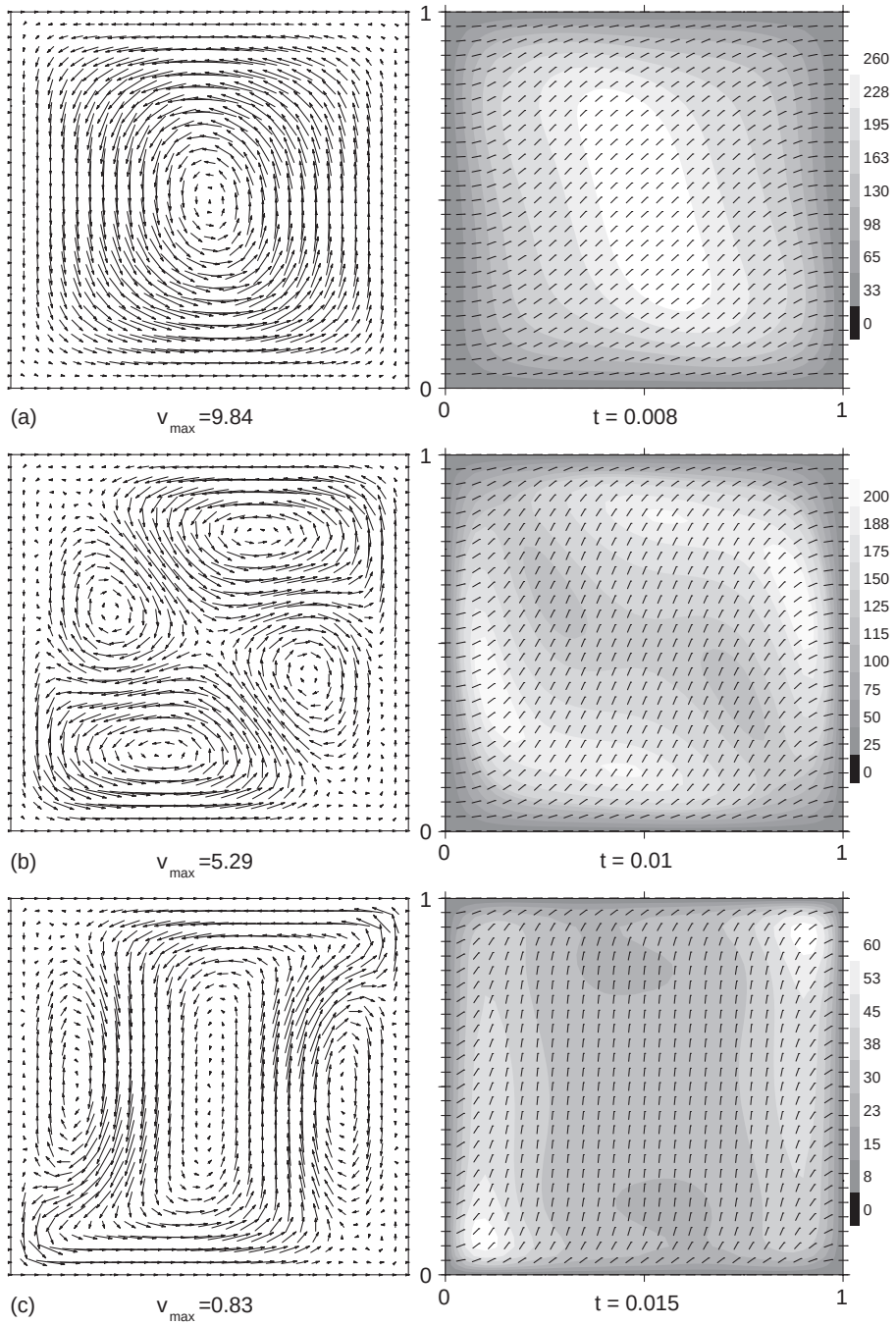

Figure 4.9 Field on in the square cell. See Fig. 4.3 for the key to the figures. (a) The director rotation is maximum in the middle; the asymmetry of the corners is due to the backflow, not to difference in the splay and bend elastic constants. (b) Now the center is relaxing slower, as are the NW and SE corners (which were faster in (a)). An interesting fourfold flow pattern is observed. (c) Late stages of relaxation; the current has not changed direction completely.

It acts like a fuse triggering the magnetic torque by rotating the director off the field normal (Eq. (4.34)). On the other hand, near the boundaries the relaxation is slowed by the shear there having opposite sign (the director tends to stay flow-aligned). Consequently, when eventually the relaxation ceases in the middle of the cell, the outer parts are still relaxing. Now the force (4.30) changes direction, trying to start a clockwise current. It is opposed by the $\nabla\varphi$- dependent force (4.31), which is strongest near the boundaries. As a result, the flow dies out in the middle of the cell first, followed by a cessation at the boundaries.

Again the situation is quite different for the vertical case (Fig. 4.10). However, unlike the field-off relaxation, now it will be the more interesting one. Here the anticlockwise flow due to the force (4.30) is initiated immediately, since now $\nabla\omega$ points along the director. Moreover, in the middle of the cell the shear starts to rotate the director at a maximum rate as a result of being normal to the director (Eq. (4.32)). On the other hand, near the boundaries the shear is opposite, thus turning the director in the reverse sense, again at a maximum rate (Fig. 4.10(a)). Here we are dealing with two effective mechanisms that turn on the magnetic torque, one in the middle of the cell generating an accelerated anticlockwise rotation, the other at the boundaries causing clockwise rotation, which is also amplified by the magnetic field. Hence, this gives rise to a strong anticlockwise current first (positive feedback again), as confirmed by Fig. 4.10(a). However, the force (4.31), becoming more important as the deformation increases, opposes the clockwise rotation. The flow is thus subject to a kind of frustration. As a result of this, it is able to change direction very rapidly, as the force (4.30) ceases. One can make an estimate of the director angle, at which the net force changes sign, using $\omega = \frac{1}{2}H^2 \sin 2\varphi$ with Eqs. (4.30) and (4.31), yielding

$$f = \frac{1}{2}\alpha_2 H^2 \left(2\cos^2 2\varphi + \cos 2\varphi - 1\right)\varphi'.$$

This gives $\varphi = 30^\circ$ for the angle of force reversal. Since the angle is maximum in the center of the sample, this is where the flow reversal is initiated. After some time, the interior has almost relaxed when the outer director field just begins to rotate in the right sense (Fig. 4.10(b)). The gradient of ω is reversed, the force (4.30) changes direction, now acting in accordance with the force (4.31). The clockwise current accelerates the relaxation of the outer part (positive feedback) while additionally slowing the rotation in the center (Fig. 4.10(c)). Interestingly, this current is larger than the initial anticlockwise current.

Thus, for the field-on relaxation, the interesting scenario also involves two steps: in the beginning a weak magnetic torque generates backflow due to non-uniform rotation. In some regions, the backflow accelerates the rotation which has a major effect because in this way the magnetic torque becomes progressively larger. Consequently, these regions are relaxed much more quickly than those for which the backflow has a retarding effect. As a result, they are already far above the angle of maximum magnetic torque when the delayed regions arrive at it. Now the latter regions relax faster, which causes the backflow also to change direction. The two-step scenario is fully developed in the vertical case, whereas the horizontal cell relaxes more or less in one step, as described previously.

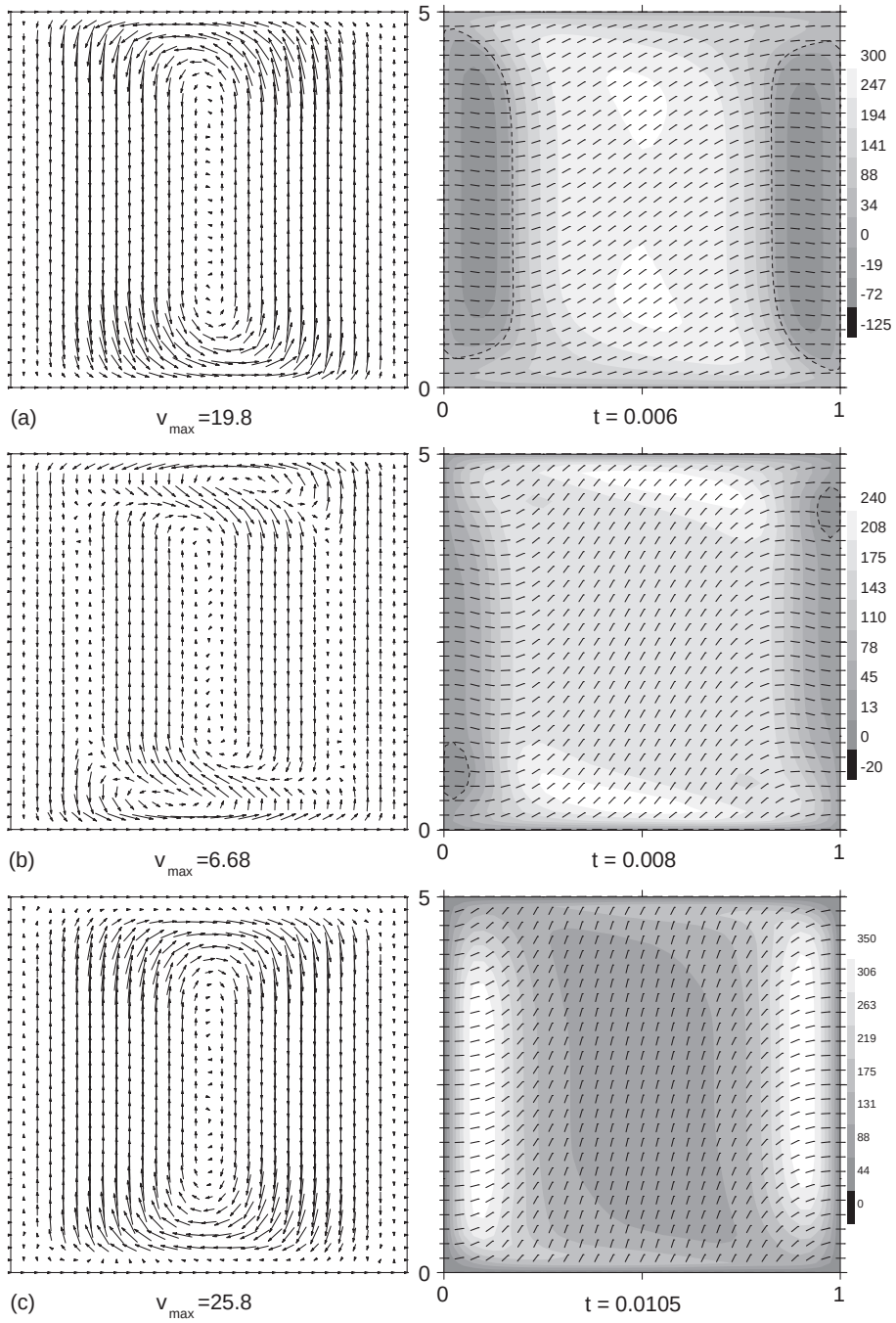

Figure 4.10 Field on in the vertical cell with $L_y/L_x = 5$ (note the scale): two-step relaxation. See Fig. 4.3 for the key to the figures. (a) Flow-induced backward rotation near vertical boundaries is amplified by the field (contour of zero rotation is shown dashed). (b) Backflow is changing direction, note the director deformation near the vertical boundaries. (c) The flow has changed direction, as well as the gradient of $\dot{\varphi}$. The situation is similar to that in (a), but reversed. Note that the velocities are large in magnitude.

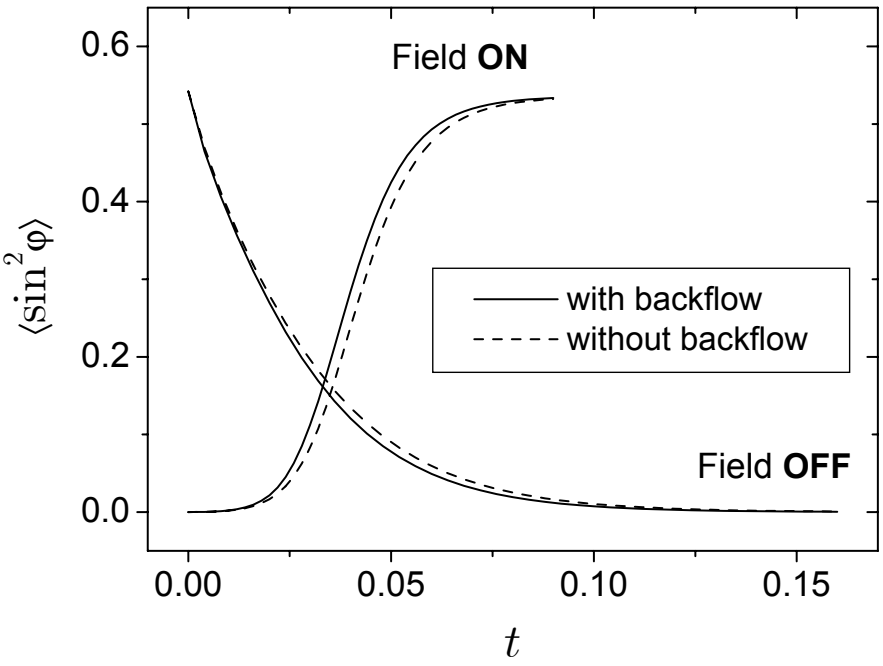

Figure 4.11 Time dependence of $\sin^2 \varphi$ (square cell), averaged over the cell, for cases with and without taking into account the backflow. Magnetic field of strength $H = 10$ is turned on and off.

The sudden formation of four vortices in the square cell can also be explained by this mechanism, only that now all four boundaries are important, resulting in a more complex fourfold flow pattern (Fig. 4.9(b)). Clearly the flow reversing mechanism is present in this case also, yet toward the end the original flow direction is restored. However, calculations for $L_y/L_x = 2$ already yield a definite flow reversion.

Finally, it should be mentioned that the processes just studied do not depend critically on the sign of the Leslie coefficient α_3, which sets the flow-aligning or flow-tumbling properties of the nematic, subject to the simple shear flow. If α_3 is set to zero or even its sign is reversed (keeping its value small), no radical changes are observed. For our discussion to be valid, only the condition $|\alpha_3/\alpha_2| \ll 1$ must be satisfied.

4.5.3 Comparison with the simplified treatment

The relaxation with the backflow is to be compared now with the simplified relaxation without taking into account the backflow. Figure 4.11 shows the time dependence of $\sin^2 \varphi$, averaged over the square cell, for both the full and simple treatments. Here the effect of the backflow is mainly to speed-up the relaxation process, a situation that is most frequently observed. In some cases, however, the influence of the backflow is more complicated and one cannot speak simply about changes of the relaxation rate. This occurs in the vertical cell if a strong enough field is applied so that the two-step process becomes very distinct (Fig. 4.12). At a lower

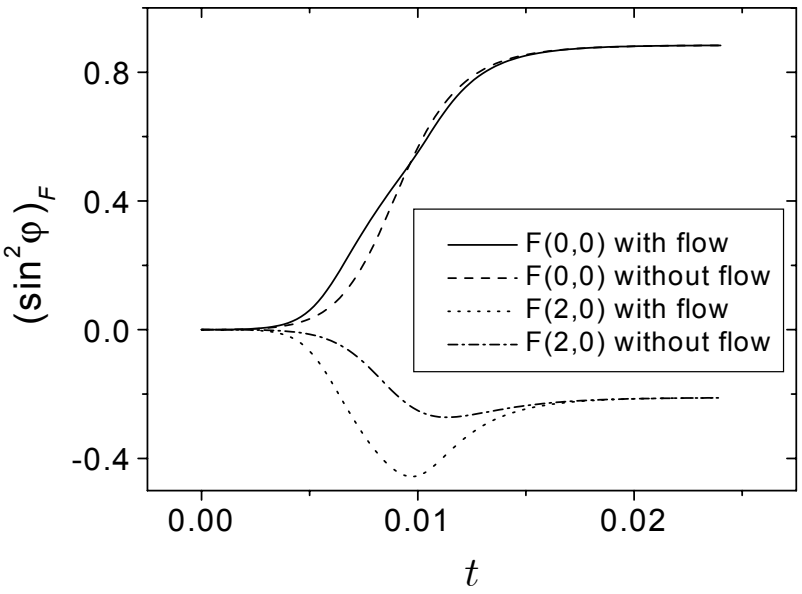

Figure 4.12 Time dependence of the largest cosine Fourier components of $\sin^2\varphi$, for the full and simplified treatments (vertical cell, magnetic field of strength $H = 20$ is turned on). The average is denoted by $\mathsf{F}(0,0)$, whereas $\mathsf{F}(2,0)$ stands for the component belonging to $\cos(2\pi x/L_x)$. It is shown that the average behavior can be more complicated than normal (compare Figs. 4.11, 4.13, or 4.14). Note that the difference is much larger for the $\mathsf{F}(2,0)$ components than for the averages, indicating that due to the backflow the rotation is indeed faster in the middle of the cell and slower near the boundaries (see also Fig. 4.10).

field strength, on the other hand, the simple regime is again restored (Fig. 4.13).

The importance of the geometry is clearly seen if one compares Figures 4.12 and 4.14, showing the time dependence of the Fourier components of $\sin^2\varphi$ in the vertical and horizontal cells, respectively. The fields are rescaled relative to the critical field

$$H_c^2 = \frac{K_{33}}{K_{11}}\,(\pi/L_x)^2 + (\pi/L_y)^2\,, \tag{4.37}$$

so that the ratio H/H_c is the same in both cases, allowing one to make a direct comparison. Evidently, when turning on the field, the backflow effect is much stronger in the vertical cell (two-step process) than in the horizontal cell (single-step process). As far as the field-off relaxation is concerned, the same conclusion holds. There the effect is stronger in the horizontal geometry, which in this case yields the two-step scenario.

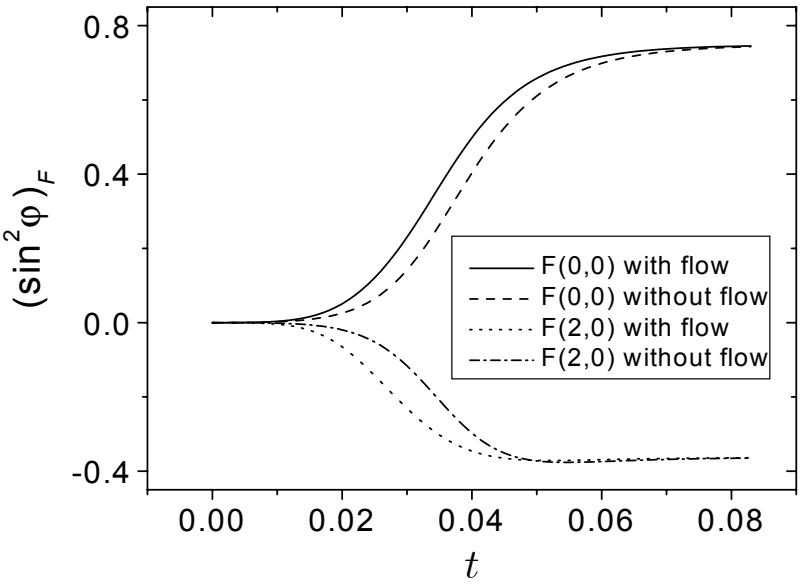

Figure 4.13 Time dependence of the cosine Fourier components of $\sin^2\varphi$, defined in Fig. 4.12, for the full and simplified treatments (vertical cell, magnetic field of strength $H = 10$ is turned on). Note that due to the weaker field the average behavior is less complex, when compared with Fig. 4.12.

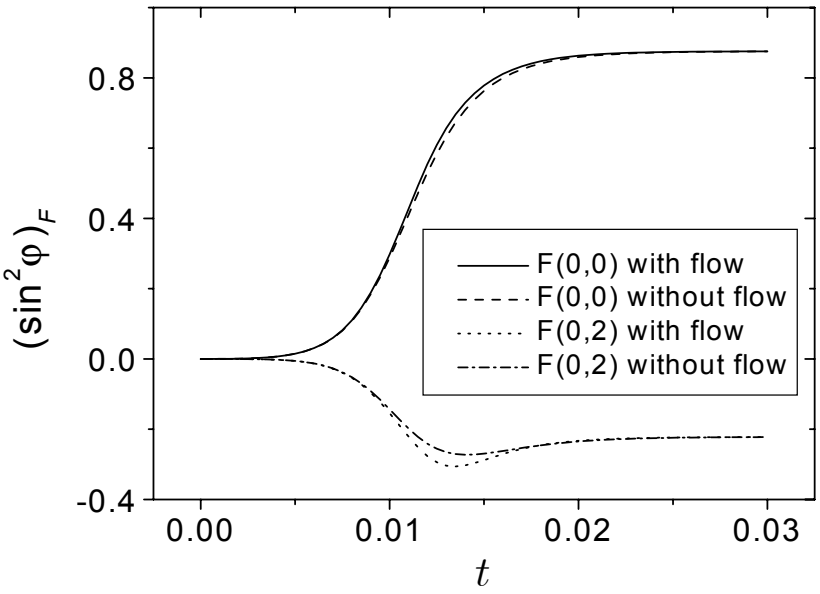

Figure 4.14 Time dependence of the cosine Fourier components of $\sin^2\varphi$, defined in Fig. 4.12, for the full and simplified treatments (horizontal cell, magnetic field of strength $H = 20$ is turned on). The figure should serve as a contrast to Fig. 4.12, showing that the backflow effect is less pronounced in the horizontal cell.

4.6 Amplifying the kickback effect

4.6.1 2D problem

If one takes the field-aligned configuration (the initial configuration in Fig. 4.3) and applies a secondary magnetic field in the x direction immediately after the y field has been turned of, the kickback produced by the backflow is amplified by the secondary magnetic field. A domain of opposite director rotation is formed, Fig. 4.15, separated from the rest of the sample by a domain wall with thickness of the order of the magnetic coherence length ξ_m, Eq. (4.15). The strengths of the primary and secondary magnetic fields are 20 and 40 units (4.29), respectively. Once the domain is formed it begins to shrink, which is a slow process compared with the formation and is driven by the domain wall curvature. The final configuration is undeformed, just like in the field-off case depicted in Fig. 4.3.

Let us estimate the shrinking time of the domain. Neglecting the flow and the elastic anisotropy, the shrinking rate of a thin circular domain wall with radius R is [56, p. 213]

$$\frac{dR}{dt} = -\frac{1}{R}, \tag{4.38}$$

where length and time are scaled by L and τ_L (Eq. 4.28), respectively, yielding

$$R^2(0) - R^2(t) = 2t. \tag{4.39}$$

Note that the shrinking rate does not depend on the magnetic field. Assuming $R(0) \approx 1/4$, the shrinking time is estimated to $t \approx 1/32$, which is supported by Fig. 4.16.

The presence of the domain wall is reflected in any integral property of the cell $A(t)$, e.g., in the cell average $\langle \sin^2 \varphi \rangle$, Fig. 4.16. In the case of a linear dependence of A on the wall length (the above average is such a case), one can write

$$A(t) = A(0) + C\left[R(t) - R(0)\right], \tag{4.40}$$

where C is a constant. Then it follows from Eq. (4.39) that

$$t = C_1\left[A(t) - A(0)\right]^2 + C_2\left[A(t) - A(0)\right]. \tag{4.41}$$

The constants C_1 and C_2 are determined by fitting the polynomial (4.41) to the slowly falling region in Fig. 4.16. The numeric data and the fit are ploted in Fig. 4.17 showing excellent agreement.

4.6.2 Quasi-3D problem

Let us now consider a more general example, which is closer to experimental set-ups than the 2D problem. By contrast, the director and the flow velocity can point out of the plane this time, while there is still no dependence on the z coordinate. Two switching examples have been chosen. The nematic sample is confined to an

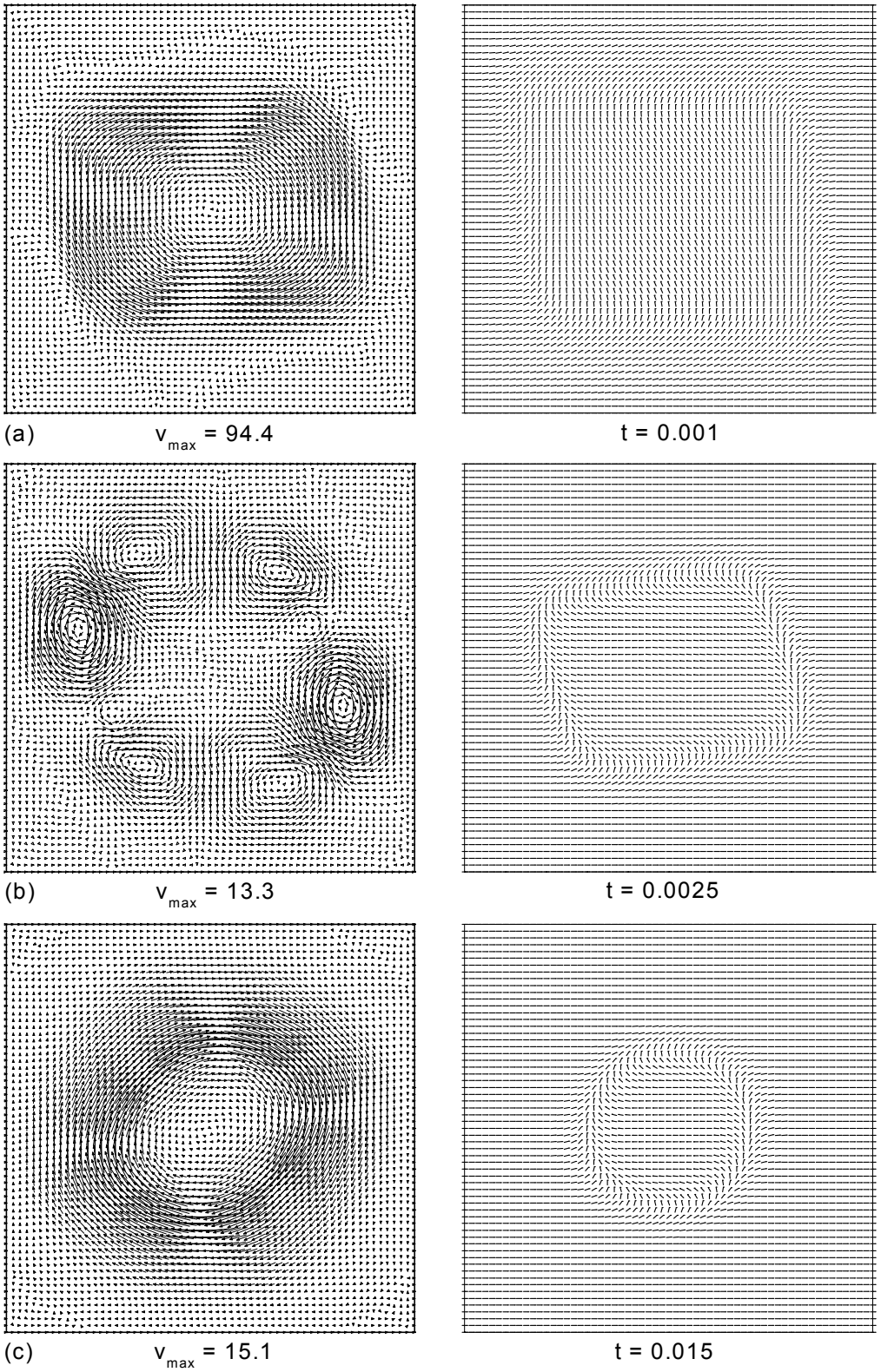

Figure 4.15 Amplification of the kickback: flow (left column) and director fields in selected moments of time. (a) The kickback caused by the anticlockwise flow gets amplified by the horizontal magnetic field. (b) The domain has formed, the flow changes direction. (c) Shrinkage of the domain, now the flow is clockwise.

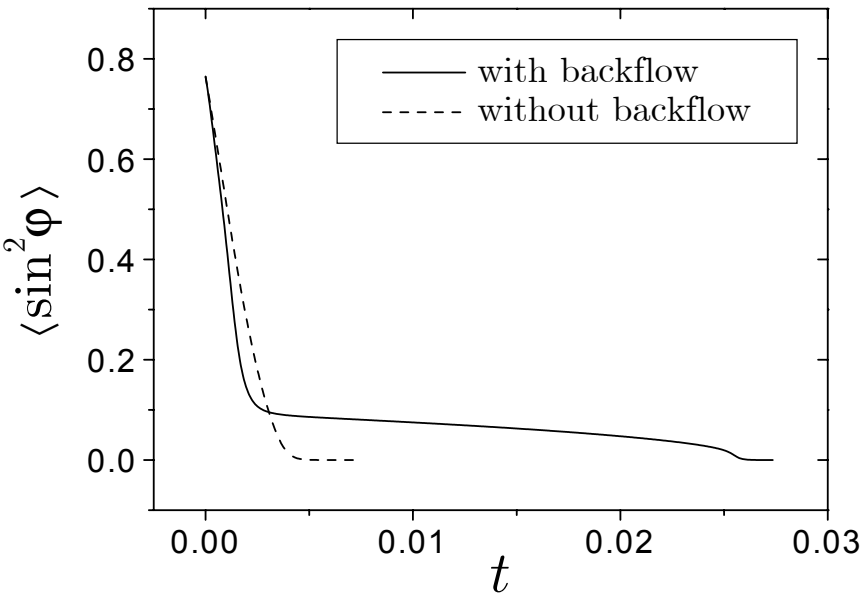

Figure 4.16 Comparison of switching processes with and without the flow: time dependence of the y director component squared, $\sin^2 \varphi$, averaged over the cell. The backflow-affected switching proceeds in three steps. First almost the whole sample aligns with the x field, except for the domain wall. The characteristic time of this process is $\xi_m^2 = 1/H^2 = 1/900$. Then the central domain is slowly shrinking, driven by the domain wall curvature. In the end, when the size of the domain is comparable to its thickness, the characteristic time of the relaxation is again ξ_m^2. Time is scaled by τ_L, Eq. (4.28).

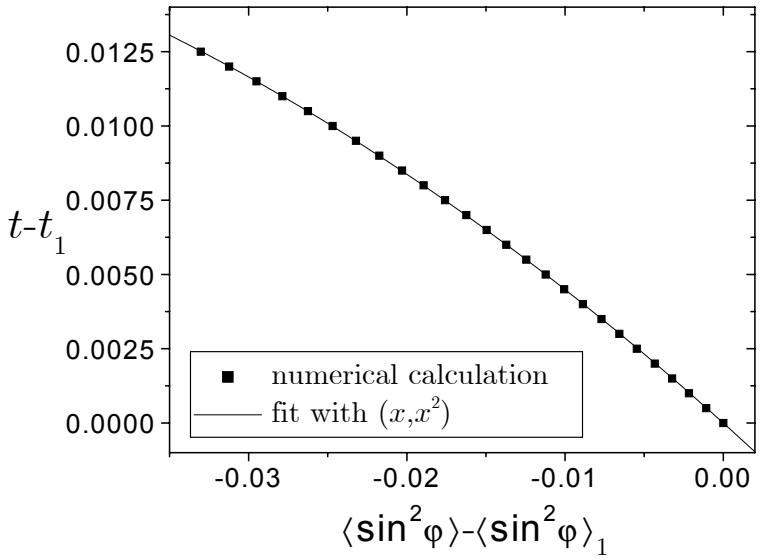

Figure 4.17 The fit of the polynomial (4.41) to the numeric data for $\langle \sin^2 \varphi \rangle$ in the time interval between $t_1 = 0.0075$ and $t_2 = 0.02$, when the domain wall is well defined.

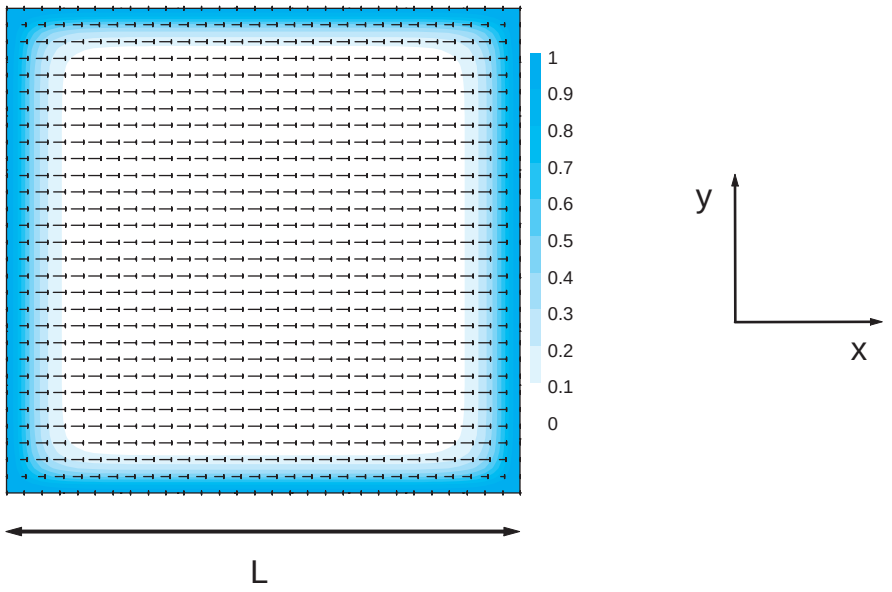

Figure 4.18 The initial director field configuration. Shading (although redundant in the case of the director field) represents the out-of-plane (z) component, while the in-plane components are drawn as nails as customary. Magnetic field with coherence length of $L/30$ is applied in the x direction.

infinitely long capillary of square cross section. The domain of calculation corresponds to the cross-section (a square in the xy plane) and is thus two-dimensional. The anchoring is infinitely strong, its direction is parallel to the tube axis (z axis). Initial conditions are identical in both cases: the sample is aligned by an in-plane magnetic field with the coherence length (4.15) of 1/30 of the tube thickness L, pointing along the x axis (Fig. 4.18). Following the discussion in Section 4.3, for a 100 μm thick capillary the corresponding field is around 0.3 T, and the characteristic time (4.16) is about 0.2 s.

The switching process is started by suddenly rotating the magnetic field to a perpendicular direction. The switching time of the field must be short compared with the characteristic time (4.16). In the first example, the final field is parallel to the z axis, whereas in the second example, it lies in the yz plane at an angle 70° with respect to the z axis. It will be shown that, due to the backflow, the switching process is again altered completely.

4.6.3 Axial magnetic field

After the magnetic field has been switched to the z direction, near the boundary the director is rotated out of the plane by elastic and field torques. On the other hand, the elastic and field torques are almost zero in the center. If one disregards the backflow, the director will align with the new field by a clockwise rotation about the y axis, proceeding from the boundary toward the center.

The backflow, however, can produce a large effect in this case, since the director

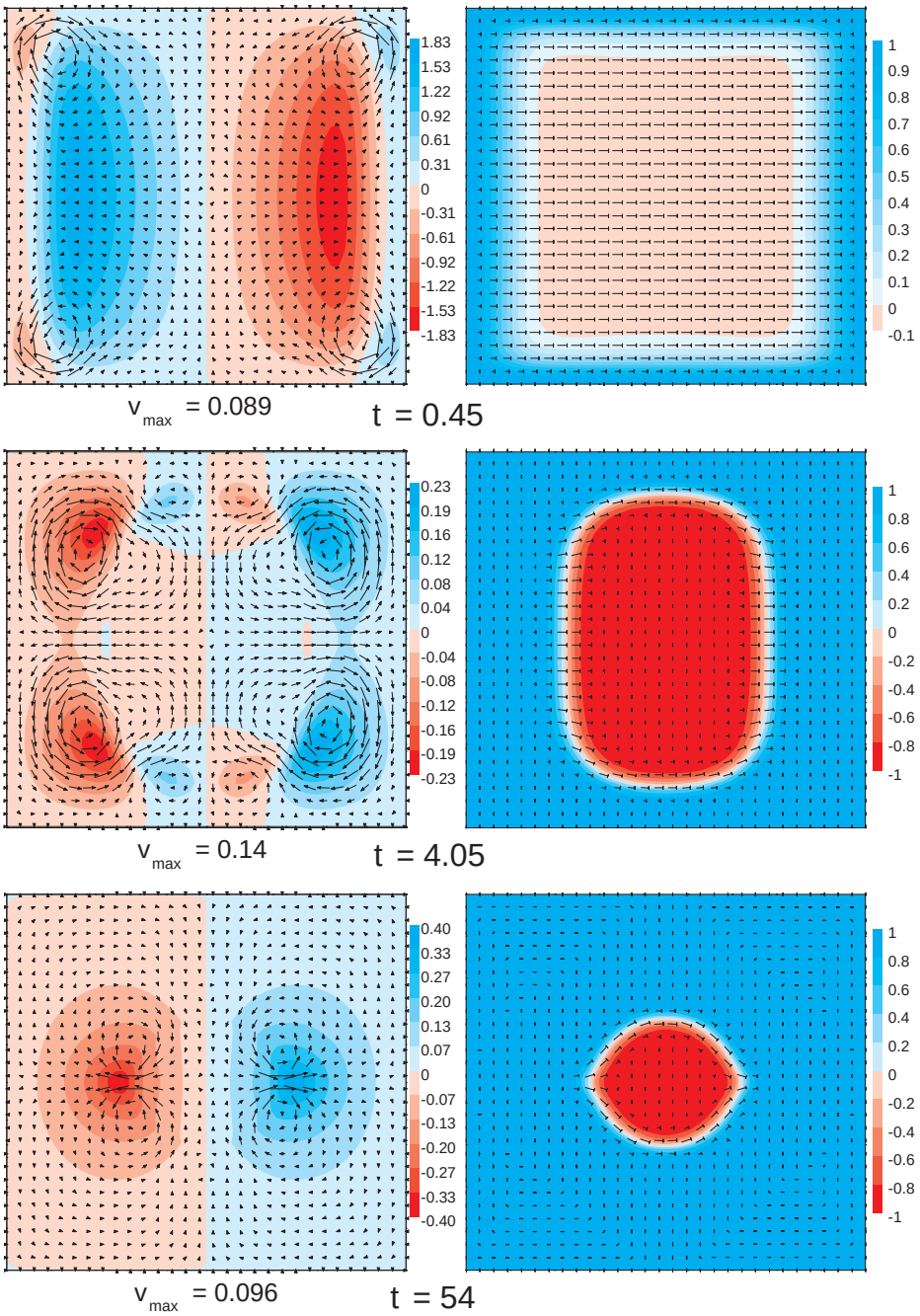

Figure 4.19 Axial magnetic field: velocity (left column) and director fields in selected moments of time (in units of τ as defined in Eq. (4.16)). The number of mesh points displayed has been reduced by a factor of two in each direction to gain clarity. The key to the figures is given with Fig. 4.18. Blue and red levels represent components up and down, respectively. The maximum in-plane velocity is denoted v_{max}. The velocity unit is v_0 as defined in (4.19). The reader should not confuse the heads of nails with the nails themselves, where the directors point almost in the z direction. (a) The kickback caused by the out-of-plane flow. (b) The kickback is amplified by the magnetic field, a domain is formed. (c) As the domain shrinks, a major part of the domain wall becomes a twist wall due to the elastic anisotropy: K_{11} and K_{33} are about twice as large as K_{22}.

orientation in the central region is labile with respect to the field, and thus quite sensible to perturbations. The rate of director rotation has two minima — at the boundary and in the center, and a maximum in between. As a result, an out-of-plane fluid flow is generated (Fig. 4.19, (a)), where the velocity changes sign three-times as we move along x direction, whereas on passing along y it is single-signed. The mechanisms governing this phenomenon are explained in Section 4.5.1. The flow rotates the director in the center in the opposite direction than expected (the kickback effect). This rotation is amplified by the magnetic field. Thus, we are left with the center rotating in the opposite direction as the outer part of the sample, which leads to the formation of a domain (Fig. 4.19, (b)). The shrinking time $t = R^2(0)/2$ (Eq. (4.39)), where $R(0) \approx L/3\xi_m = 10$ is the initial radius of the domain, is estimated to $t \approx 50$ in units of τ, Eq. (4.16). On the other hand, the characteristic time for the formation of the domain is just τ.

4.6.4 Oblique magnetic field

In order to show that the effect is not limited only to a certain direction of the final magnetic field, a second example is to be demonstrated. The initial configuration is the same as in the previous case (Fig. 4.18), but now the final field is in the yz plane at an angle 70° with respect to the z axis. It is important that the initial and final fields are still perpendicular to each other, or close enough to this, i.e., a few degrees. If not so, the field torque outweighs the backflow-generated one even in the beginning, and the backflow can give only quantitative effects. The situation is similar as in the previous example, only that now the flow is both out-of-plane and in-plane and the domain wall is more complex (Fig. 4.20).

It is worth mentioning that, if the final field is too close to the cross-section plane (a few degrees), even in the absence of the flow the director rotation is complicated by the elastic anisotropy. Namely, due to the anisotropy, the director deviates slightly from the x direction initially, which causes the director to rotate in opposite directions in different parts of the sample. Despite the backflow is important in this case also, we do not aim to give examples, since they are too complicated and thus not particularly instructive.

4.7 Summary

In this Chapter, nematodynamic problems have been studied in their full form, making no approximation other than a low Reynolds number, which is practically exact for the problems concerned. First, one must note the remarkable non-triviality of the generated velocity fields, i.e., the formation of several vortices, despite the simple geometry and strictly laminar flow. It is a consequence of the delicate interconnection between the director and the flow field. In addition, it has been shown that the form of the backflow, as well as its time evolution, depend very much on the geometry of the system, as does the influence of the backflow on the director reorientation. It is stronger for the two-step processes, which are characterized by

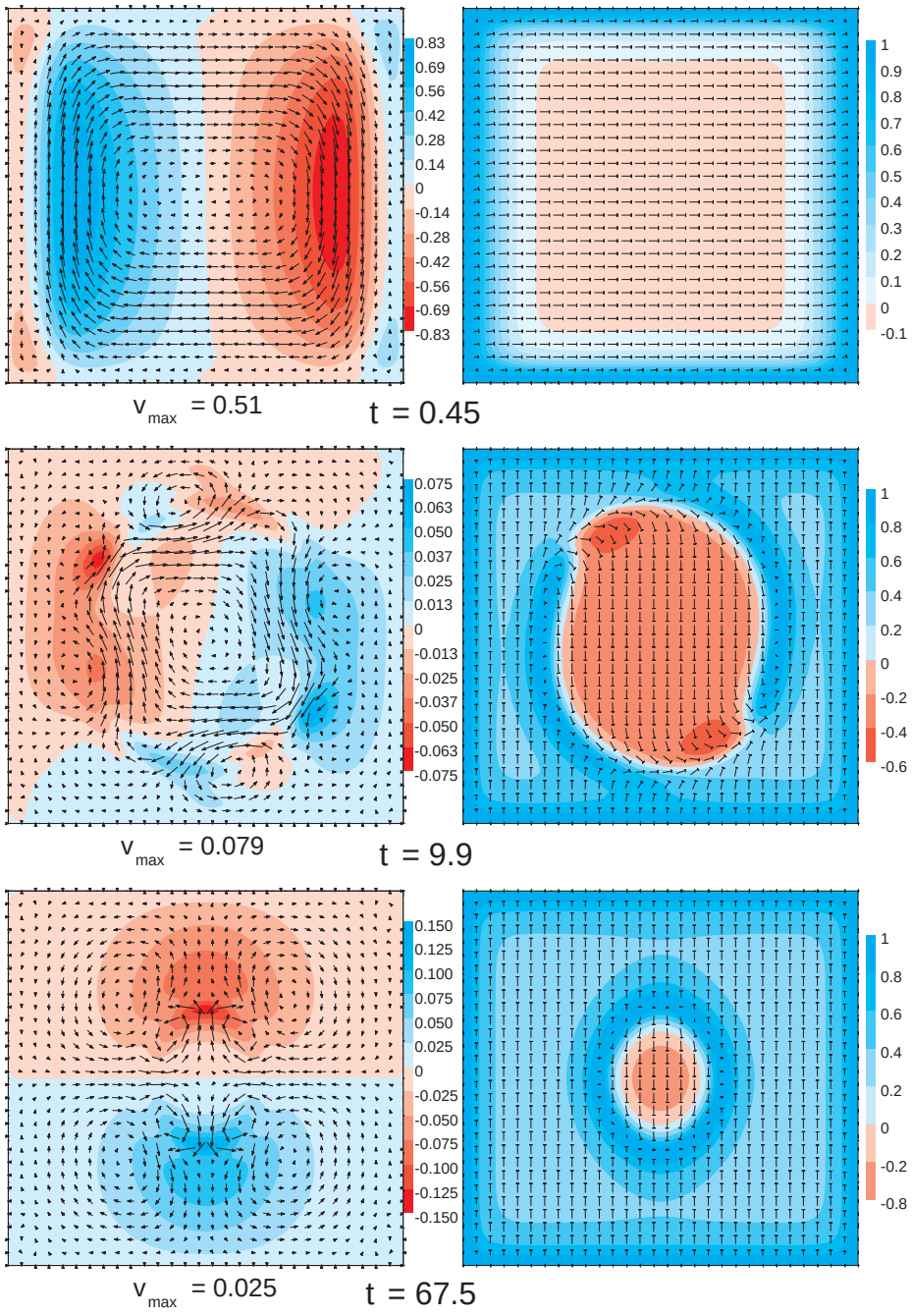

Figure 4.20 Oblique magnetic field: velocity (left column) and director fields in selected moments of time. The number of mesh points displayed has been reduced by a factor of two in each direction to gain clarity. The key to the figures is given with Figs. 4.18 and 4.19. (a) Both the out-of-plane and in-plane flow velocities are comparable in magnitude, resulting in the kickback around an oblique axis. (b) A part of the splay-bend domain wall first created (not shown) is transformed to a twist wall due to the elastic anisotropy, resulting in a complex wall structure. (c) As the domain shrinks, the structure of the wall becomes simpler.

a global reversal of the flow direction.

Besides numerical solutions, the qualitative picture of the backflow problem is also highlighted in this Chapter. Thus, following the discussion in Section 4.5.2, one is able to foresee the global flow dynamics in the cell, without having to perform any extensive numerical calculations. In particular, it is worth pointing out again that the backflow scenario depends crucially on the relative orientation of the magnetic field with respect to the long axis of the cell. It has been assumed that $|\alpha_3/\alpha_2| \ll 1$ holds for the two Leslie coefficients, whereas the sign of α_3 has proved not to be significant.

It has been shown that there are cases where the backflow effect is crucial. If in a part of the sample the director is near an unstable equilibrium with respect to the field, the backflow usually produces a perturbation strong enough to change the director rotation in that part. Of course, only those cases are interesting, where the backflow has a frustrating influence on the director field, i.e., it creates regions of opposite director rotation. Such relaxation processes have been referred to as the two-step processes, as opposed to the one-step processes, where backflow is less important.

Infinitely strong anchoring has been assumed throughout the Chapter 4. In order to observe any relevant backflow effects in practice, the anchoring should be strong enough ($\xi/\xi_m \ll 1$), which can be readily achieved in experiments. Numerical evidence for the ceasing backflow effect in the case of finite anchoring has been given toward the end of [57]. Disregarding any surface viscosity effects, one can make a simple estimate for the case when the anchoring becomes finite, $\xi > 0$, but remains strong, $\xi/\xi_m \ll 1$. Comparing the director profiles near the boundary for the infinite and the finite anchoring in the presence of the magnetic field, one finds the director gradient to decrease as $\xi_m/(\xi_m + \xi) \approx 1 - \xi/\xi_m$. Upon removal of the field (or, in the 3D examples, rotating the field into a perpendicular direction), the director is rotated by elastic forces (Eq. (4.9)), decreasing as $\xi_m^2/(\xi_m+\xi)^2 \approx 1-2\xi/\xi_m$. It then follows that the divergence of the α_2 and α_3 terms in Eq. (4.11), which represents the source driving the flow in Eq. (4.10), decreases as $1 - 3\xi/\xi_m$ as the anchoring gets weaker. Hence, the magnitude of the backflow and its torque exerted on the director (Eq. (4.9)) decrease the same way.

As indicated by additional calculations not presented, the qualitative picture does not depend on the exact geometry of the tube cross section, i.e., the square could be replaced by a circle or a rectangle, etc., provided that the aspect ratio stays roughly the same. Also, the detailed structure of the domain wall appears to depend on the ratio of the elastic constants, as mentioned in captions to the Figures 4.19 and 4.20.

The reorientation problems described in this Chapter may be regarded as an overture to the primary challenge — the influence of hydrodynamic flow on defect dynamics. From the early days of our research we have speculated that these are the processes where the flow should really come into play. Richer in experience and, in particular, equipped with the numerical method, we are now ready to meet the challenge. Of course, there is still a crucial step that yet has to be done — we must go beyond the director description. There are two paths leading from here and

we will take both, one after another. For nematic defects, one has no choice other than resorting to the dynamic theory of the tensor order parameter. On the other hand, defects in a vector order parameter field like that of the smectic-C phase are mastered by a direct generalization of the Ericksen-Leslie theory.

5

Dynamics of a vector order parameter

In this Chapter, the dynamic theory for a general vector order parameter will be derived. It represents a generalization of the standard Ericksen-Leslie theory to include the nonhydrodynamic degree of freedom — the magnitude of the vector. One should stress that the Ericksen-Leslie theory is a vectorial theory, and therefore a consistent generalization is the one to the full vector order parameter, not to the tensor. Moreover, the Ericksen-Leslie theory is not at all connected with the tensor order parameter, except for the missing polar effects (e.g., electric polarization) — the elastic free energy and the coupling to the flow are of the vectorial nature. As we have not come across this statement in the literature, we decided to support it in this Chapter. The general three-dimensional case will be considered. Although vectorial quantities like the electric polarization appear in this case, we will omit the electric and magnetic degrees of freedom and limit the discussion to the elastic distortions and flow coupling only. A two-dimensional version of the theory will be used in Chapter 8 for the description of the SmC thin film system.

5.1 Free-energy density

We will focus on the homogeneous and elastic parts of the free-energy density $f(\mathbf{c}, \nabla\mathbf{c})$, where $\mathbf{c}$ is the vector order parameter:

$$f = \frac{1}{2}A\,c^2 + \frac{1}{4}C\,c^4 + \frac{1}{2}L_{ijkl}\,(\partial_i c_j)(\partial_k c_l). \tag{5.1}$$

The homogeneous terms (the first two terms) describe the phase transition, $A = A'(T - T^0)$, $A' > 0$, $C > 0$, and give the equilibrium modulus of $\mathbf{c}$, $c_0 = \sqrt{-A/C}$, which is the condensed quantity. In principle, the elastic part could contain also second derivative terms $L_{ijk}\,\partial_i\partial_j c_k$, but these yield, besides the terms already contained in (5.1), only surface contributions [50, p. 77]).

The demanding task is to find the elastic coefficients L_{ijkl} that are allowed by symmetry. One requires that f is invariant to the inversion ($\mathbf{r} \to -\mathbf{r}$, $\mathbf{c} \to -\mathbf{c}$), which implies that L_{ijkl} must be invariant as well. Furthermore, the permutation symmetry (2.10), $L_{ijkl} = L_{klij}$, must be obeyed. It turns out that the set of scalar

L_{ijkl}	elastic term	comment
$\delta_{ik}\delta_{jl}$	$L_1(\partial_i c_j)^2$	isotropic
$\delta_{ij}\delta_{kl}$	$L_2(\partial_i c_i)^2$	splay
$\delta_{il}\delta_{jk}$	$2L_3(\partial_i c_j)(\partial_j c_i)$	$\partial_i(c_j\partial_j c_i - c_i\partial_j c_j) + (\partial_i c_i)^2$, surface
$c_i c_k \delta_{jl}$	$L_4\, c_i c_k(\partial_i c_j)(\partial_k c_j)$	$[\mathbf{c}\cdot(\nabla\mathbf{c})]^2$, derivative parallel to $\mathbf{c}$
$c_j c_l \delta_{ik}$	$L_5\, c_j c_l(\partial_i c_j)(\partial_i c_l)$	$[(\nabla\mathbf{c})\cdot\mathbf{c}]^2$, $\delta\mathbf{c}$ parallel to $\mathbf{c}$
$(c_k c_l\delta_{ij} + c_i c_j\delta_{kl})$	$2L_6\, c_j c_k(\partial_j c_k)(\partial_i c_i)$	$[\mathbf{c}\cdot(\nabla\mathbf{c})\cdot\mathbf{c}]\,(\nabla\cdot\mathbf{c})$, length-splay
$(c_j c_k\delta_{il} + c_i c_l\delta_{jk})$	$2L_7\, c_j c_k(\partial_i c_j)(\partial_k c_i)$	$[(\nabla\mathbf{c})\cdot\mathbf{c}]\cdot[\mathbf{c}\cdot(\nabla\mathbf{c})]$, length-bend
$c_i c_j c_k c_l$	$L_8\, c_i c_j c_k c_l(\partial_i c_j)(\partial_k c_l)$	$[\mathbf{c}\cdot(\nabla\mathbf{c})\cdot\mathbf{c}]^2$, deriv. and $\delta\mathbf{c}$ parall. to $\mathbf{c}$
$c_p c_r \epsilon_{pij}\epsilon_{rkl}$	$L_9(c_p\epsilon_{pij}\partial_i c_j)^2$	twist

Table 5.1 Elastic terms for the vector order parameter, Eq. (5.1), without the prefactor 1/2 defined in Eq. (5.1). In the nonquadratic terms the factor 2 has been included for convenience.

Figure 5.1 The (a) length-splay and (b) length-bend distortions, accounted for by the L_6 and L_7 terms, respectively.

invariants to form the elastic contribution is not unique, i.e., some invariants formed with ϵ_{ijk} can be expressed by those formed with δ_{ik}. We decide to introduce the minimum number of invariants containing ϵ_{ijk}. Among the sequence of invariants like

$$(\partial_i c_i)^2, \quad c_j^2(\partial_i c_i)^2, \ldots \tag{5.2}$$

we choose the one that is lowest order in c. This does not mean, of course, that terms of order c^2 and higher are dropped everywhere in L_{ijkl}. The nonzero components L_{ijkl} and the corresponding scalar invariants are listed in Table 5.1. Elastic constants L_i, independent of the length of $\mathbf{c}$, have been introduced. The L_1 term is an isotropic term, i.e., it treats all distortions equally. The L_2 and L_9 terms are the splay and twist terms, respectively. The L_3 term is essentially a surface term. The L_4 term is related to the bend distortion, i.e., it is nonzero if the derivative of $\mathbf{c}$ in the direction of $\mathbf{c}$ is nonzero. The terms with L_5, L_6, L_7, and L_8 are different from zero only if the length of $\mathbf{c}$ varies. The L_6 and L_7 terms are particularly interesting: they correspond to distortions involving the variation of the length of $\mathbf{c}$ and a simultaneous splay or bend deformation (Fig. 5.1). There is no such term connected with the twist distortion.

A comparison with the Frank distortion terms (4.1) can be made to connect the Frank elastic constants with the fundamental elastic constants L_i. The splay and twist terms are already among the invariants in Table 5.1. The bend term is expressed as follows:

$$[\mathbf{c}\times(\nabla\times\mathbf{c})]^2 = c_ic_k(\partial_ic_j)(\partial_kc_j) + c_jc_l(\partial_ic_j)(\partial_ic_l) - c_jc_k(\partial_ic_j)(\partial_kc_i). \tag{5.3}$$

Only the first term (the L_4 term) contributes if c^2 is constant. In addition, there must be equal contributions from the isotropic (L_1) term to the splay, twist, and bend distortion. Thus,

$$\begin{aligned} K_{11} &= c^2L_1 + c^2L_2, &(5.4)\\ K_{22} &= c^2L_1 + c^4L_9, &(5.5)\\ K_{33} &= c^2L_1 + c^4L_4, &(5.6)\end{aligned}$$

where also the leading order dependence of the Frank elastic constants on the length of $\mathbf{c}$ has been obtained (recall that the Frank terms involve the unit vector). To see the contribution from the L_1 term explicitly, one expresses the bend term in another way:

$$[\mathbf{c}\times(\nabla\times\mathbf{c})]^2 = c_p^2\left[(\partial_ic_j)^2 - (\partial_ic_j)(\partial_jc_i)\right] - [\mathbf{c}\cdot(\nabla\times\mathbf{c})]^2. \tag{5.7}$$

Hence, if c^2 is constant, Eq. (5.7) represents a relation between the invariants, so that one of them is redundant. In the Frank expression, one gets rid of the isotropic term $(\partial_ic_j)^2$. Furthermore, the second term in the bracket can now be written as a divergence, as indicated in Table 5.1. This leads to

$$(\partial_ic_j)^2 = (\nabla\cdot\mathbf{c})^2 + \frac{1}{c^2}[\mathbf{c}\cdot(\nabla\times\mathbf{c})]^2 + \frac{1}{c^2}[\mathbf{c}\times(\nabla\times\mathbf{c})]^2 + \partial_i(c_j\partial_jc_i - c_i\partial_jc_j), \tag{5.8}$$

showing that in fact the L_1 term merely renormalizes the constants for splay, twist, and bend.

As mentioned in Section 2.2, the elastic free energy density can be written as a sum of square terms only. All elastic terms in Table 5.1 are already in the square form, except the L_3, L_6, and L_7 terms. After taking care of these, one gets:

$$\begin{aligned} f^{el} = {} & \tfrac{1}{2}(L_1-2L_3)(\partial_ic_j)^2 + \tfrac{1}{2}(L_2-L_6)(\partial_ic_i)^2 + \tfrac{1}{2}L_3(\partial_ic_j+\partial_jc_i)^2 + \\ & \tfrac{1}{2}(L_4-L_7)(c_j\partial_jc_i)^2 + \tfrac{1}{2}(L_5-L_7)(c_j\partial_ic_j)^2 + \tfrac{1}{2}L_6(\partial_ic_i+c_jc_k\partial_jc_k)^2 + \\ & \tfrac{1}{2}L_7(c_j\partial_ic_j+c_k\partial_kc_i)^2 + \tfrac{1}{2}(L_8-L_6)(c_ic_j\partial_ic_j)^2 + \tfrac{1}{2}L_9(c_k\epsilon_{kij}\partial_ic_j)^2. \end{aligned} \tag{5.9}$$

For the free energy density to be positive definite the coefficients of the square terms must all be positive, which introduces inequality relations between the elastic parameters L_i.

5.2 Coupling to the flow

To describe the coupling to the flow, we must find the expressions for the viscous stress tensor and the generalized viscous force on the vector $\mathbf{c}$, i.e., we must determine

S_{ijkl}	dissipation term	R_{ijkl}	dissipation term
$\delta_{ij}\delta_{kl}$	$(\mathsf{A}_{ii})^2$, compressible		
$\frac{1}{2}(\delta_{ik}\delta_{jl}+\delta_{jk}\delta_{il})$	$\eta_0(\mathsf{A}_{ij})^2$	$\frac{1}{2}(\delta_{ik}\delta_{jl}-\delta_{jk}\delta_{il})$	$(\mathsf{W}_{ij})^2$, forbidden

Table 5.2 Parts of the matrices S and R, not depending on $\mathbf{c}$. These are the terms that remain in the case of the isotropic fluid ($\mathbf{c}=0$). There is no $\mathbf{c}$-independent contribution to M. The dissipation given by these terms must vanish for a rigid rotation, which interdicts the term $(\mathsf{W}_{ij})^2$.

the matrices S, M, R, C, D, and B in Eqs. (2.35)-(2.37) with the properties (2.39). In addition, the entropy source density (2.38) must be invariant to the inversion, implying that the matrices S, M, R, and B are even in $\mathbf{c}$, whereas C and D are odd. Again, the set of scalar invariants to form the entropy source density is not unique, i.e., some invariants formed with ϵ_{ijk} can be expressed by those formed with δ_{ik}. Once more, we decide to introduce the minimum number of invariants containing ϵ_{ijk}. The terms describing the dissipation in the isotropic fluid are collected in Table 5.2, those appearing additionally in the anisotropic case in Table 5.3. Viscous parameters η_i independent of the length of $\mathbf{c}$ have been introduced.

There must be no dissipation (2.38) and no forces (2.35)-(2.37) for a rigid rotation, $\mathbf{v}=\boldsymbol{\omega}\times\mathbf{r}$, $\dot{\mathbf{c}}=\boldsymbol{\omega}\times\mathbf{c}$, for which

$$\mathsf{A}=0, \quad \omega_k=\frac{1}{2}\epsilon_{ijk}\mathsf{W}_{ij}, \quad \dot{c}_i=-\mathsf{W}_{ij}c_j. \tag{5.10}$$

Requiring this for the isotropic part (Table 5.2) forbids the $(\mathsf{W}_{ij})^2$ term. In the anisotropic part (Table 5.3) it forbids the term $c_pc_r\epsilon_{pij}\epsilon_{rkl}\mathsf{W}_{ij}\mathsf{W}_{kl}$ and introduces the following relations between the material parameters:

$$\begin{aligned}\eta_8&=\eta_7=\eta_3,\\ \eta_5&=\eta_4.\end{aligned} \tag{5.11}$$

Finally, the symmetric and antisymmetric parts of the viscous stress tensor, Eqs. (2.35) and (2.36), read

$$\begin{aligned}\sigma^s_{ij} &= \eta_0\mathsf{A}_{ij}+\tfrac{1}{2}\eta_1(\mathsf{A}_{ik}c_kc_j+\mathsf{A}_{jk}c_kc_i)+\eta_2\mathsf{A}_{kl}c_kc_lc_ic_j+\\ &\quad \tfrac{1}{2}\eta_4(N_ic_j+N_jc_i)+\eta_6c_k\dot{c}_kc_ic_j,\\ \sigma^a_{ij} &= \tfrac{1}{2}\eta_3(N_ic_j-N_jc_i)+\tfrac{1}{2}\eta_4(\mathsf{A}_{ik}c_kc_j-\mathsf{A}_{jk}c_kc_i),\end{aligned} \tag{5.12}$$

and the generalized viscous force on the vector $\mathbf{c}$, Eq. (2.37), reads

$$-h^v_i=\eta_3N_i+\eta_4\mathsf{A}_{ij}c_j+\eta_6\mathsf{A}_{jk}c_jc_kc_i+\eta_9c_j\dot{c}_jc_i, \tag{5.13}$$

where

$$N_i=\dot{c}_i+\mathsf{W}_{ij}c_j \tag{5.14}$$

is the vector of the relative rotation of $\mathbf{c}$ with respect to the rotation of the fluid. One can compare Eqs. (5.12) and (5.13) with the Ericksen-Leslie expressions (4.13) and

matrix	matrix term	dissipation term
S_{ijkl}	$\frac{1}{2}(c_ic_j\delta_{kl}+c_kc_l\delta_{ij})$	$c_ic_j\mathsf{A}_{ij}\mathsf{A}_{kk}$, compressible
	$\frac{1}{4}(c_ic_k\delta_{jl}+c_ic_l\delta_{jk}+c_jc_k\delta_{il}+c_jc_l\delta_{ik})$	$\eta_1\, c_ic_k\mathsf{A}_{ij}\mathsf{A}_{kj}$
	$c_ic_jc_kc_l$	$\eta_2\, c_ic_jc_kc_l\mathsf{A}_{ij}\mathsf{A}_{kl}$
R_{ijkl}	$\frac{1}{4}(c_ic_k\delta_{jl}+c_jc_l\delta_{ik}-c_jc_k\delta_{il}-c_ic_l\delta_{jk})$	$\eta_3\, c_ic_k\mathsf{W}_{ij}\mathsf{W}_{kj}$
	$c_pc_r\epsilon_{pij}\epsilon_{rkl}$	$c_pc_r\epsilon_{pij}\epsilon_{rkl}\mathsf{W}_{ij}\mathsf{W}_{kl}$, forbidden
M_{ijkl}	$\frac{1}{4}(-c_ic_k\delta_{jl}-c_jc_k\delta_{il}+c_ic_l\delta_{jk}+c_jc_l\delta_{ik})$	$\eta_4\, c_ic_k\mathsf{A}_{ji}\mathsf{W}_{jk}$
C_{ijk}	$c_k\delta_{ij}$	$c_k\dot{c}_k\mathsf{A}_{ii}$, compressible
	$\frac{1}{2}(c_i\delta_{jk}+c_j\delta_{ik})$	$\eta_5\, c_i\dot{c}_j\mathsf{A}_{ij}$
	$c_ic_jc_k$	$\eta_6\, c_ic_jc_k\dot{c}_k\mathsf{A}_{ij}$
D_{ijk}	$\frac{1}{2}(-c_i\delta_{jk}+c_j\delta_{ik})$	$\eta_7\, c_i\dot{c}_j\mathsf{W}_{ji}$
B_{ij}	δ_{ij}	$\eta_8\, \dot{c}_i^2$
	c_ic_j	$\eta_9\, (c_i\dot{c}_i)^2$

Table 5.3 Parts of the matrices S and R, depending on $\mathbf{c}$, and the remaining matrices. These terms appear additionally in the case of the anisotropic fluid. The term containing ϵ_{ijk} is forbidden due to the requirement of vanishing dissipation at a rigid rotation.

(4.6), relating the five independent Leslie viscous coefficients α_i to the fundamental coefficients η_i:

$$\begin{aligned}
\alpha_4 &= \eta_0,\\
\alpha_5+\alpha_6 &= c^2\eta_1,\\
\alpha_1 &= c^4\eta_2,\\
\gamma_1 &= c^2\eta_3,\\
\gamma_2 &= c^2\eta_4,
\end{aligned} \tag{5.15}$$

with $\gamma_1=\alpha_3-\alpha_2$ and $\gamma_2=\alpha_3+\alpha_2$ as customary. The leading order dependence of the Leslie coefficients on the length of $\mathbf{c}$ has been obtained. In the general case, there are two additional viscous parameters η_6 and η_9, connected with the dissipation when $\dot{\mathbf{c}}$ is parallel to $\mathbf{c}$. They describe the component of the generalized force parallel to $\mathbf{c}$ and introduce the time derivative of $\mathbf{c}$ to the symmetric part of the viscous stress tensor. Furthermore, the η_4 contribution to the generalized force is not restricted to the direction perpendicular to $\mathbf{c}$ any longer.

Finally, let us write down the dissipation, i.e., the entropy source density:

$$\begin{aligned}
T\dot{s}^i &= \eta_0(\mathsf{A}_{ij})^2+\eta_1(\mathsf{A}_{ij}c_j)^2+\eta_2(\mathsf{A}_{ij}c_ic_j)^2+\eta_3N_i^2+\\
&\quad 2\eta_4N_i\mathsf{A}_{ij}c_j+2\eta_6\mathsf{A}_{ij}c_ic_jc_k\dot{c}_k+\eta_9(c_i\dot{c}_i)^2.
\end{aligned} \tag{5.16}$$

As mentioned in Section 2.3, the entropy source density (5.16) can be diagonalized

to square terms only:

$$\begin{aligned} T\dot{s}^i &= \eta_0(\mathsf{A}_{ij})^2 + \left(\eta_1 - \frac{\eta_4^2}{\eta_3}\right)(\mathsf{A}_{ij}c_j)^2 + \left(\eta_2 - \frac{\eta_6^2}{\eta_9}\right)(\mathsf{A}_{ij}c_ic_j)^2 + \\ &\quad \eta_3 h_i^2 + \eta_9 g^2, \end{aligned} \tag{5.17}$$

with

$$h_i = N_i + \frac{\eta_4}{\eta_3}\mathsf{A}_{ij}c_j, \tag{5.18}$$

$$g = c_i\dot{c}_i + \frac{\eta_6}{\eta_9}\mathsf{A}_{ij}c_ic_j. \tag{5.19}$$

Hence, there are only five square terms determining the dissipation, with the coefficients that have to be positive. The two additional parameters are η_4/η_3 (the analogue of the reaction parameter γ_2/γ_1 in the Ericksen-Leslie theory) and η_6/η_9. They define the rotation in the flux space to yield the fluxes chosen originally, i.e., N_i instead of (5.18) and $c_i\dot{c}_i$ instead of (5.19).

We are now able to write down the dynamic equations (2.40)-(2.42). There is no point in really writing them down here.

6

Defects

In this Chapter, enough background on the defects will be covered to understand the annihilation processes studied in next Chapters. It is not our aim to give a thorough perspective of the subject here. In particular, we do not go into the group-theoretical considerations of defect topology — the homotopy theory [58,59]. Nevertheless, we do use some of its results relevant in our context. We will restrict the discussion to point defects in a two-dimensional system or line defects in a three-dimensional system, without discussing the point defects in the 3D system, as they will not be studied in the Thesis. The discussion will apply both to defects of the director and vector order parameters — the latter are merely a subset of the former.

Defects are a "registration mark" of systems with broken symmetry. Let us first try to give a useful definition of the defect. Naively we can say that the defect is an irregularity in the order parameter field, i.e., a discontinuity. It can take place in a single point, a line, or a plane, resulting in zero-, one-, and two-dimensional defects. Their fundamental properties depend on the order parameter, or more precisely, on its symmetry. Of course, physically it is hardly possible to speak about any discontinuities, so there may be a problem with our naive definition of the defect. In fact, in the nematic the discontinuity is present only as long as the director description with a fixed degree of order is considered. If this restriction is abandoned and changes of the degree of order and/or the biaxiality are allowed, a continuous solution is obtained [60–64]. Therefore, a more general definition of the defect must be searched for. Fig. 6.1 shows a point defect in two dimensions or a cross-section of a line defect in three dimensions. Orientational defects of the order parameter that carries information on a direction are called disclinations. There are two types of disclinations, wedge (Fig. 6.1) and twist disclinations [55, p. 126]. We will concentrate on the wedge disclinations only, as they are easier to envisage.
If a loop is imagined around the defect and then traversed counterclockwise so as to return to the starting point, a winding number s can be defined as a measure of the total angle θ the director/vector is rotated by on this trip, $s = \theta/2\pi$. Since the loop passes over defectless structure only, the continuity of the director/vector field imposes that the angle of rotation must be an integer multiple of π or 2π,

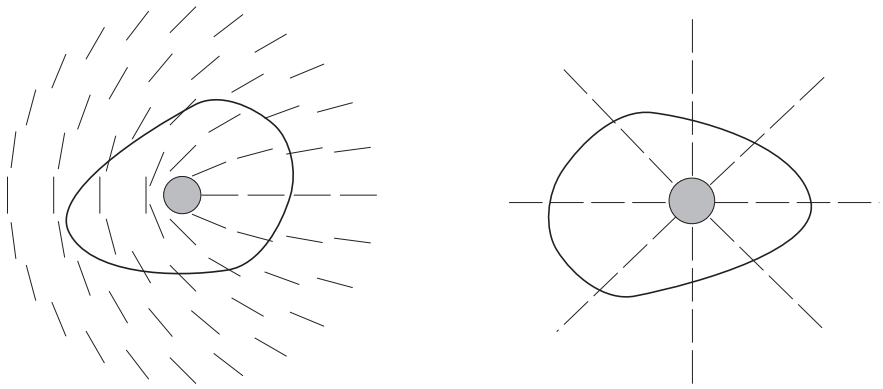

(a) $s = 1/2$ (b) $s = 1$

Figure 6.1 Examples of wedge disclinations. A loop is placed around each defect to define its winding number s, (a) $s = 1/2$, (b) $s = 1$. In the vector case, (a) does not represent a possible configuration.

Figure 6.2 Fingerprint "defects" resemble disclinations in the nematic. A defect-antidefect pair with strengths $1/2$ and $-1/2$ appears on my forefinger.

respectively:

$$s = \begin{cases} 0, \pm\frac{1}{2}, \pm 1, \pm\frac{3}{2}, ... & ; \quad \text{director} \\ 0, \pm 1, \pm 2, \pm 3... & ; \quad \text{vector} \end{cases} . \tag{6.1}$$

The winding number does not depend on the size or actual shape of the loop but solely on the type of the defect encircled. Therefore, it identifies the defect completely and is also referred to as the strength of the defect. Even if the singularity in the center (the core of the defect) is somehow smeared (e.g., by melting — restoring the isotropic phase, to be the case below), the winding number does not change. In fact, to determine the strength s of the defect we do not need any information on what the central configuration is. Therefore, the core region is not of importance for the macroscopic description of the so-called topological defects, i.e., defects that cannot be converted to a defectless structure by means of any continuous transformation of the director/vector field [58]. Topologically speaking, all defects transformable into each other by continuous transformations are identical. This means that those which can be transformed in this way to a defectless structure, are not defects in the topological sense. At this point one should mention that the wedge and twist disclination lines are topologically identical.

Usually, topological defects are energetically stable, although they do not correspond to states of the lowest free energy [65]. Indeed, when trying to transform them to a defectless structure, a high energy barrier occurs due to discontinuities that inevitably take place at such a transformation.

6.1 Disclinations of a 2D director/vector

A two-dimensional order parameter is a convenient example to start with. The system may be two- or three-dimensional, it is only the director/vector which is restricted to a plane. Hence, the discussion will apply to point disclinations in the 2D system or line disclinations (disclination lines) in the 3D system. In the latter case the free energies (6.5), (6.7), (6.11), (6.9), and (6.12) must be interpreted as the energies per unit length of the disclination line. The classification of defects is quite illustrative here, and in the one constant approximation (Eq. (4.2)) the calculation of structures is simple [66, p. 147]. An example of the physical system possessing the 2D vector order parameter is the smectic-C liquid crystal studied in Chapter 8 as a representative of the XY-model.

Apart from the surface terms, there is no difference in the lowest order director and vector elastic free energies, i.e., the Frank expression applies to both cases. In the one constant approximation (4.2), the equilibrium condition for a point disclination located at the center of the coordinate system reads [67]

$$\nabla^2\theta = 0, \tag{6.2}$$

where θ is the polar angle of the director/vector,

$$\mathbf{n} = (\cos\theta, \sin\theta). \tag{6.3}$$

The solution of Eq. (6.2) can depend only on the polar angle ϕ and must satisfy the continuity condition for the director/vector. Thus,

$$\theta = s\phi + \theta_0 = s\,\mathrm{arctg}\frac{y}{x} + \theta_0, \quad s = 0, (\pm\tfrac{1}{2}), \pm 1, (\pm\tfrac{3}{2}), ..., \tag{6.4}$$

where θ_0 is a free parameter. The (half-)integral number s is the strength of the defect exactly as defined above. The elastic free energy of the defect structure is obtained by integration of Eq. (4.2) for the solution (6.4):

$$\mathcal{F}_d = \frac{K}{2}\int_{r_0}^{R} r dr \int_0^{2\pi} d\phi \left[\left(\frac{\partial\theta}{\partial x}\right)^2 + \left(\frac{\partial\theta}{\partial y}\right)^2\right] = \pi K s^2 \ln\frac{R}{r_0}, \tag{6.5}$$

where R is a typical size of the sample, and r_0 is a microscopic cut-off required for the free energy not to diverge. Physically, this means that at distances near r_0 the director/vector configuration (6.4) cannot possibly be correct. In this region the deformation becomes large, so that the Frank elastic theory ceases to be valid and changes in the scalar invariants of the order parameter must be taken into account. In first approximation, a core of radius r_0 with the system in the isotropic (melted) state is invented, having then

$$S = \begin{cases} 0 & ; \quad r < r_0 \\ S_0 = \mathrm{const} & ; \quad r > r_0 \end{cases}, \tag{6.6}$$

where S is the scalar order parameter of the nematic or the length of the vector order parameter. Of course, this is not the configuration with the minimal free energy. The core free energy F_c due to the presence of the isotropic phase is

$$\mathcal{F}_c = \pi r_0^2 \Delta f, \tag{6.7}$$

where Δf is the difference in free energy densities of the isotropic and the ordered phase. By minimizing the total free energy $\mathcal{F}_d + \mathcal{F}_c$, the radius of the core is set to

$$r_0 = \sqrt{\frac{Kn^2}{2\Delta f}}, \tag{6.8}$$

so it increases linearly with the strength of the defect s. The size of the core is of the order of the correlation length ξ, Eqs. (7.18) or (8.8), which is in the nanometer range. It is very small if compared to wavelength of light so one can conclude that optics cannot be used for investigation of defect cores. Finally, the total free energy of the defect structure in this approximation is

$$\mathcal{F} = \mathcal{F}_c + \mathcal{F}_d = \pi s^2 K \left(\frac{1}{2} + \ln\frac{R}{r_0}\right). \tag{6.9}$$

In case multiple defects with strengths s_i are present, due to the linearity of Eq. (6.2) the equilibrium configuration is obtained simply by summing the solutions (6.4) for a single defect:

$$\theta = \sum_i (s_i\phi_i + \theta_{0i}) = \sum_i s_i\,\mathrm{arctg}\frac{y - y_i}{x - x_i} + \theta_0'. \tag{6.10}$$

The free energy of two defects is [65, p. 529]

$$\mathcal{F} = \mathcal{F}_1 + \mathcal{F}_2 + 2\pi K s_1 s_2 \ln \frac{R}{r}, \tag{6.11}$$

where r is the distance between the centers of the defects. The first two terms stand for the free energies (6.9) of single defects, whereas the third terms represents their interaction free energy. Evidently, defects with equally signed strengths repel each other, while those with opposite signs of the strength are attracted. Explicitly, the free energy of a defect pair with $s_2 = -s_1$ reads

$$\mathcal{F} = 2\pi s^2 K \left(\frac{1}{2} + \ln \frac{r}{r_0} \right), \quad s = |s_1|, \quad r_1 = r_2 = r_0, \tag{6.12}$$

i.e., the logarithmic divergence with system size is eliminated in this case.

Let us now discuss basic properties of the disclinations of the two-dimensional director/vector order parameter. Our main interest will be in how topologically different defects are characterized and then, how they may combine. The disclinations have already been characterized by their winding number or strength s. For the two-dimensional director/vector it is found that disclinations of different strengths are topologically different [58], i.e., they cannot be continuously transformed into each other. Furthermore, two defects with strengths s_1 and s_2 can combine in a continuous transformation to form a defect with strength $s_1 + s_2$, i.e., in combining the winding numbers are simply summed [58]. Particularly, it follows that two defects with opposite winding numbers can combine to form a defectless structure with zero winding number $s = 0$. Even if the pair remains unannihilated, Eq. (6.12) shows that the logarithmic divergence is eliminated if $s_1 + s_2 = 0$, so the free energy of the defects is small, provided that they are not very far apart. This can be understood a priori, since using a loop that encircles both defects a winding number $s = s_1 + s_2 = 0$ is detected, which reflects a defectless structure with low distortion energy outside the loop.

Generally, defects with oppositely signed (not necessarily equal in magnitude) strengths will combine in order to reduce the distortion energy. On the other hand, it is energetically favorable for a defect with a large strength to decay into defects with lower strengths, which can then move apart reducing the distortion energy. In principle, one should be more precise and apply Eq. (6.12) to this cases, accounting for the core energies and cut-offs r_0 that depend on the winding number. However, these are small energy corrections, too subtle to be described in the current approximation. Nevertheless, Eq. (6.12) shows, that changing the separation of the defects for as little as only a few core sizes already predominates the other free energy contributions.

6.2 Disclinations of a 3D director/vector

Allowing for a three-dimensional order parameter, the topological picture is changed dramatically. Continuous transformations changing the winding number by an integer are now possible [58]. This implies that topologically all defects with integer

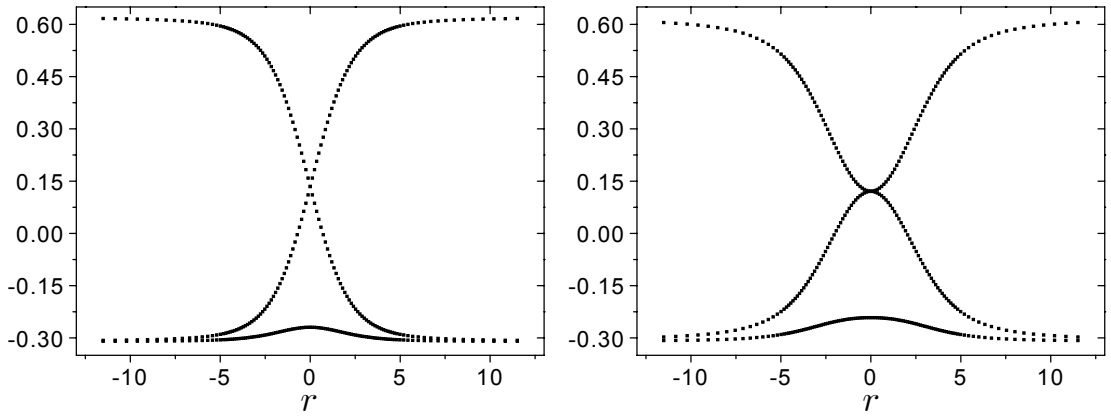

(a) $s = \pm 1/2$ (b) $s = \pm 1$

Figure 6.3 Radial dependence of the Q-tensor eigenvalues for (a) the $\pm 1/2$ and (b) ± 1 disclinations. Length is scaled by the correlation length (7.18). Analytic expansions for small r are given in Eq. (9.8).

strengths are no defects at all, since they can be continuously transformed to a defectless structure. For the defect in Fig. 6.1(b) such a transformation (a so-called escape in the third dimension [68,69]) is achieved by a progressive rotation of directors around the perpendicular axes lying in the plane when going from the boundary towards the center. Hence, in the case of the vector order parameter there exist no topological disclination lines (or points in the 2D system). Similarly, half-integer defects are continuously transformable into each other, thus being topologically identical. Hence, in the case of the director order parameter there exists only a single topological line defect (or point defect in the 2D system); we choose it to be the disclination line with winding number $s = 1/2$, Fig. 6.1(a). The combination law is again simply the addition of winding numbers [58]. With only one topological defect, there is little possibility left: two disclinations with strengths $s = 1/2$ can combine to form a defectless structure with $s = 0$.

Let us just mention that there exist an exact analogy between the disclination lines and magnetic systems [65, p. 530].

6.3 Structure of disclination cores

In the case of the vector order parameter $\mathbf{c}$ the structure of the disclination core is very simple, i.e., the magnitude c of the vector vanishes in the center. In the one elastic constant approximation, the general solution for small r is

$$c \propto r^{|s|}, \tag{6.13}$$

where the vector $\mathbf{c}$ is expressed as

$$\mathbf{c} = c(r)\left(\hat{\mathbf{e}}_r \cos\psi + \hat{\mathbf{e}}_\phi \sin\psi\right), \quad \psi = (s-1)\phi + \psi_0. \tag{6.14}$$

In the case of the director, the full tensor order parameter must be solved for [60–62]. In the one elastic constant approximation (7.1), the solution for small r is

given in Eq. (9.8). The cross section through the strength $\pm 1/2$ and ± 1 disclinations is depicted in Fig. 6.3. Far from the core the ordering is uniaxial, but also in the center, where the largest in absolute eigenvalue is negative, i.e., the distribution of molecules is planar. This can be best seen in Fig. 6.4 containing the complete information on the Q-tensor field in the disclination cores.

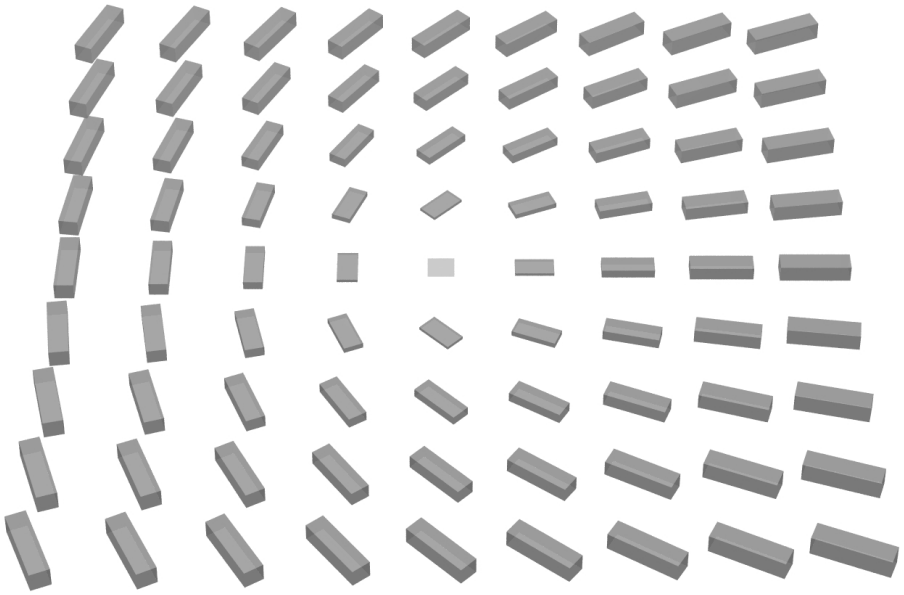

(a) $s = 1/2$

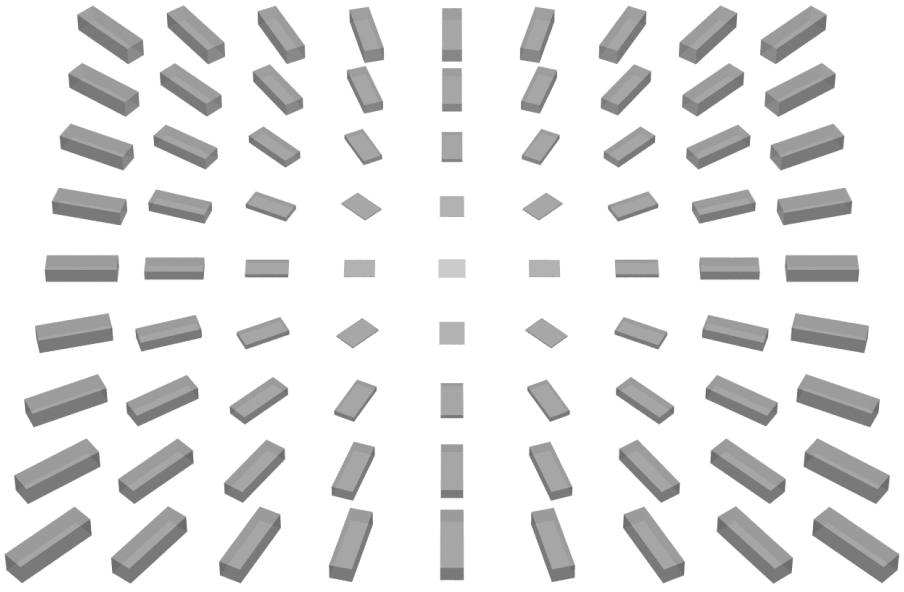

(b) $s = 1$

Figure 6.4 Cross sections through the disclination lines with $s = 1/2$ and $s = 1$. The Q-tensor eigensystem is represented by the box, the lengths of the edges correspond to the eigenvalues (a constant is added to make them non-negative).

7

Pair-annihilation of disclination lines in nematics

7.1 Introduction

The research of defects in order parameter fields corresponding to various condensed matter systems is driven by many aspects of motivation. Defects can be readily observed, either directly (e.g., by optical methods) or through other physical properties of the system, which are crucially modified in the presence of defects. In many cases of application defect-free structures are required, while in the others (e.g., in some liquid crystal displays) structures containing defects might be essential. In the latter case, one must know something about static or dynamic properties of defects. Theoretically, defects offer a rich playground for mathematically oriented excursions. Their topological properties can be very interesting and nontrivial, if only the order parameter has enough degrees of freedom. Defects play a decisive role in any phase transition, since in the late stages the ordering is governed exclusively by the dynamics of the defects created at the transition. An important part of the motivation arises from the universality of defects, i.e., they can occur in any system with a rich enough order parameter. Their major properties are independent of the underlying physics, determined solely by symmetries and dimensionalities of the order parameter, the defect, and the system. Lately the aim towards the exploitation of this universality has been experienced in the area, motivating the research of laboratory-friendly condensed matter systems such as liquid crystals in order to yield knowledge in completely different realms of physics (e.g., the physics of the universe, elementary particles, and fields) [70–74].

In order to study the statics or dynamics of defects in nematic liquid crystals, the full tensorial description of the nematic ordering must be considered. Nevertheless, there have been some attempts using the director description. The monopole-antimonopole annihilation of point defects has been studied in the scaling regime by Pargellis *et al.* [75]. The annihilation of a wedge disclination pair in a hybrid nematic cell and the annihilation of straight disclination lines have been studied by Minoura *et al.* [76] and Denniston [77], respectively. Peroli, Bajc, *et al.* [78–81] have studied the annhilation of point defects in a capillary. The dynamics of loop disclinations has been modelled by Sonnet and Virga [82]. Stark and Ventzki [83] have calculated the Stokes drag of spherical particles in a nematic solvent.

There are two reasons for the necessity of the tensor description. First, the half-integer defects are only possible when the order parameter possesses the tensorial symmetry. One can evade this problem by using a director description that preserves this symmetry [84]. However, the approach is still inadequate for the second reason, which is the inability of describing the defect core. The core must necessarily be included, for it is only in this way that the length scale is defined to which other lengths can be compared, i.e., the interdefect distance! Also, in the absence of the core problems regarding the discretisation arise, e.g., the artifactural pinning of defects. Puncturing a hole at the spot of the defect core and shrinking it to a point as suggested by Gartland *et al.* [85] cannot be of benefit, as the length scale is still not introduced, not to mention the obscure boundary conditions emerging at the cutting surface. A uniaxial tensor description with a varying length of the director has been used by Pismen and Rubinstein [86]. The complete tensor approach has been taken by Kilian [87]. A nice tensorial calculation using an adaptive mesh refinement approach has been performed by Fukuda *et al.* [88].

If one wants to include hydrodynamic effects, normally described by the Ericksen-Leslie theory [22,23], Chapter 4, a generalization of the latter is required to describe the coupling of the tensorial dynamics and the flow [89–92]. Still keeping the director description, one might expect to remedy the problem just by allowing a variation of the degree of order. It turns out, however, that in the defect center the equations so obtained are ill-conditioned and incapable of accurately describing the hydrodynamic part of the problem.

The effect of hydrodynamic flow on kinetics of nematic-isotropic transition has been studied by Fukuda [93], a similar topic, however with a different method — the lattice Boltzmann algorithm [94], has been studied by Denniston *et al.* [95]. Recently a work on hydrodynamics of topological defects was published by Tóth, Denniston, and Yeomans [96]. They studied the effect of backflow and elastic anisotropy on the pair-annihilation of straight line defects with strengths $\pm 1/2$, again using the lattice Boltzmann algorithm. Their treatment, however, is not based on the Ericksen-Leslie theory and involves only two viscous coefficients. There is also a significant amount of experimental work on the dynamics of defects in nematics [97,76,98].

The aim of this Chapter is to present the solution to the pair-annihilation of straight disclination lines with strengths $\pm 1/2$, starting from the dynamic theory for the tensor order parameter [92]. We consider an unconfined bulk system. In the theory [92], only those dissipation terms are included that reduce to the Leslie terms in the uniaxial limit with a constant degree of order. Therefore, the tensorial theory involves the same number of viscous parameters as the Ericksen-Leslie theory, expressed as simple linear combinations of the Leslie viscosity coefficients.

Symmetry properties of the stress tensor with respect to changing the sign of the winding number will be discussed, resulting in a simple identification of stress tensor terms, responsible for the observed flow asymmetry and the acceleration of the annihilation process. Further, it is to be shown that the hydrodynamic effect depends on the director phase angle, i.e., unlike the order parameter dynamics in case of elastic isotropy considered here, it is not invariant under the homogeneous rotation of directors. Again the corresponding stress tensor term will be pointed

out.

It should be stressed that although the tensorial approach works very well at small defect separations, the passage to >1 μm length scales that can be resolved experimentally is hindered by enormous computational complexity of the problem and the large (several orders of magnitude) ratio of the defect separation to the size of the defect core.

7.2 Dynamic equations

The starting point is the bulk free energy density expression in terms of Q [10, p. 156]:

$$f = \phi(\mathsf{Q}) + \frac{1}{2}L\,(\partial_i \mathsf{Q}_{jk})(\partial_i \mathsf{Q}_{jk}), \tag{7.1}$$

where the homogeneous part is given by

$$\phi(\mathsf{Q}) = \frac{1}{2}A\,\mathsf{Q}_{ij}\mathsf{Q}_{ji} + \frac{1}{3}B\,\mathsf{Q}_{ij}\mathsf{Q}_{jk}\mathsf{Q}_{ki} + \frac{1}{4}C\,(\mathsf{Q}_{ij}\mathsf{Q}_{ji})^2. \tag{7.2}$$

It was taken into account that $C_1\,(\mathsf{Q}_{ij}\mathsf{Q}_{ji})^2 + C_2\,\mathsf{Q}_{ij}\mathsf{Q}_{jk}\mathsf{Q}_{kl}\mathsf{Q}_{li} = (C_1 + 1/2C_2)(\mathsf{Q}_{ij}\mathsf{Q}_{ji})^2$ and a new constant $C = C_1 + C_2/2$ was introduced. In the elastic part of (7.1), only the term with $L_1 \equiv L$ is retained, resulting in isotropic elasticity. Terms of third order in Q are needed to reach the splay-bend elastic anisotropy [99], the effects of which have been studied in [96].

Requiring the Q tensor be traceless and symmetric, the Euler-Lagrange equation for the free energy functional

$$\mathcal{F} = \int dV\,[f(\mathsf{Q}, \nabla\mathsf{Q}) - \lambda\mathsf{Q}_{ii} - \lambda_i \epsilon_{ijk}\mathsf{Q}_{jk}] \tag{7.3}$$

gives the homogeneous and elastic part of the generalized force on the tensor order parameter Q:

$$\mathsf{h}^{he}_{ij} = L\,\partial_k^2 \mathsf{Q}_{ij} - \frac{\partial\phi}{\partial\mathsf{Q}_{ij}} + \lambda\delta_{ij} + \lambda_k \epsilon_{kij}. \tag{7.4}$$

The Lagrange-multiplier terms merely state that the isotropic and antisymmetric components of (7.4) are not specified and have to be determined by the constraints, i.e., the isotropic and antisymmetric parts must be subtracted from the force h^{he}_{ij} (projection to the traceless symmetric subspace). To put it in another way, h^{he} must be projected onto the symmetric and traceless subspace of Q. The elastic stress tensor is obtained in a standard manner, Eq. (2.26), as

$$\sigma^e_{ij} = -\frac{\partial f}{\partial(\partial_i \mathsf{Q}_{kl})}\partial_j \mathsf{Q}_{kl}. \tag{7.5}$$

The viscous stress tensor and the viscous generalized force on the Q tensor are [92]

$$\sigma^v_{ij} = \beta_1 \mathsf{Q}_{ij}\mathsf{Q}_{kl}\mathsf{A}_{kl} + \beta_4 \mathsf{A}_{ij} + \beta_5 \mathsf{Q}_{ik}\mathsf{A}_{kj} + \beta_6 \mathsf{Q}_{jk}\mathsf{A}_{ki} + \frac{1}{2}\mu_2 \mathsf{N}_{ij} - \mu_1 \mathsf{Q}_{ik}\mathsf{N}_{kj} + \mu_1 \mathsf{Q}_{jk}\mathsf{N}_{ki}, \tag{7.6}$$

$$-\mathsf{h}^v_{ij} = \frac{1}{2}\mu_2 \mathsf{A}_{ij} + \mu_1 \mathsf{N}_{ij}, \tag{7.7}$$

where

$$\mathsf{N}_{ij} = \frac{d\mathsf{Q}_{ij}}{dt} + \mathsf{W}_{ik}\mathsf{Q}_{kj} - \mathsf{Q}_{ik}\mathsf{W}_{kj}, \tag{7.8}$$

with the material time derivative $d\mathsf{Q}_{ij}/dt = \partial \mathsf{Q}_{ij}/\partial t + (\mathbf{v}\cdot\nabla)\mathsf{Q}_{ij}$ and the symmetric and antisymmetric parts of the velocity gradient A and W, Eq. (2.34). Only those terms have been included that in the uniaxial limit with a constant degree of order reduce to the standard Leslie viscous terms α_i. Thus, the viscous coefficients in (7.6) and (7.7), linked by the relation $\mu_2 = \beta_6 - \beta_5$, can be expressed in terms of the Leslie coefficients and the constant value of the scalar order parameter [92].

Finally, the equation of motion for the Q-tensor is the traceless symmetric part (denoted by $\perp$) of the generalized force balance,

$$\left\{\mathsf{h}^{he} + \mathsf{h}^v\right\}_\perp = 0, \tag{7.9}$$

with the constraints

$$\mathsf{Q}_{ii} = 0, \quad \epsilon_{ijk}\mathsf{Q}_{jk} = 0. \tag{7.10}$$

The generalized Navier-Stokes equation within the low-Reynolds-number approximation (omitting the nonlinear advective derivative term $(\mathbf{v}\cdot\nabla)\mathbf{v}$), regularly used to describe the order parameter elasticity driven dynamics in liquid crystals (Chapter 4), reads

$$\rho\frac{\partial v_i}{\partial t} = -\partial_i p + \partial_j(\sigma^v_{ji} + \sigma^e_{ji}), \tag{7.11}$$

with the density ρ and the viscous and elastic stress tensors given in (7.6) and (7.5). Usually, also the steady state approximation is made, omitting the time derivative term (Chapter 4). The pressure field p must be such that the incompressibility condition

$$\partial_i v_i = 0 \tag{7.12}$$

is satisfied.

7.3 Characteristic scales

Let us rewrite the free energy density using the uniaxial ansatz (3.11)

$$\mathsf{Q}_{ij} = \frac{1}{2}S(3n_i n_j - \delta_{ij}), \tag{7.13}$$

$$f = \tfrac{3}{4}A\,S^2 + \tfrac{1}{4}B\,S^3 + \tfrac{9}{16}C\,S^4 + \tfrac{3}{4}L\,(\nabla S)^2 + \tfrac{9}{4}L\,S^2(\nabla\mathbf{n})^2. \tag{7.14}$$

The Euler-Lagrange equation for S, putting $\nabla\mathbf{n}$ to zero, reads

$$\tfrac{3}{2}L\,\nabla^2 S - \frac{\partial f}{\partial S} = 0. \tag{7.15}$$

For a homogeneous system, the second term must vanish in equilibrium, from where the bulk equilibrium value of S is obtained,

$$S_0 = \frac{1}{2}\left(-B/3C + \sqrt{(B/3C)^2 - 8A/3C}\right). \tag{7.16}$$

Linearizing Eq. (7.15) for small deviations from equilibrium, $S(\mathbf{r}) = S_0 + \Delta S(\mathbf{r})$, one gets

$$\nabla^2 \Delta S - \frac{2}{3L}\frac{\partial^2 f}{\partial S^2}\Big|_{S_0} \Delta S = 0, \tag{7.17}$$

from where a characteristic length scale can be extracted — the nematic correlation length

$$\xi = \sqrt{\frac{3}{2}\frac{L}{f''|_{S_0}}}. \tag{7.18}$$

Using the correlation length (couple of nanometers usually) and a corresponding characteristic time (Eq. (4.16))

$$\tau = \gamma_1 \xi^2 / K = \mu_1 \xi^2 / L, \tag{7.19}$$

where γ_1 is the director rotational viscosity and K is the director elastic constant, Eq. (7.9) and the stationary Eq. (7.11) are both put to a dimensionless form. The time τ is the characteristic relaxation time of the order parameter deformation on the length scale of ξ, which is typically tens of nanoseconds. In the following, dimensionless quantities will be used, i.e. $r \leftarrow r/\xi$ for length, $t \leftarrow t/\tau$ for time and $v \leftarrow v\tau/\xi$ for the velocity. After doing so, the material parameters enter the equations only through combinations given in (7.22) and (7.23).

Let us estimate the Reynolds number and the unsteadiness parameter of the flow, i.e., the ratio of characteristic dynamic times of the flow field and the order parameter field. The estimate differs from those made in Chapter 4, in that now there is no simple relation between characteristic deformation length (7.18) of the order parameter field and its relaxation time. Instead, one can empirically identify the latter with the annihilation time. This yields the Reynolds number and the unsteadiness parameter of

$$Re = \frac{\rho K}{\gamma_1^2}\frac{R_0^2}{t} \approx 10^{-6} \cdot \frac{R_0^2}{t}, \tag{7.20}$$

where R_0^2 is the initial defect separation and t is the annihilation time. The isotropic viscosity was put equal to γ_1 for brevity. The value of R_0^2/t, obtained empirically, is of the order of a few units. What is more, following the phenomenological equation of motion given by Pleiner [100,101,96],

$$\frac{dR}{dt} \propto \frac{1}{R}\,\ln^{-1}\left(\frac{R}{\xi'}\right), \tag{7.21}$$

where $R(t)$ is the actual defect separation and ξ' scales with ξ, the value of R_0^2/t exhibits only a weak logarithmic dependence on R. Thus, for large enough defect separations compared with ξ, the empirical estimate is quite general in validity. In conclusion, the Reynolds number and the unsteadiness parameter are tiny indeed, so that in Eq. (7.11) both the advective and partial time derivatives can be omitted.

7.4 Technicalities and material parameters

The numerical method used is described in Chapter 4. The calculations were done on an inhomogeneous square mesh, consisting of a fine mesh of 160x160 points in the center containing both defects, and a coarser inhomogeneous grid with increasing spacing around it to yield the total of 280x280 points. The position of the defects was determined by finding a local minimum of the trace $\mathsf{Q}_{ij}\mathsf{Q}_{ij}$.

The velocity was set to zero at the boundary. In order to meet the situation present in a bulk system, the defect separation was small compared to the size of the computational area (the ratio of the two was 3/20) and the derivatives of the order parameter normal to the boundary were set to zero. Initially, the Q tensor was set to $\mathsf{Q}_{ij} = \frac{S_0}{2}(3n_in_j - \delta_{ij})$, where $\mathbf{n} = (\cos\phi, \sin\phi)$ and $\phi = \sum_{k=1}^{2} m_k \arctan\left(\frac{y-y_k}{x-x_k}\right)$, which is the one elastic constant equilibrium director configuration with two defects of strength m_k positioned at (x_k, y_k), Eq. (6.10). Afterwards, enough computing steps without the hydrodynamics were performed to first establish the full tensorial configuration. The initial defect separation was above 70 correlation lengths (7.18), in order to reach the far regime of motion, where the defects are well isolated. As one realizes, there are three length scales in the system, which should be well enough separated: the correlation length and the defect spacing as the relevant physical scales, plus the container size as the technical one.

The viscosity coefficients in (7.6) and (7.7) were obtained from the standard Leslie coefficients corresponding to MBBA [49, p. 231] as described in [92]. Numerical values of the relevant ratios are

$$\mu_2/\mu_1 \approx -1.92, \quad \beta_1/\mu_1 \approx 0.17, \quad \beta_4/\mu_1 \approx 1.99, \quad \beta_5/\mu_1 \approx 0.70, \quad \beta_6/\mu_1 \approx -0.79. \tag{7.22}$$

The Landau coefficients A, B, C and the elastic constant L in (7.1) and (7.2) were taken from [102]. Numerical values of the relevant ratios are

$$A\xi^2/L \approx -0.064, \quad B\xi^2/L \approx -1.57, \quad C\xi^2/L \approx 1.29, \tag{7.23}$$

with the correlation length (7.18) $\xi \approx 2.11$ nm. The characteristic time (7.19) $\tau \approx 32.6$ ns completes the set of material parameters.

7.5 Results and discussion

The results for the pair annihilation of $\pm 1/2$ defects (Fig. 7.1) are presented in Fig. 7.2. It should be pointed out that due to the high computational complexity of the problem and the broad range of length scales involved, only defect separations of less than 1 μm and annihilation times of less than 1 ms can be reached. This means that for the time being there still exists a large gap between numeric capabilities and possible experimental observations.

In Fig. 7.2 one notices two distinct features: due to the hydrodynamic flow the annihilation is faster and asymmetric. Fig. 7.3 shows that it is particularly the $+1/2$ defect whose motion is affected by the flow. Also clearly demonstrated by Fig. 7.3

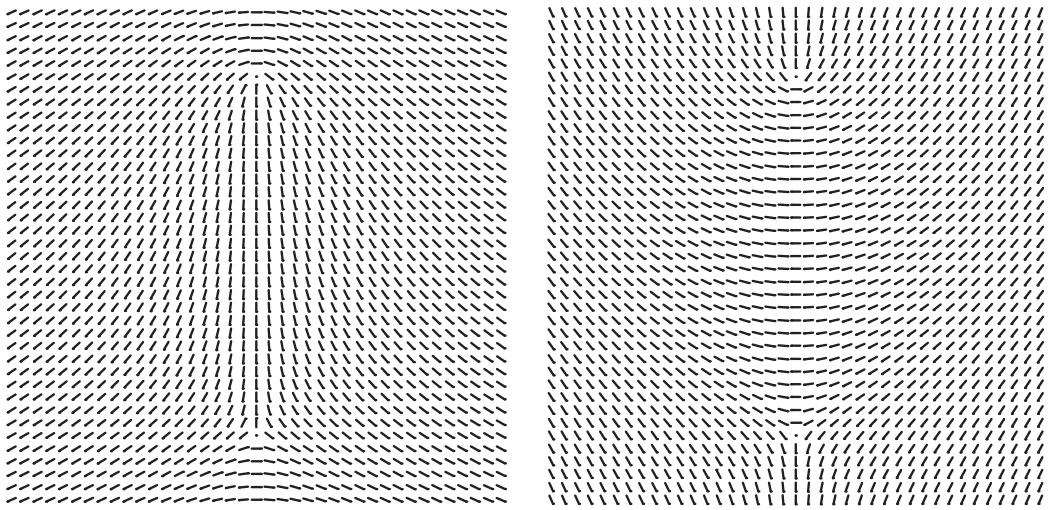

Figure 7.1 A schematic representation of a pair of $\pm 1/2$ defect lines: the eigenvectors corresponding to the largest absolute eigenvalue of Q (directors) are depicted in the cross-sectional plane, perpendicular to the disclination lines. Two isomorphs (a) and (b) are shown, differing only in a homogeneous rotation of the directors. For clarity, the number of mesh points has been reduced by a factor of 4 in each dimension and the correlation length has been increased by a factor of 2 (only the central homogeneous region of the mesh is shown).

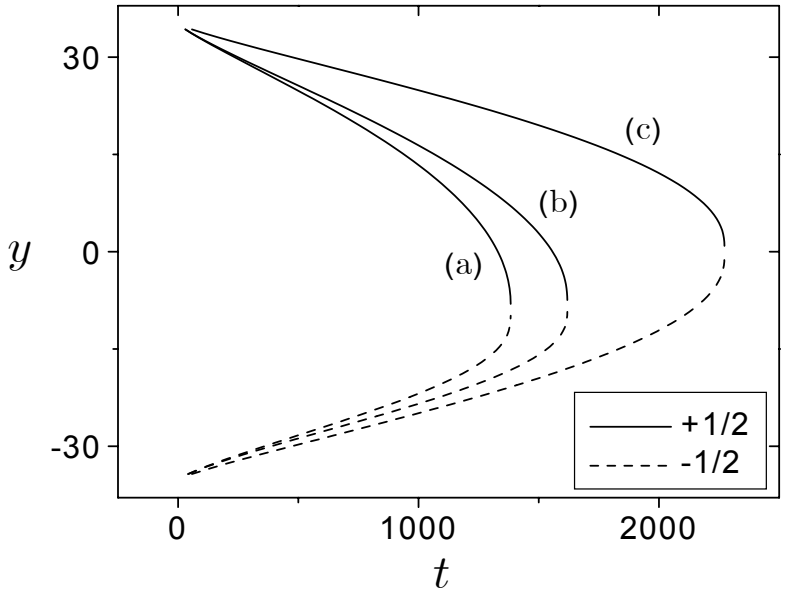

Figure 7.2 Position of the defects as a function of time, measured from the initial middle point between the defects. Three situations are displayed: the two isomorphs (a) and (b) (see Fig. 7.1) and the case without the flow (c), where the isomorphs become degenerate. Recall that length is measured relative to $\xi \approx 2.1$ nm, and time is measured relative to $\tau \approx 33$ ns.

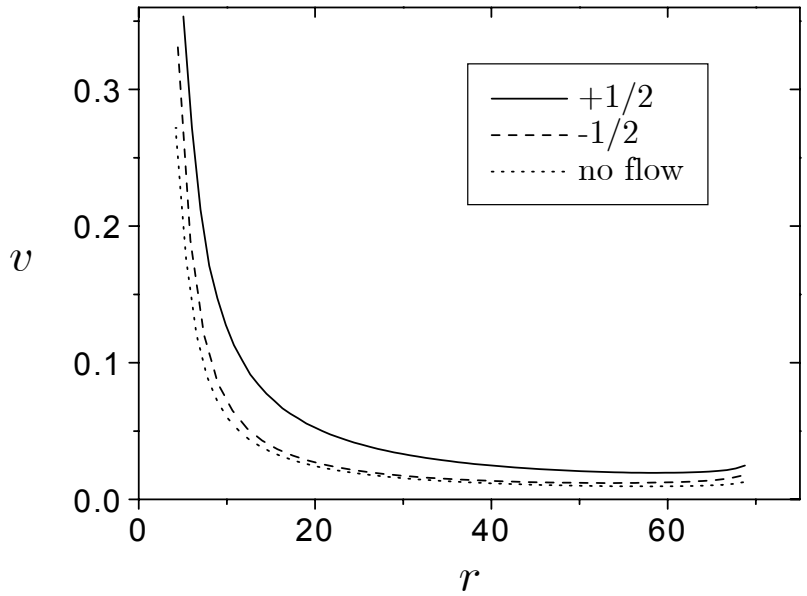

Figure 7.3 Velocity of the defects as a function of the interdefect distance (isomorph (a)). For comparison, the same is shown for the case without the hydrodynamic flow. The velocity of the $+1/2$ defect is strongly increased by the flow. Note the nonmonotonic behavior at early stages of the process, where the initial equilibrium Q-tensor configuration is adapting to a dynamic one. The distance and the velocity are measured relative to $\xi \approx 2.1$ nm and $\xi/\tau \approx 65$ nm/μs, respectively.

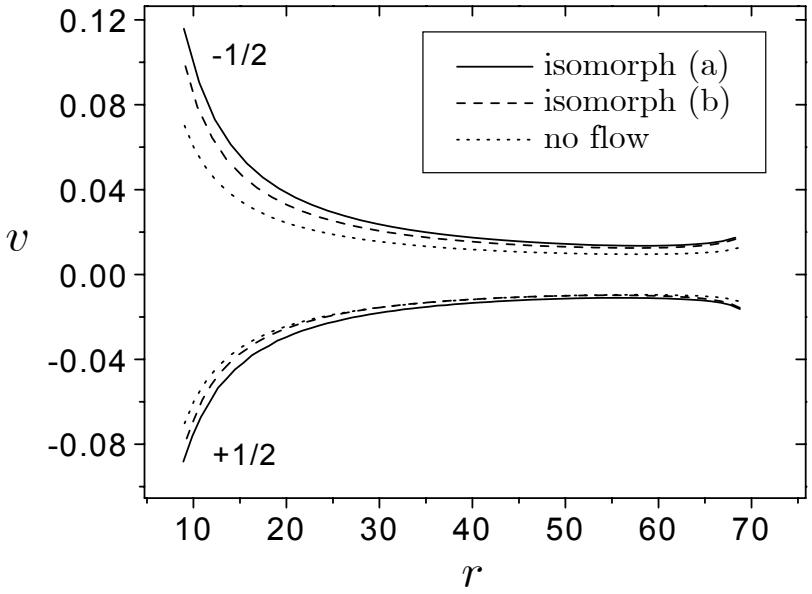

Figure 7.4 Velocity of the defects without the contribution of advection as a function of the interdefect distance. Without the hydrodynamic flow, both defects move symmetrically. Note that the part of the velocity coming from the order parameter dynamics is larger for the $-1/2$ defect. Also note the difference between the isomorphs originating from the different coupling to flow and different flow field itself, both of which are mostly due to the μ_2 viscous term.

(see also Figs. 7.4 and 7.5) is the nonmonotonic behavior of the defect velocities at early stages of the annihilation [86], [72, p. 58]. It is a consequence of starting with the equilibrium configuration of fixed defects rather than with a dynamic one, which is being approached by the system in the course of annihilation. Since our simulations represent only the very late stage of an actual annihilation process, this nonmonotonic behavior should be viewed as an unphysical artifact of the initial condition. Later we will show that it can be eliminated by starting with a proper dynamic configuration, even without throwing away computational resources for simulating larger defect separations. Alternatively, it can be regarded as an inertial effect due to an effective mass that can be attributed to the defect [100]. As the defect moves with a speed v, it distorts the order parameter around it, the distortion depending on v. The part of the distortion energy quadratic in v can be regarded as an effective kinetic energy, from where the effective mass can be extracted.

First, let us concentrate on qualitative features of the flow-driving mechanism by inspecting the stress tensors (7.5) and (7.6). One is tempted to explain the easily perceived characteristic of the flow field (Fig. 7.6(a)): due to advection the $+1/2$ defect is sped up, while the flow is much weaker around the $-1/2$ defect.

As estimated in Chapter 4 and verified numerically, the "passive" β_1, β_5, and β_6 terms in the viscous stress tensor (7.6) (or their counterparts in the standard Ericksen-Leslie theory, α_1, α_5, and α_6), describing the dependence of the fluid vis-

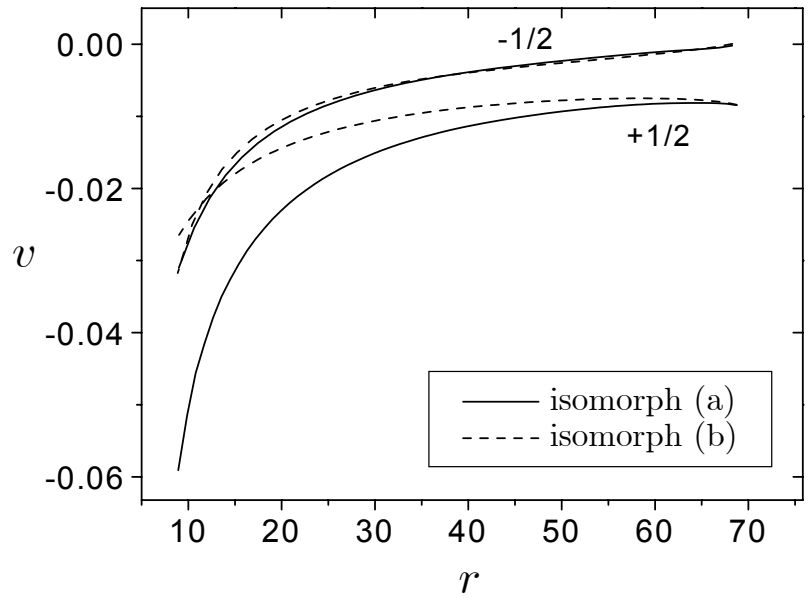

Figure 7.5 The advective contribution to the velocity of the defects for the two isomorphic cases. The surprisingly large difference between the velocities of the $+1/2$ defect is mainly due to the μ_2 viscous term. At small separations not shown, the motion driven by the order parameter dynamics (Fig. 7.4) becomes dominant.

cosity on the order parameter, give only minor quantitative effects. Therefore one can ignore them in striving to gain a qualitative picture. On the other hand, the remaining μ_1 and μ_2 terms, which contain the order parameter time derivative $\dot{\mathsf{Q}}$, and also the elastic stress tensor (7.5), represent the source driving the flow and therefore have to be analyzed carefully.

7.5.1 The flow asymmetry

At this stage, we are interested only in symmetries, i.e., the behavior of the stress tensor terms considered upon changing the order parameter field locally as to transform the $+1/2$ and $-1/2$ defects one into the other. In one elastic constant approximation, this can be achieved by mirroring the Q tensor on the axis joining the defects (the y axis, Fig. 7.1) [95]: $\mathsf{Q}_{xy} \to -\mathsf{Q}_{xy}$, since the free energy density (7.1) is left unchanged by this procedure. Any stress tensor terms, invariant with respect to this transformation, treat both defects equally and clearly do not contribute to the flow asymmetry. On the other hand, any noninvariant terms must be identified as the flow symmetry-breaking components.

By definition (7.5) the elastic stress tensor is invariant, which is a direct consequence of the elastic isotropy. As a result, the flow field is the same for both defects (Fig. 7.6(b)). In addition, its direction is such as to reduce the interdefect separation and thereby the free energy of the system. This follows immediately from the definition of any stress tensor, Eq. (2.25).

The viscous terms will be analyzed for the case $\mathbf{v} = 0$, i.e., only the driving ($\dot{\mathsf{Q}}$-

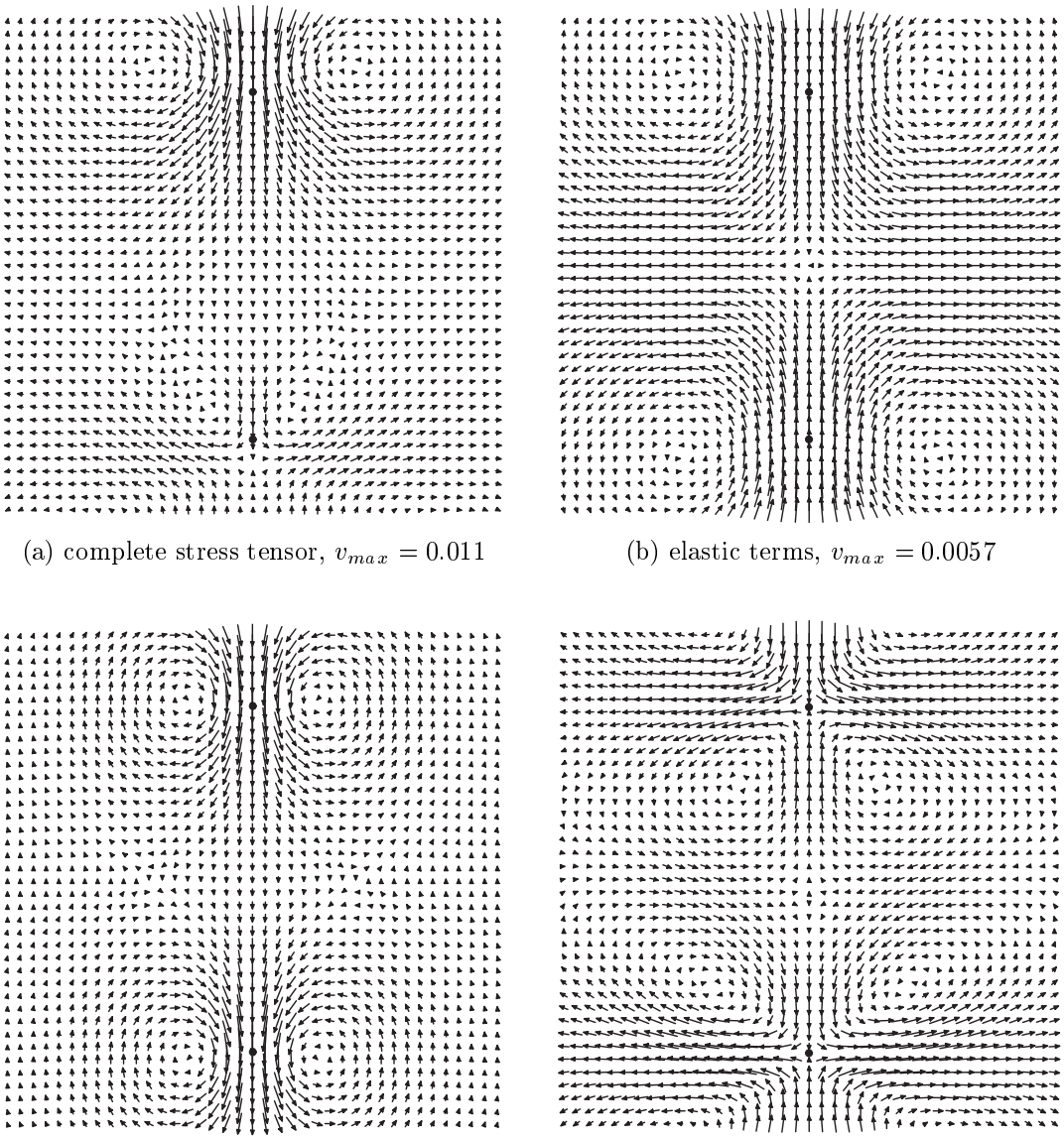

(a) complete stress tensor, $v_{max} = 0.011$

(b) elastic terms, $v_{max} = 0.0057$

(c) μ_1 term, $v_{max} = 0.0085$

(d) μ_2 term, $v_{max} = 0.0041$

Figure 7.6 Flow fields resulting from different driving stress tensor terms: (a) the complete stress tensor, (b) elastic stress, (c) the μ_1 viscous term, and (d) the μ_2 viscous term. In all cases also the isotropic β_4 viscous term is included. For clarity, the number of mesh points has been reduced by a factor of 4 in each dimension; only the central homogeneous region of the mesh is shown. The approximate positions of defects are marked with circles, the radius of the defect core is roughly four grid points. The maximum velocity magnitude v_{max} corresponding to the longest velocity vector is given for each flow field (relative to ξ/τ).

dependent) part in (7.8) will be considered. The μ_2 term has no definite symmetry for some of its components transform symmetrically and some antisymmetrically. At the defect spots the flow driven by this term is rather weak compared to the contribution from the other terms in question, because $\dot{\mathsf{Q}}$ is extremal there yielding a vanishing divergence. Hence, the μ_2 term does not give a dominant contribution to the advective motion of the defects.

On the other hand, the μ_1 term is fully antisymmetric with respect to the transformation, yielding exactly the opposite flow for the $-1/2$ defect as compared with that near the $+1/2$ defect (Fig. 7.6(c)). One notices that the flow is the strongest at the defect positions in this case. Thus, due to advection this term alone can give rise to the flow asymmetry observed. One can verify by inspecting Eqs. (7.6) and (7.7) that the relative magnitude of this antisymmetric contribution to the advective derivative term $(\mathbf{v}\cdot\nabla)\mathsf{Q}$ in (7.9) is approximately proportional to μ_1, provided that all other material parameters are kept fixed. On the other hand, scaling all viscosities equally with respect to the elastic constant leaves the dynamics unchanged completely and merely alters the characteristic time (7.19), a statement based purely on dimensional grounds (see Section 7.2).

In addition to the flow asymmetry, the annihilation process is also significantly sped up when compared to the annihilation without the flow. Following the previous discussion, this effect is caused mostly by the elastic stress driven flow. Thus, the annihilation dynamics offers a nice example showing the importance of the elastic stress in liquid crystals, which is usually considered less significant, e.g. in LC cells. Additionally, the elastic and μ_1 viscous terms act in concord near the $+1/2$ defect, whereas for the $-1/2$ defect they combine destructively. This explains the different velocity magnitudes in the vicinity of the defects (Fig. 7.6(a)).

7.5.2 Reorientation-driven defect motion vs flow advection

It is also of one's interest to quantify the ratio of defect motion due to advection as opposed to the motion propelled by the order parameter dynamics. Figures 7.4 and 7.5 show that the velocities in question are quite comparable in magnitude. Moreover, in Chapter 9, where the repulsive motion of two 1/2 disclination is studied, we find that the contribution of the advective transport to the total motion increases with the increasing interdefect separation (Fig. 9.10). We expect this to be the case also for the attraction. Once again this reflects the importance of the flow in defect dynamics as compared with the limited perturbing effects it normally has, e.g. in LC cells, Chapter 4. Furthermore, one must realize that also a secondary flow effect besides advection is important, namely the influence of the flow on the order parameter dynamics. It is clear from Fig. 7.4 that the order parameter dynamics itself is faster because of the coupling to the flow. Comparing Figs. 7.4 and 7.5 one can state that the contribution of this coupling to the flow asymmetry is less important than that of the advection, whereas its accelerating effect is just as important.

7.5.3 Influence of the director orientation angle on the flow

In one elastic constant approximation, the free energy density (7.1) and thus the order parameter dynamics are invariant with respect to a homogeneous rotation of the eigensystem of the Q-tensor in every space point. Consequently, defect pairs differing only in this constant phase angle of director rotation — let us call them *isomorphs* (Fig. 7.1) — behave exactly in the same way (e.g., for the case of a +1 defect such isomorphs are the radial and tangential defects, as well as any other form between the two). With the flow present, however, this symmetry is broken (Fig. 7.2). It is quite instructive to study the dependence of the important stress tensor terms upon such a rotation. Besides the elastic term (7.5), the μ_1 pair of terms is also left unchanged by the rotation. This is why the effect of advection should be roughly similar for all isomorphs. It is worth mentioning that also the influence of the flow on the Q-tensor given by the μ_1 term in (7.7) is not affected by the rotation.

On the other hand, the μ_2 stress tensor term is not invariant. One can see in Figure 7.5 that it introduces significant differences even as far as the advection of the defects is concerned. For general isomorphs the μ_2 term yields a flow field lacking the symmetry of reflection on the axis joining the defects. Additionally, the μ_2 term in the viscous force (7.7) is different for different isomorphs. It is due both to the different coupling of the flow to the order parameter dynamics and to the differences in advection that the isomorphs are not equivalent dynamically. As verified numerically, the β_1, β_5, and β_6 terms again bring only a very small difference.

7.6 Summary

We have studied the attraction and annihilation of straight line defects with strength $\pm 1/2$ in bulk nematics. Our approach is based on the Ericksen-Leslie-like dynamic theory for the tensor order parameter of the nematic liquid crystals. It has been shown that due to the hydrodynamic flow, the annihilation is faster and asymmetric. Further, we have identified the governing stress tensor terms: the μ_1 and μ_2 viscous terms and the elastic stress. Symmetries of the terms upon inverting the sign of the winding number and performing a homogeneous in-plane rotation of the Q-tensor eigensystem have been discussed. Both the μ_1 term and the elastic stress are invariant upon the rotation and hence identical for all isomorphs. The μ_1 term is antisymmetric with respect to changing the sign of the defects, thereby contributing dominantly to the annihilation asymmetry. On the other hand, the elastic stress is symmetric, so that it causes the annihilation process to go on faster. The only terms distinguishing between different isomorphs are the μ_2 terms in (7.6) and (7.7) (they also distinguish between the $+1/2$ and $-1/2$ defect). Thus, one can conclude that the difference in dynamics between the isomorphs is governed by the ratio μ_2/μ_1. The remaining β_1, β_5, and β_6 terms in the viscous stress tensor (7.6) introduce only inferior corrections to the flow field.

One should emphasize once more that due to length scales several orders of magnitude apart and enormous computational complexity of the problem, with the

present method one is unable to reach the >1 μm range of interdefect distances, which can be resolved in experiments. Nevertheless, it is quite reasonable to believe that the hydrodynamic effects described in this Chapter, i.e., the flow asymmetry and the reduction of the annihilation time, will be present and even stronger at larger defect separations.

8

Pair-annihilation of vortices in SmC films

Our research of defect dynamics in SmC films has been motivated by a preliminary experiment on the free-standing SmC thin film system by Link *et al.* [103–106], showing an unexpected behavior of a pair of annihilating vortices. This triggered speculations on the flow effects being responsible for it. Apart from an approximate analytical study of forces on a single defect by Pleiner [100], there have been no hydrodynamic studies of defects in SmC films reported so far. For a nonhydrodynamic treatment see the work by Pargellis *et al.* [107].

In this Chapter, we define the SmC order parameter and set the scene for an adequate description of defect dynamics in SmC films. The SmC thin film system is reduced to the XY-model. Then we show that the pair-annihilation of vortices with winding numbers ± 1 (Fig. 8.2) is accompanied by strong hydrodynamic flow, which speeds up the process as compared with the model situation without the flow, and, assisted by the elastic anisotropy, gives rise to asymmetry in defect speeds.

8.1 SmC order parameter

In the phase sequence I — N — SmA — SmC, the SmC phase occurs, if present, at the lowest temperature. In the SmA phase, the director $\mathbf{n}$ is normal to the smectic layers, whereas in the SmC phase, this symmetry is broken and the director is tilted. Experimentally most convenient liquid crystal system for the study of defects is the free-standing SmC thin film, only a few smectic layers in thickness. The projection of the director onto the smectic plane is a two-dimensional vector, called the c-director, which is the order parameter of the SmC phase. One has to point out immediately, that the c-director, despite its name, is in fact a vector, i.e., $\mathbf{c} \neq -\mathbf{c}$. The length of the vector (also called the tilt or amplitude) is the condensed quantity that becomes nonzero at the transition, while its angle (or phase) is the hydrodynamic quantity with a Goldstone mode. Originally, the c-director has been considered a unit vector, representing only the hydrodynamic degree of freedom. For description of defects, however, one must include also the variation of its length. In general, the c-director is coupled to the smectic order parameter and possesses also the nematic tensorial structure. To first approximation, both will be neglected, assuming a uniaxial nematic ordering with a constant degree of order and straight

and fixed smectic layers with a constant thickness, irrespective of the c-director.

Topological defects of the c-director are disclination lines with integer winding numbers, i.e., vortices. Half integer strengths are not allowed due to $\mathbf{c} \neq -\mathbf{c}$. In order to avoid discontinuities in the $\mathbf{c}$ field, the tilt must be allowed to vary. With that, in the defect core the system reverts locally to the SmA configuration.

It must be stressed that the order parameters of the SmC and nematic phases are fundamentally different, and it is the SmC thin film system — within the restrictions given below — rather than the nematic that is a representative of the XY-model. Therefore, it is believed that the SmC dynamics has a wider range of applicability, which essentially motivates its analysis. Moreover, the ± 1 vortex is unstable in the nematic case (Chapter 9) — it is decomposed into a repelling pair of $\pm 1/2$ disclinations, so that its dynamics cannot be followed. Thus, one has to resort to the vector order parameter to study vortices.

8.2 Dynamic equations

The starting point is the hydrodynamic theory of SmC liquid crystals proposed by Carlsson, Leslie, Stewart, and Clark [108,109]. It assumes a constant smectic layer thickness and a constant average tilt of the molecules. In order to describe the structure of the vortices, however, at least the constraint of constant tilt has to be relaxed, i.e., a slight generalization of the theory is necessary. At the same time, a substantial simplification will be made, that is, a system with variations only in two dimensions and with straight smectic layers will be assumed, eliminating the layer normal degree of freedom completely and fixing it to $\hat{\mathbf{e}}_z$. Experimentally, SmC thin films are much closer to the two-dimensional theoretical description than the nematics in Chapter 7, where the disclination lines can curve and fluctuate. Due to the thin film geometry, two spatial variables x and y, with $\nabla = \hat{\mathbf{e}}_x \partial_x + \hat{\mathbf{e}}_y \partial_y$, and a planar flow, $\mathbf{v} = v_x \hat{\mathbf{e}}_x + v_y \hat{\mathbf{e}}_y$, are assumed. Hence, we have reduced the SmC thin film system to the XY-model. It can be shown that under these assumptions, the constant-tilt SmC theory [108,109] reduces to the Ericksen-Leslie (EL) theory of the nematic liquid crystal exactly. In addition, the modulus of $\mathbf{c}$, corresponding to the sine of the tilt, will be allowed to vary [100]. We have thus arrived at a two-dimensional version of the vector order parameter dynamics, considered in Chapter 5. Nothing changes in the 2D case, except for the missing twist term in Eq. (5.1). There is, however, a principal difference in the inversion symmetry of the general 3D vector and c-director systems, stemming from the fact that in reality the 2D c-director is embedded in the 3D space and that $\mathbf{n} = -\mathbf{n}$ still holds: $\mathbf{c}$ is invariant to a global inversion $\mathbf{c} \to -\mathbf{c}$. As a result, the free energy and the dissipation of the SmC system are invariant to separate inversions of the coordinate and the order parameter, i.e., they are invariant to $\mathbf{r} \to -\mathbf{r}$, $\mathbf{c} \to \mathbf{c}$, as well as to $\mathbf{r} \to \mathbf{r}$, $\mathbf{c} \to -\mathbf{c}$, as opposed to the 3D system. For example, the distortions depicted in Fig. 8.1 are not equivalent in the general vector case, whereas in the case of the c-director defined on straight smectic layers they are identical. One just needs to flip over the smectic layers to see this. Nevertheless, this distinction does not play a role with the free

Figure 8.1 The distortions (a) and (b) of a general vector field are not equivalent, whereas in the SmC system modelled they are.

energy of the form (5.1) and the dissipation of the form (2.38), as they are already invariant to the separate inversions.

In spite of the thin film geometry, we ignore the surface terms in the free energy density. Moreover, in order to keep the number of material parameters as low as possible, we will neglect a great number of the elastic terms in Table 5.1. However, we do want to account for the splay-bend elastic anisotropy, which in SmC liquid crystals can be large due to spontaneous polarization effects [110–112]. Then the free energy density can be conveniently expressed as

$$f = \frac{1}{2}A\,c^2 + \frac{1}{4}C\,c^4 + \frac{1}{2}B_1(\nabla \times \mathbf{c})^2 + \frac{1}{2}B_2(\nabla \cdot \mathbf{c})^2. \tag{8.1}$$

By comparison with the elastic terms in Table 5.1, one can show that up to the surface terms the relations

$$B_1 = L_1, \quad B_2 = L_1 + L_2 \tag{8.2}$$

hold. Thus, disregarding the surface terms, the terms with L_4-L_8 have been consistently omitted from Eq. (8.1). Their relevance is limited to regions, where the modulus of $\mathbf{c}$ varies, i.e., to the defect cores.

In the original constant-tilt description [108], the elastic part involves 9 coefficients, which for fixed and straight smectic layers reduce to a bend and splay term only. In our case, allowing for a variation of the length of $\mathbf{c}$ the bend and splay elastic constants B_1 and B_2 are tilt-independent, Eq. (8.2). If one wanted to use a director of unit length instead of $\mathbf{c}$, Eq. (8.1) would imply the elastic constants to depend on the tilt θ as $\tilde{B}_i \propto c^2 = \sin^2\theta$, which is in accord with the symmetry considerations in [108].

The Euler-Lagrange equation for the free energy functional $\mathcal{F} = \int dV f(\mathbf{c}, \nabla\mathbf{c})$ gives the homogeneous and elastic part of the generalized force acting on the vector $\mathbf{c}$:

$$h_i = -(A + Cc^2)c_i + B_1\,\partial_j^2 c_i + (B_2 - B_1)\,\partial_i\partial_j c_j. \tag{8.3}$$

The elastic stress tensor is obtained from (8.1) using Eq. (2.26):

$$\sigma_{ij}^e = -\frac{\partial f}{\partial(\partial_i c_k)}\partial_j c_k. \tag{8.4}$$

Originally, the theory [109] involves 20 viscous terms, of which only the standard Leslie terms are left in the present limit of lateral flow, straight smectic layers and no gradients in the direction of the layer normal. Accounting in addition for the variable

length of $\mathbf{c}$, Eqs. (5.12) and (5.13) represent the proper description of the dissipative forces in our system. Nevertheless, to resort to the known material parameters, we we will reduce the number of viscous terms to the Leslie terms only, omitting the terms with the coefficients η_6 and η_9 in Eqs. (5.12) and (5.13). Again, the omitted terms affect only the core region of the defect. Hence, the viscous stress tensor is

$$\begin{aligned}\sigma^v_{ij} &= \eta_0\,\mathsf{A}_{ij} + \eta_2\,c_k c_l \mathsf{A}_{kl} c_i c_j + \tfrac{1}{2}\eta_3\,(N_i c_j - c_i N_j) + \\ &\quad \tfrac{1}{2}\eta_4\,(N_i c_j + c_i N_j) + \tfrac{1}{2}(\eta_1 - \eta_4)\,c_i \mathsf{A}_{jk} c_k + \tfrac{1}{2}(\eta_1 + \eta_4)\,\mathsf{A}_{ik} c_k c_j, \end{aligned} \tag{8.5}$$

and the generalized viscous force on the vector $\mathbf{c}$ is

$$-h^v_i = \eta_3\,N_i + \eta_4\,\mathsf{A}_{ij} c_j, \quad N_i = \dot{c}_i + \mathsf{W}_{ij} c_j, \tag{8.6}$$

with the material time derivative $\dot{\mathbf{c}} = \partial\mathbf{c}/\partial t + (\mathbf{v}\cdot\nabla)\mathbf{c}$ and the symmetric and antisymmetric parts of the velocity gradient A and W, Eq. (2.34). Although Eqs. (8.5) and (8.6) are exactly those of the Ericksen-Leslie theory (Eqs. (4.11) and (4.6)), there is a fundamental distinction in that here the viscous parameters do not depend on the condensed quantity — the tilt, whereas the original Leslie coefficients do (Eq. (5.15)).

One must emphasize, that by allowing the modulus of $\mathbf{c}$ to vary in Eqs. (8.1), (8.5), and (8.6), we make a natural generalization of the EL description to the case of the non-unit vector order parameter. Hereby we automatically recover also the correct tilt dependence of the viscous forces, which in [109] must be regulated by tilt-dependent coefficients, suggested by symmetry arguments. For nematics, in contrast, only the tensorial description will provide the proper dependence of the material parameters on the degree of order/biaxiality. Hence, it is exactly the modelled SmC film system rather than the nematic to which the EL theory applies rigorously (within the restrictions considered).

The equation of motion for the vector $\mathbf{c}$ reads briefly

$$\mathbf{h} + \mathbf{h}^v = 0. \tag{8.7}$$

Together with the generalized Navier-Stokes equation (2.41) and the incompressibility condition (2.42) it forms the set of three partial differential equations governing the dynamics of the SmC film system.

The equations are cast in dimensionless form by introducing a characteristic length, i.e., the tilt correlation length

$$\xi = \sqrt{\frac{B_0}{(A + 3Cc_0^2)}}, \tag{8.8}$$

couple of nanometers usually, and a characteristic time

$$\tau = \frac{\eta_3 \xi^2}{B_0}, \tag{8.9}$$

where $B_0 = (B_1 + B_2)/2$. The time τ is the characteristic relaxation time of the $\mathbf{c}$ deformations on the length scale of ξ, or equivalently, the dynamic time of the

modulus of **c**, typically tens of nanoseconds. In the following, dimensionless quantities will be used, i.e. $r \leftarrow r/\xi$ for length, $t \leftarrow t/\tau$ for time and $v \leftarrow v\tau/\xi$ for the velocity. Doing so, the material parameters enter the equations only through ratios given below.

8.3 Technicalities and material parameters

The numerical method is the same as in Chapter 7. The calculations were done on a square mesh, consisting of a fine homogeneous mesh of 80x80 points in the center containing both defects, and an inhomogeneous grid with increasing spacing around it to yield the total of 140x140 points. The velocity was set to zero at the boundary. In order to simulate a bulk system, the defect separation was small compared to the size of the computational area (the ratio of the two was 3/20) and the derivatives of the order parameter normal to the boundary were set to zero.

A generic set of viscous parameters in (8.5) and (8.6) was used, corresponding to the Leslie coefficients of the nematic substance MBBA [49, p. 231], with the relevant ratios $\eta_4/\eta_3 \approx -1.0$, $\eta_2/\eta_3 \approx 0.085$, $\eta_0/\eta_3 \approx 1.1$, $\eta_1/\eta_3 \approx 0.19$, The Landau coefficients A, C, and the elastic constants in (8.1) were in the ratios of $A\xi^2/B_0 \approx -0.50$, $C\xi^2/B_0 \approx 2.0$ (yielding equilibrium tilt value of 30°), with the correlation length $\xi \approx 2.4$ nm. The characteristic time $\tau \approx 88$ ns completes the set of material parameters.

Early stages of the annihilation process exhibit a dependence on the initial configuration (Fig. 8.4). Starting with the equilibrium structure containing two fixed defects, a transition period exists, during which the equilibrium configuration is changing to a dynamic one [72,86], Chapter 7. It can be also regarded as the inertial effect due to the effective mass [100], as mentioned in Chapter 7. As the relaxation time of the **c** field on the length scale of the interdefect distance R is proportional to R^2 and so is the annihilation time in the limit of $R/\xi \gg 1$, the transition period makes up roughly a constant fraction of the annihilation time, which is unpleasant as it wastes the computational resources. Therefore, a scaling technique was used to obtain a more suitable starting configuration, based on the self-similarity of the **c** field, attained when far away from the start but still in the limit $R \gg \xi$. The defects were left to annihilate to half the initial separation, followed by a rescaling of the **c** field to the initial defect separation and a short simulation run to equilibrate the tilt. This starting configuration is considered as a useful approximation — in reality, the scaling regime, where $R \propto (t_0 - t)^{1/2}$ would hold, is approached only at very large distances due to logarithmic corrections [101].

8.4 Results and discussion

First we focus on the hydrodynamic effects on the pair-annihilation in the one elastic constant approximation, $B_1 = B_2$. Significant asymmetry in the defect motion and reduction of the annihilation time as compared to the nonhydrodynamic treatment is observed (Fig. 8.3), very similar to the case of $\pm 1/2$ defects in nematics (Chapter

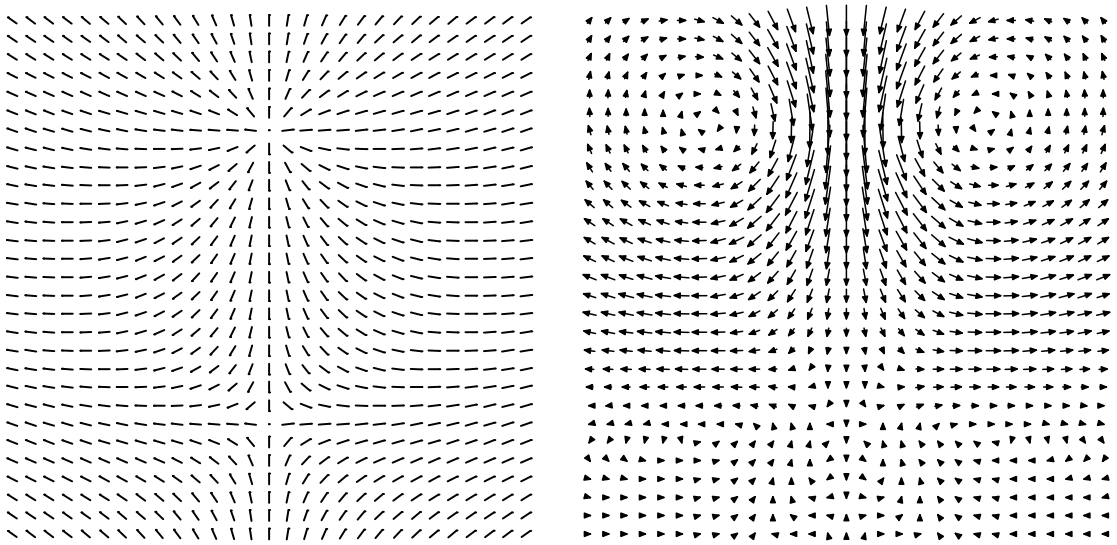

Figure 8.2 Left: radial-hyperbolic pair of annihilating ± 1 disclinations in $\mathbf{c}$ field (the grid has been coarsened for clarity, only the central region of the mesh is shown). Vector heads have been omitted for legibility; yet there is no ambiguity, since in the absence of any external fields the system is invariant under a global transformation $\mathbf{c} \to -\mathbf{c}$. Right: the central part of the corresponding flow field. The $+1$ defect is subject to strong advection, as opposed to the -1 one.

7). It is possible to understand this easily by inspecting the flow-driving terms in the stress tensor (those containing $\dot{\mathbf{c}}$): the elastic terms (8.4) and the η_3 and η_4 terms in the viscous stress (8.5). The main flow effect appears to be the advection, i.e., the hydrodynamic mass transport, which is to be discussed in the following. The viscous influence on the $\mathbf{c}$ vector comes second, though it is not negligible.

If one performs a reflection of the $\mathbf{c}$ vectors in the line joining the defects, the winding number of the defects is reversed, but the order parameter dynamics stays the same in the one elastic constant approximation. To recover the original configuration (up to an irrelevant global minus sign), a π rotation of the sample around an axis perpendicular to the film through the middle point between the defects is required. Performing the reflection on the stress tensor terms mentioned, one can verify that the η_3 term is antisymmetric (provided that the flow is generated by this term only and that the η_1 and η_2 terms are neglected), the η_4 term has no definite symmetry, while the elastic stress is symmetric by definition. This means that the flow generated by the elastic stress is symmetric with respect to the rotation about the perpendicular axis, while the one driven by the η_3 viscous term is antisymmetric (Fig. 8.5). With other words, the elastic stress driven flow carries the defects symmetrically toward each other (Fig. 8.5(b)), as in this way the free energy is reduced. Thereby it contributes to the speedup of the process. On the other hand, the flow driven by the η_3 term carries both defects with equal speeds and in the same direction, downward in Fig. 8.5(c). This is the main reason for the $+1$ defect moving

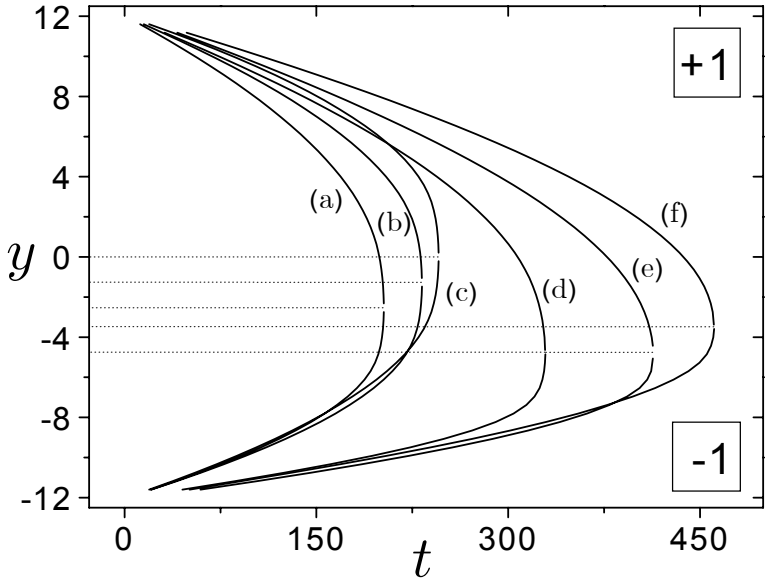

Figure 8.3 Position of the defects vs. time, measured from the initial middle point between the defects. The cases with one elastic constant: (a) RH (Fig. 8.2) and (b) TH defect pair, (c) the case without hydrodynamics, (d) RH pair with the η_3 coefficient doubled. Combined effect of flow and elastic anisotropy, with the average elastic constant B_0 fixed: (e) $B_1/B_2 = 5$ (RH), (f) $B_2/B_1 = 5$ (TH). Length and time are measured relative to $\xi \approx 2.4$ nm and $\tau \approx 88$ ns, respectively.

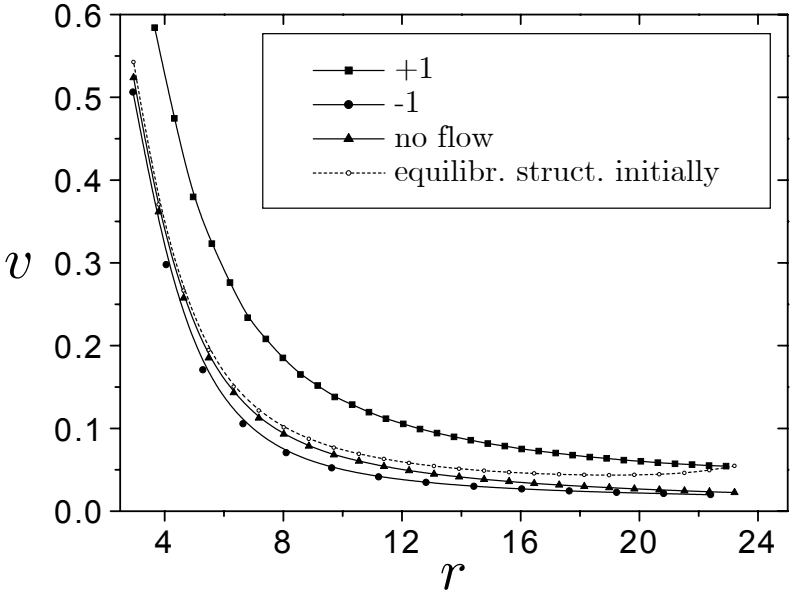

Figure 8.4 Velocity of the defects (relative to $\xi/\tau \approx 27$ nm/μs) vs. inter defect distance, one elastic constant. The +1 defect is strongly sped up by the flow, the -1 is slightly slowed down (there the flow is opposite to its motion, Fig. 8.2). Starting with the equilibrium configuration of fixed defects, a nonmonotonic behavior is observed (dashed).

faster. What is more, on this basis it can be understood why the flow near the +1 defect is much stronger as compared with that near the −1 defect (Fig. 8.5(a)): in the first case the flow fields from the two sources are added, while in the second they combine destructively. Finally, the velocity magnitude of both flows relative to the speed of defect motion just due to reorientation of $\mathbf{c}$ is proportional to η_3/η_0.

The asymmetric η_4 viscous term complicates the situation (Fig. 8.5(d)). It is this term that is mainly responsible for the different flow effect in case of different defect pairs (e.g. radial-hyperbolic (RH) vs. tangential-hyperbolic (TH, a homogeneous $\pi/2$ rotation of $\mathbf{c}$ vectors on the RH structure), Fig. 8.3 (a), (b)), since the η_3 and the elastic terms are left unchanged by the homogeneous rotation, and so is the viscous torque on the $\mathbf{c}$ vector, given by the η_3 part of the viscous force (8.6). The passive viscous terms (η_1, η_2, η_4) need not be discussed in the qualitative picture.

The asymmetry of defect motion is given rise to also by elastic anisotropy. In SmC chiral systems, this can be large due to $\mathbf{c}$-vector deformation induced gradients of polarization $\mathbf{P}$ and thus appearance of an electric charge, $e = -\nabla \cdot \mathbf{P}$. The polarization vector lies in the smectic plane, usually perpendicularly to $\mathbf{c}$, thus increasing the bend elastic constant [110]. However, in very thin systems surface polarization might dominate [112], strengthening the resistance to the splay deformation [111]. The annihilation processes at different ratios of the elastic constants are presented in Fig. 8.6, combined effect of the flow and the anisotropy is demonstrated in Fig. 8.3, curves (e) and (f). Without the flow, inverting the ratio and correspondingly changing the structure, RH $\leftrightarrow$ TH, does not change the dynamics, so it is enough to consider one type of elastic anisotropy only.

8.5 Summary

Under the restrictions mapping the SmC thin film system to the XY-model, we have reduced the SmC dynamic theory [108,109] to the EL theory. We have demonstrated, that the latter, naturally generalized to the variable modulus of the vector order parameter, exactly describes the model system containing vortices. Numerically, we have shown that the influence of hydrodynamics depends primarily on the ratio of rotational and translational viscosity η_3/η_0, controlling the hydrodynamic acceleration of the process and the defect speed asymmetry, and on the ratio η_4/η_0, breaking invariance upon configurations, differing only by a homogeneous rotation of the vectors $\mathbf{c}$. To a lesser extent, the motion asymmetry is contributed to also by the elastic anisotropy. On the other hand, rescaling the elastic constants with respect to the viscosities has no effect on the dynamics other than changing the characteristic time.

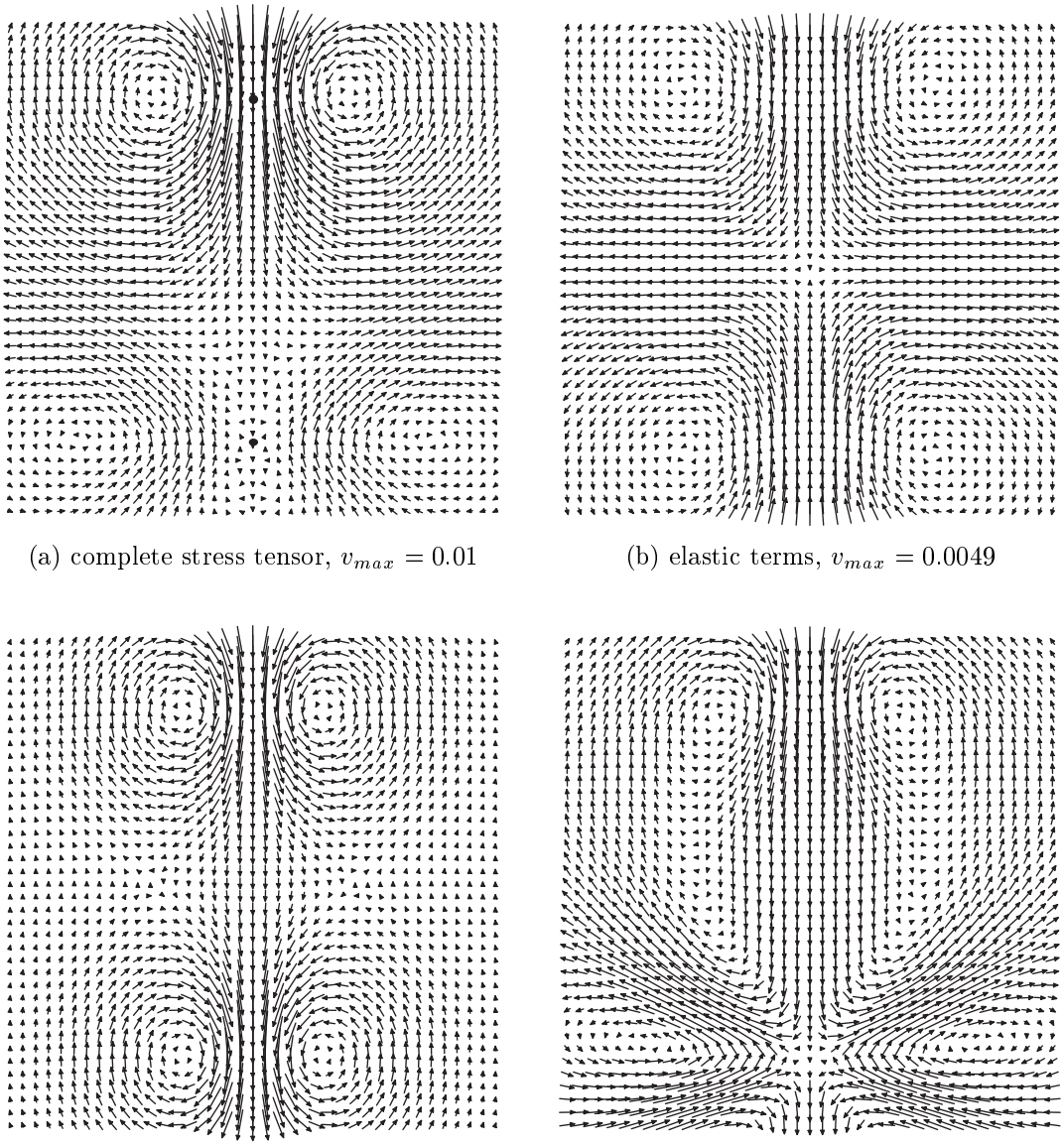

(a) complete stress tensor, $v_{max} = 0.01$

(b) elastic terms, $v_{max} = 0.0049$

(c) η_3 term, $v_{max} = 0.0043$

(d) η_4 term, $v_{max} = 0.0019$

Figure 8.5 Flow fields resulting from different driving stress tensor terms: (a) the complete stress tensor, (b) elastic stress, (c) the η_3 viscous term, and (d) the η_4 viscous term. In all cases also the isotropic η_0 viscous term is included. For clarity, the number of mesh points has been reduced by a factor of 2 in each dimension; only the central homogeneous region of the mesh is shown. In (a) the approximate positions of defects are marked with circles, the radius of the defect core is roughly two grid points. The maximum velocity magnitude v_{max} corresponding to the longest velocity vector is given for each flow field (relative to ξ/τ as defined in Eqs. (8.8) and (8.9)).

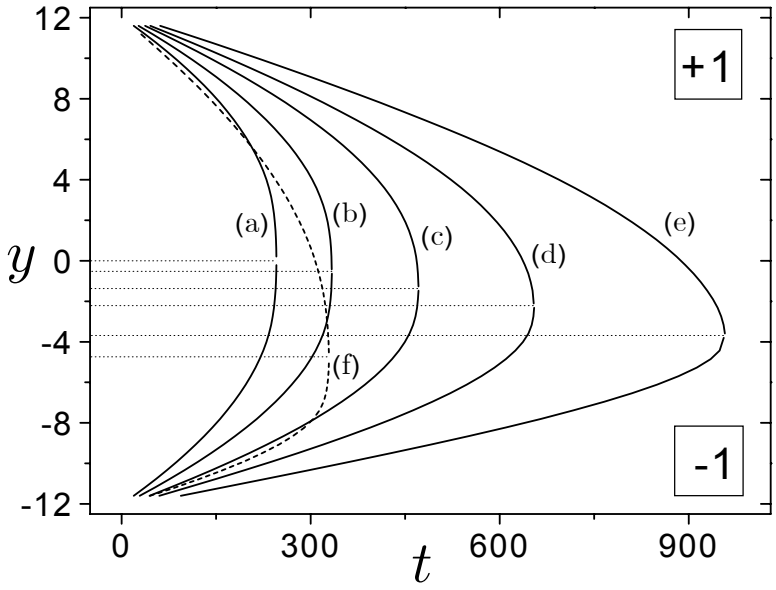

Figure 8.6 The effect of elastic anisotropy (without the hydrodynamics). The ratio of elastic constants is (a) 1, (b) 2, (c) 4, (d) 8, and (e) 16; B_0 is kept constant. (f) For comparison, the hydrodynamic one elastic constant case with η_3 doubled is shown.

9

Decay of integer disclinations in nematics

In this Chapter, we study in some respects an opposite phenomenon to the annihilation — the decay of disclinations with integer strengths and the subsequent motion of the resulting disclinations. The study has been motivated by a numerically observed instability of the strength 1 disclination line, leading to the decomposition into a pair of repelling strength 1/2 disclinations.

Like in Chapter 7, straight and infinitely long disclination lines are assumed. First we focus on the early stage of the process, performing a stability analysis of the integer strength disclination. We want to check whether there exists any local stability. Should it not, it will be interesting to see what is the nature of the fluctuations responsible for the instability, i.e., which components of the order parameter are coupled. With this intention we study the complete Q-tensor dynamics without the flow for small deviations from the initial structure.

The fluctuation problem of the strength 1 disclination line has been studied in the director description with and without variable degree of order by Ziherl and Žumer [113,114]. In the former case, a model radial profile for the scalar order parameter was assumed, but with an incorrect behavior near the origin. In the spherical geometry, the stability of a radial point defect (hedgehog) has been studied in [115] by constructing a specific perturbation without solving the eigenmode problem, and in [116] by assuming the Lyuksyutov's constraint [117] and a restriction to a subspace of perturbations. We solve a general linearized Q-tensor fluctuation problem for a disclination line with any integer winding number. This enables us to find the growing fluctuations, which are responsible for the instability of the integer disclination. For the strength 1 disclination, we determine the correction to the growth rate of the critical fluctuations due to the flow. In the nonlinear regime, we study numerically the influence of the flow on the repulsive motion of the $\pm 1/2$ disclinations, created after the decay of the strength ± 1 disclination.

9.1 Fluctuation problem

In this Section, we study the dynamics of perturbations of a long and straight nematic disclination line with a general integer winding number. Cylindrical coordi-

nates (r, ϕ, z) with corresponding orthonormal base vectors $(\hat{\mathbf{e}}_r, \hat{\mathbf{e}}_\phi, \hat{\mathbf{e}}_z)$ will be used. The disclination line coincides with the z axis.

In the one elastic constant approximation (9.3), the free energy is invariant upon a homogeneous rotation of the Q-tensor. This implies that the Q-eigensystem will rotate as $\psi = \psi_0 + (s-1)\phi$ with respect to the above base vectors when we encircle a defect of strength s located at the origin; ψ is the angle between the director and $\hat{\mathbf{e}}_r$ and ψ_0 is the free parameter of the defect configuration, corresponding to the angle between the director at $\phi = 0$ and the x axis (e.g., for $+1$ defects $\psi_0 = 0$ represents the radial defect, while the circular one has $\psi_0 = \pi/2$). There is no dependence on ϕ other than this rotation, i.e., the scalar invariants of Q (the degree of order and biaxiality) are independent of ϕ. It is due to this generalized cylindrical symmetry of the unperturbed defect structure that the eigenmode problem is tractable.

Let us define another orthonormal triad $(\hat{\mathbf{e}}_1, \hat{\mathbf{e}}_2, \hat{\mathbf{e}}_z)$,

$$\begin{bmatrix} \hat{\mathbf{e}}_1 \\ \hat{\mathbf{e}}_2 \end{bmatrix} = \begin{bmatrix} \cos\psi & \sin\psi \\ -\sin\psi & \cos\psi \end{bmatrix} \begin{bmatrix} \hat{\mathbf{e}}_r \\ \hat{\mathbf{e}}_\phi \end{bmatrix}. \tag{9.1}$$

With this, in the unperturbed configuration (or ground state, as referred to below) the Q-tensor eigensystem coincides with the triad everywhere. Further, we define the five orthonormal symmetric traceless base tensors [118–120], Fig. 9.1,

$$\begin{aligned} \mathsf{T}_0 &= 1/\sqrt{6}(3\hat{\mathbf{e}}_z \otimes \hat{\mathbf{e}}_z - \mathsf{I}), \\ \mathsf{T}_1 &= 1/\sqrt{2}(\hat{\mathbf{e}}_1 \otimes \hat{\mathbf{e}}_1 - \hat{\mathbf{e}}_2 \otimes \hat{\mathbf{e}}_2), \\ \mathsf{T}_{-1} &= 1/\sqrt{2}(\hat{\mathbf{e}}_1 \otimes \hat{\mathbf{e}}_2 + \hat{\mathbf{e}}_2 \otimes \hat{\mathbf{e}}_1), \\ \mathsf{T}_2 &= 1/\sqrt{2}(\hat{\mathbf{e}}_z \otimes \hat{\mathbf{e}}_1 + \hat{\mathbf{e}}_1 \otimes \hat{\mathbf{e}}_z), \\ \mathsf{T}_{-2} &= 1/\sqrt{2}(\hat{\mathbf{e}}_z \otimes \hat{\mathbf{e}}_2 + \hat{\mathbf{e}}_2 \otimes \hat{\mathbf{e}}_z), \end{aligned} \tag{9.2}$$

with $\mathrm{Tr}(\mathsf{T}_i \mathsf{T}_j) = \delta_{ij}$. By virtue of the definition (9.1), the resulting eigenmode equations will be independent of ψ_0, but will depend on the winding number s through spatial derivatives of the base tensors (9.2).

In one elastic constant approximation, Eq. (7.1), the standard free energy density in terms of Q reads

$$f = \tfrac{1}{2}A\,\mathrm{Tr}\mathsf{Q}^2 + \tfrac{1}{3}B\,\mathrm{Tr}\mathsf{Q}^3 + \tfrac{1}{4}C\,(\mathrm{Tr}\mathsf{Q}^2)^2 + \tfrac{1}{2}L\,\mathrm{Tr}(\nabla\mathsf{Q}\cdot\nabla\mathsf{Q}), \tag{9.3}$$

where in the last term the contraction over the gradient components is denoted by the dot. Expressing the Q-tensor as

$$\mathsf{Q}(\mathbf{r}, t) = a_i(\mathbf{r}, t)\mathsf{T}_i(\mathbf{r}), \quad i = -2, -1, 0, 1, 2, \tag{9.4}$$

and inserting it into Eq. (9.3) while being careful with the gradient $\nabla = \hat{\mathbf{e}}_r\partial/\partial r + \hat{\mathbf{e}}_\phi\partial/r\partial\phi$ of the base tensors, f is expressed in terms of the tensor components a_i. The balance of generalized forces leads to the equations of motion for the components a_i, in a dimensionless form:

$$\mu_1\dot{a}_i = \nabla\cdot\frac{\partial f}{\partial\nabla a_i} - \frac{\partial f}{\partial a_i} = \frac{\partial}{\partial r}\frac{\partial f}{\partial\frac{\partial a_i}{\partial r}} + \frac{1}{r}\frac{\partial f}{\partial\frac{\partial a_i}{\partial r}} + \frac{\partial}{r\partial\phi}\frac{\partial f}{\partial\frac{\partial a_i}{r\partial\phi}} - \frac{\partial f}{\partial a_i}. \tag{9.5}$$

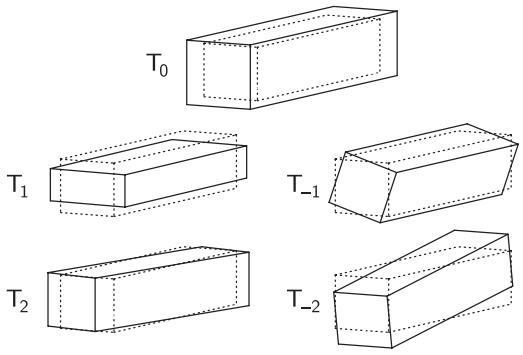

Figure 9.1 Schematic representation of the perturbations described by the base tensors (9.2) for a uniaxial distribution with a positive degree of order (dashed). The Q-tensor eigensystem is represented by the box, the length of the edges corresponds to the eigenvalue (plus a constant). The long axis of the box (usually called the director) is parallel to $\mathbf{e}_z$. T_0 describes a perturbation of the degree of order, T_1 describes a biaxial perturbation, T_{-1}, T_2, T_{-2} represent rotations of the eigensystem. The interpretation of the perturbations varies according to which of the axes has been identified with the director. Irrespective of this, the perturbations given by T_{-1}, T_2, and T_{-2} possess Goldstone modes, while those given by T_0 and T_1 are massive.

By symmetry, the ground state consists solely of the components a_0 and a_1, as opposed to perturbations, where all the components are allowed. According to Eq. (9.5), the ground state components, $q_0 = a_0$, $q_1 = a_1$, satisfy

$$\frac{\partial^2 q_0}{\partial r^2} + \frac{1}{r}\frac{\partial q_0}{\partial r} - \frac{A}{L}\,q_0 - \frac{1}{\sqrt{6}}\frac{B}{L}\,(q_0^2 - q_1^2) - \frac{C}{L}(q_0^2 + q_1^2)q_0 = 0, \tag{9.6}$$

$$\frac{\partial^2 q_1}{\partial r^2} + \frac{1}{r}\frac{\partial q_1}{\partial r} - \frac{4s^2}{r^2}\,q_1 - \frac{A}{L}\,q_1 + \sqrt{\frac{2}{3}}\frac{B}{L}\,q_0 q_1 - \frac{C}{L}(q_0^2 + q_1^2)q_1 = 0, \tag{9.7}$$

and in the vicinity of $r = 0$ behave as

$$q_0 \approx c_0 + c_2\, r^2, \quad q_1 \approx b\, r^{|2s|}, \tag{9.8}$$

with $c_2 = c_0(A + Bc_0/\sqrt{6} + Cc_0^2)/4$ and c_0, b extracted from the numerical solution if needed. Putting

$$a_i(\mathbf{r}, t) = \begin{cases} q_i(\mathbf{r}) + x_i(\mathbf{r}, t) & ; \quad i = 0, 1 \\ x_i(\mathbf{r}, t) & ; \quad i = -1, 2, -2 \end{cases}, \tag{9.9}$$

where $q_{0,1}$ are the ground state components and x_i are the perturbations, $x_i \ll q_{0,1}$, and linearizing the equations (9.5), one obtains two groups of coupled linear equations for the perturbations x_i:

$$\dot{x}_0 = \nabla^2 x_0 - f_0(r)\, x_0 + f_{01}(r)\, x_1, \tag{9.10}$$

$$\dot{x}_1 = \nabla^2 x_1 - \frac{4s^2}{r^2} x_1 - \frac{4s}{r^2}\frac{\partial x_{-1}}{\partial \phi} - f_1(r)\, x_1 + f_{01}(r)\, x_0, \tag{9.11}$$

$$\dot{x}_{-1} = \nabla^2 x_{-1} - \frac{4s^2}{r^2} x_{-1} + \frac{4s}{r^2}\frac{\partial x_1}{\partial \phi} - f_{-1}(r)\, x_{-1}, \tag{9.12}$$

and

$$\dot{x}_2 = \nabla^2 x_2 - \frac{s^2}{r^2} x_2 - 2s\frac{\partial x_{-2}}{\partial \phi} - f_2(r)\, x_2, \tag{9.13}$$

$$\dot{x}_{-2} = \nabla^2 x_{-2} - \frac{s^2}{r^2} x_{-2} + 2s\frac{\partial x_2}{\partial \phi} - f_{-2}(r)\, x_{-2}, \tag{9.14}$$

where $\nabla^2 x = \frac{\partial^2 x}{\partial r^2} + \frac{1}{r}\frac{\partial x}{\partial r} + \frac{\partial^2 x}{r^2 \partial \phi^2}$ is the Laplacian in cylindrical coordinates and

$$\begin{aligned} f_0(r) &= A + \sqrt{2/3} B q_0 + C(3q_0^2 + q_1^2), \\ f_1(r) &= A - \sqrt{2/3} B q_0 + C(q_0^2 + 3q_1^2), \\ f_{-1}(r) &= A - \sqrt{2/3} B q_0 + C(q_0^2 + q_1^2), \\ f_{01}(r) &= (\sqrt{2/3} B - 2C q_0) q_1, \\ f_{\pm 2}(r) &= A + B/\sqrt{6}(q_0 \pm \sqrt{3} q_1) + C(q_0^2 + q_1^2). \end{aligned} \tag{9.15}$$

In Eqs. (9.10)-(9.15), dimensionless quantities have been introduced: $r \leftarrow r/\xi$, $t \leftarrow t/\tau$, $(A, B, C) \leftarrow (A, B, C)\xi^2/L$, with the correlation length of the degree of order (7.18) and the characteristic time (7.19). It is worth pointing out that there is no difference between defects with strengths s and $-s$ except for two minus signs, which can be absorbed in the base tensors, i.e., $s \to -s$ and $\mathsf{T}_{-1,-2} \to -\mathsf{T}_{-1,-2}$ conserves the equations (9.10)-(9.15).

9.1.1 Fluctuation eigenmodes

The eigensolutions of the systems (9.10)-(9.12) and (9.13)-(9.14) are sought by separation of variables using the ansätze (we write $\cos(m\phi)$ instead of $C_1 \cos(m\phi) + C_2 \sin(m\phi)$, m is an integer)

$$\left\{ \begin{array}{c} x_0 \\ x_1 \\ x_{-1} \end{array} \right\} = \left\{ \begin{array}{c} R_0(r)\cos(m\phi) \\ R_1(r)\cos(m\phi) \\ R_{-1}(r)\sin(m\phi) \end{array} \right\} \exp(-\lambda t), \tag{9.16}$$

$$\left\{ \begin{array}{c} x_2 \\ x_{-2} \end{array} \right\} = \left\{ \begin{array}{c} R_2(r)\cos(m\phi) \\ R_{-2}(r)\sin(m\phi) \end{array} \right\} \exp(-\lambda t). \tag{9.17}$$

Proper combinations of the angular functions have been chosen in (9.16) and (9.17) to satisfy the equations. One could also include a factor $\cos(kz)$ and add the dependence on z to Eqs. (9.10)-(9.14), which is only through $\partial^2/\partial z^2$ in the Laplacian, so that the z coordinate is easily separated. Then the eigenvalue λ (the inverse time constant) would be

$$\lambda = \lambda_r + k^2, \tag{9.18}$$

where λ_r is the eigenvalue of the radial and angular part. This time we are not interested in the z dependence and have omitted it from the equations for brevity.

In either case, only eigenvalue systems for the radial functions $R_i(r)$ remain, where λ_r is the eigenvalue (we write λ instead of λ_r):

$$\nabla^2 R_0 + \left(\lambda - f_0(r) - \frac{m^2}{r^2}\right) R_0 + f_{01}(r)\, R_1 = 0, \tag{9.19}$$

$$\nabla^2 R_1 + \left(\lambda - f_1(r) - \frac{m^2{+}4s^2}{r^2}\right) R_1 - \frac{4sm}{r^2}\, R_{-1} + f_{01}(r)\, R_0 = 0, \tag{9.20}$$

$$\nabla^2 R_{-1} + \left(\lambda - f_{-1}(r) - \frac{m^2{+}4s^2}{r^2}\right) R_{-1} - \frac{4sm}{r^2}\, R_1 = 0, \tag{9.21}$$

and

$$\nabla^2 R_2 + \left(\lambda - f_2(r) - \frac{m^2{+}s^2}{r^2}\right) R_2 - \frac{2sm}{r^2}\, R_{-2} = 0, \tag{9.22}$$

$$\nabla^2 R_{-2} + \left(\lambda - f_{-2}(r) - \frac{m^2{+}s^2}{r^2}\right) R_{-2} - \frac{2sm}{r^2}\, R_2 = 0. \tag{9.23}$$

One notices that the three- and two-function operators (9.10)-(9.12) and (9.13)-(9.14) are self-adjoint, implying real eigenvalues and orthogonal eigenmodes. These must be solved for numerically, either by discretization, Bessel-function expansion, relaxation, or shooting. Although for linear systems the first two methods would usually be preferred [121], we decide to use the shooting procedure [54, p. 582] as it is simple and quite efficient when only a few eigenfunctions are searched for. In what follows, we will focus our attention to possible growing modes, i.e., those for which $\lambda < 0$.

Due to the singularity of the cylindrical coordinates, the behavior of the radial eigenfunctions near the origin must be determined analytically prior to numerically solving the eigensystems (9.19)-(9.23). One makes use of the ground state expansion (9.8), which enters the functions f_i. The unknown coefficients of the radial eigenfunction expansion have to be determined together with the eigenvalue λ. For numerical reasons, we restrict the eigenmodes to vanish at an arbitrary, but not too large a value of $r = r_0$. The modes concerned are localized and hence remain unaffected by the restriction, if only r_0 is large enough compared to the characteristic decay length of the mode. For nonlocalized modes the restriction corresponds to a physical cylindric confinement of the defect with strong anchoring; in this case, however, no numerical difficulties prevent r_0 from larger values. Thus, starting with the analytic expansion of the radial functions and a trial value of λ, the equations are integrated to r_0 by a Runge-Kutta method with an adaptive step size [54], where it is required that $R_i(r_0) = 0$. With n radial functions coupled, there are n unknown coefficients of expansion, one of which is arbitrary. Together with λ this gives n free parameters, which in the shooting procedure are determined by the n ending conditions.

9.1.2 Eigenmodes leading to decay

The modes responsible for the decay do not involve the components x_2 or x_{-2}, since by symmetry the Q-tensor eigensystem does not get rotated out of the xy plane in

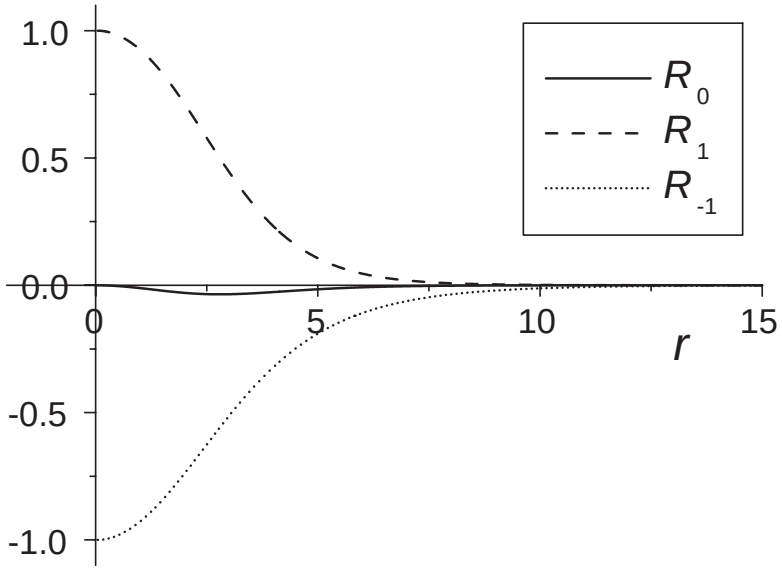

Figure 9.2 Radial eigenfunctions of the growing fluctuation, $s = 1$, $m = 2$, $\lambda \approx -0.22$. The length unit is $\xi = 2.11$ nm, the time unit is $\tau = 32.6$ ns. The fastest growing mode leading to the escape of the defect has $\lambda \approx -0.0042$.

this process. Therefore, the system (9.10)-(9.12) must be examined. The lowest-order expansion of the system (9.19)-(9.21) around the origin does not involve the ground state coefficients (9.8), but requires

$$R_0 \approx r^m, \quad R_{\pm 1} \approx \begin{cases} \pm a_1 \, r^{|m-2s|} \\ a_2 \, r^{|m+2s|} \end{cases}, \tag{9.24}$$

where the two solutions for R_1 and R_{-1} are independent and the coefficients a_1, a_2 must be determined together with the eigenvalue.

We study in detail the simplest case, i.e., the decay of the ± 1 defect. Then we make a generalization to defects of higher integer strengths. In the case of the decay of the ± 1 defect to two $\pm 1/2$ defects, the modes in question must exhibit a quadrupolar symmetry, which sets $m = 2$ in the angular part of Eq. (9.16). A single growing mode ($\lambda \approx -0.22$) is found (Figs. 9.2 and 9.3), which is localized within a few correlation lengths, while all the others (including those with different m) are decaying and nonlocalized. Due to the localization, the growing mode cannot be affected by any confinement unless it comes down to the ξ scale — it is an intrinsic feature of the defect structure. It is no sooner than at a confinement of $r_0 \approx 3.5\xi$ that the mode becomes decaying.

More precise, and applying to any integer strength, it is the function R_{-1} that is localized if and only if the eigenmode is of the growing type, which can be seen from its asymptotic behavior

$$R_{-1} \asymp r^{-1/2} \, e^{\pm\sqrt{-\lambda}\, r}. \tag{9.25}$$

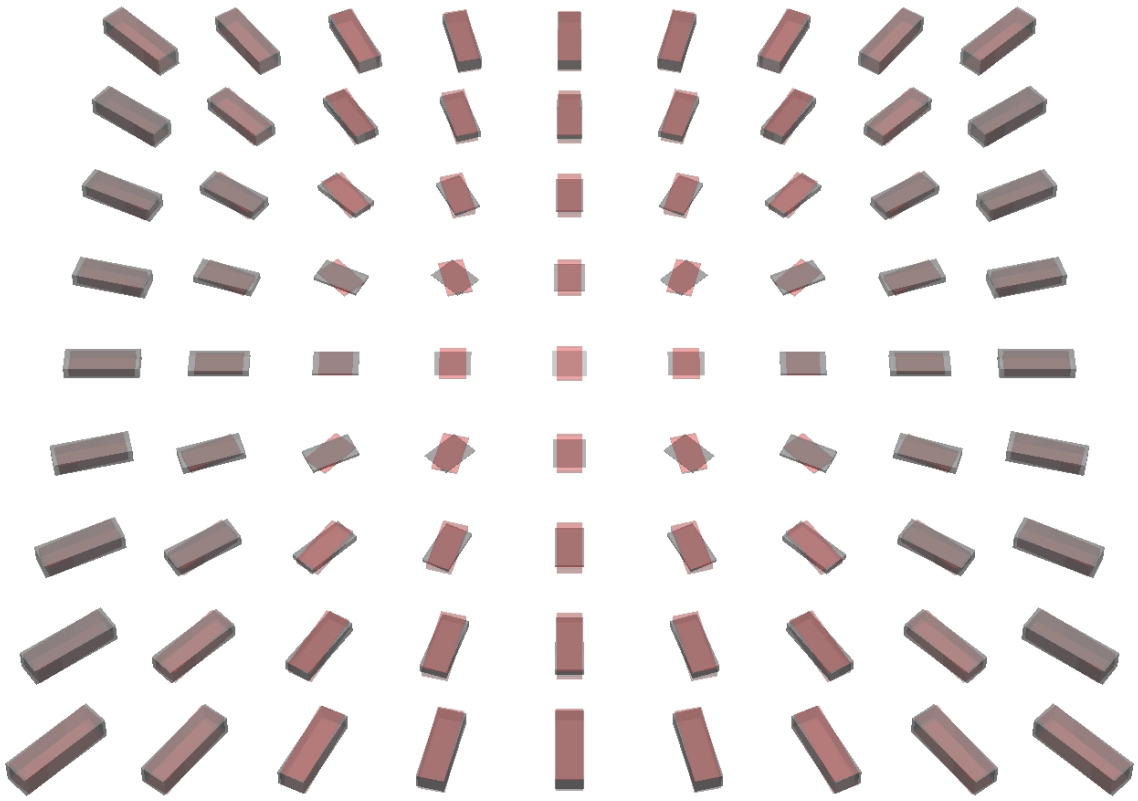

Figure 9.3 Cross section through the disclination line with $s = 1$: the ground state (gray) is perturbed by the growing mode (red, shown exaggerated), leading to two 1/2 disclinations on the x axis.

The functions R_0 and R_1 are found to be localized also for the decaying modes in the region of low enough λ. Significantly, the modes with $\lambda < 0$ have a discrete spectrum, whereas the spectrum of those with $\lambda > 0$ is continuous. Thus, the growing modes can be counted.

One can test the time evolution of the growing mode in a pure numeric simulation. Regardless of the initial perturbation, i.e., if only it contains a nonzero projection onto the growing mode, an exponential growth of any quantity linearly depending on the mode amplitude is observed after a short transient (decay of other modes), with a time constant very close to λ.

It is instructive to study the influence of the hydrodynamic flow generated by the order parameter dynamics on the growth rate of the mode. This is performed numerically, where the coupling of the flow and Q-tensor fields is described by the tensorial version of the Ericksen-Leslie theory [92], Chapter 7. The one elastic constant approximation is used, the numerical method and the material parameters are the same as in Chapter 7. It is found that the hydrodynamic correction to the growth rate is small, i.e., less than 5%, speeding up the modes. The correction is expected to be small, since the velocity of the flow generated decreases with decreasing Q (that is, decreasing $\mathrm{Tr}\mathsf{Q}^2$), as does its influence on Q (Eqs. (7.6) and (7.7)). At the same time, one should be quite reserved, since the description of the flow-to-Q-tensor coupling [92] is not complete [122], and the missing terms [123] could play an important role in the dynamics of the defect core. Besides, one must also realize that the applicability of hydrodynamic equations is questionable at length and time scales that small (1 nm, 10 ns).

In the case of defects with higher strengths there is an increasing number of growing modes, as there are more and more ways the defect can decay. It turns out that for every decomposition allowed topologically, one can find at least one growing mode, provided that none of the resulting winding numbers is too high. Each of these modes exhibits a distinctive angular symmetry, set by its value of m. Generally, a defect of strength $\pm s$ decays to m symmetrically placed $\pm 1/2$ defects surrounding a $\pm s \mp m/2$ defect, which remains in the center (Fig. 9.4). For example, a possible decay channel of a defect with strength 2 is: $2 \to -1 + 6 \times 1/2$, where the -1 defect stays in the middle, surrounded by the $1/2$ defects. The corresponding mode has a sixfold symmetry, $m = 6$. On the other hand, the $+2$ defect is stable with respect to the decay $2 \to -3/2 + 7 \times 1/2$ and higher. All possible decay paths of defects with strengths 2 and 3 are given in Tables 9.1 and 9.2. The decay to $\pm 1/2$ defects only is always the fastest.

In principle, there is no limitation to the winding numbers. There are, however, two technical points. Firstly, the core size of the defect increases proportionally to its strength s, which gets time and space consuming with progressing winding numbers. Secondly, more terms should be added to the expansion (9.24) to reach better accuracy, required particularly for the localized modes with higher values of m. The series is more complicated in this case, as it contains both the ground state coefficients (9.8) and the eigenvalue λ. It is beyond our aim to pursue accuracy issues here.

Instead, one must emphasize an important point regarding the numeric simu-

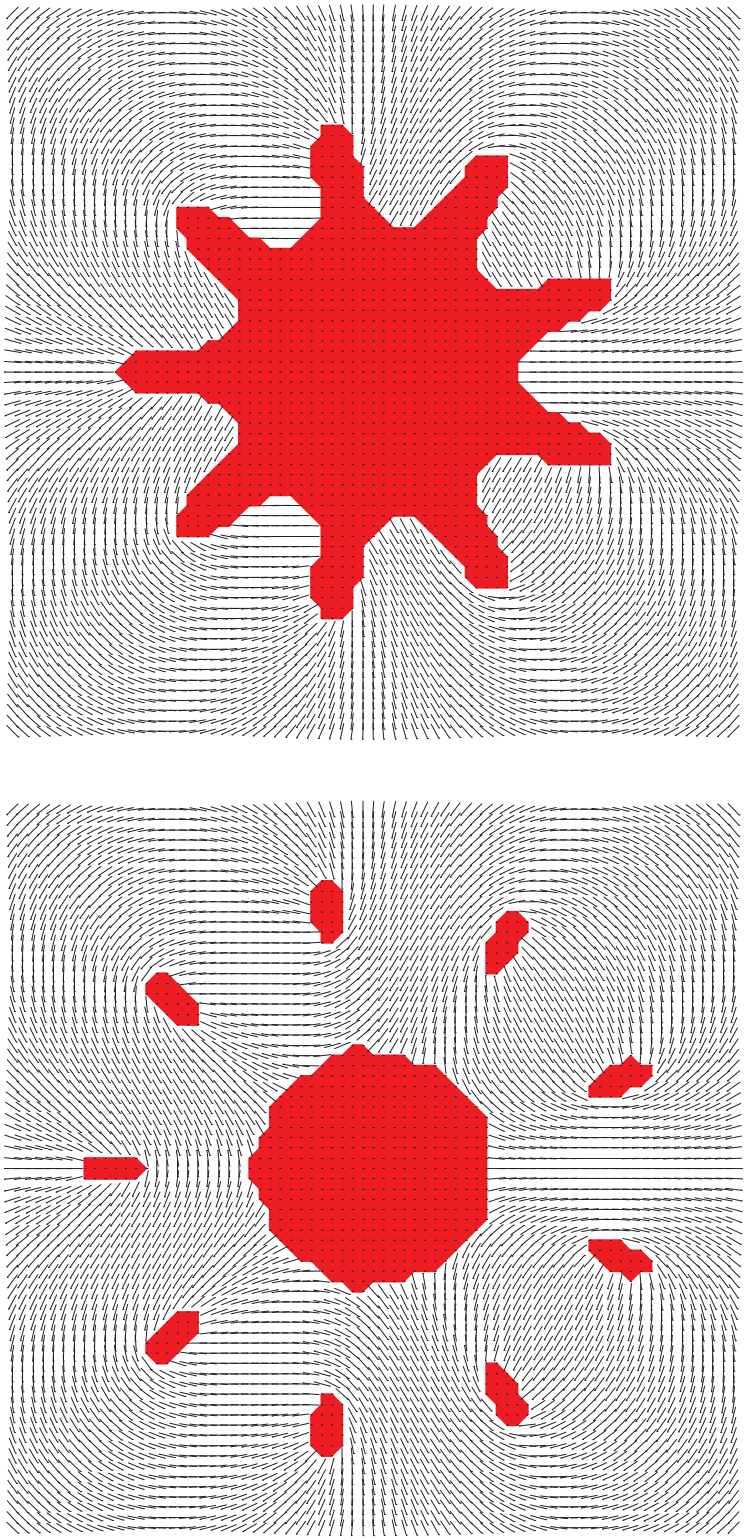

Figure 9.4 A ninefold ($m = 9$) decay of the $s = 3$ defect. On the lower diagram we can see a -3/2 defect in the center and nine 1/2 defects around it.

decay	m	$-\lambda$
$1 \to 2 \times 1/2$	2	0.22
$2 \to 1 + 2 \times 1/2$	2	0.066
$2 \to 1/2 + 3 \times 1/2$	3	0.23
$2 \to 4 \times 1/2$	4	0.39
$2 \to -1/2 + 5 \times 1/2$	5	0.23
$2 \to -1 + 6 \times 1/2$	6	0.045

Table 9.1 Fastest decay modes with a given m of the $s = 1, 2$ disclination lines

decay	m	$-\lambda$
$3 \to 2 + 2 \times 1/2$	2	0.043
$3 \to 3/2 + 3 \times 1/2$	3	0.15
$3 \to 1 + 4 \times 1/2$	4	0.26
$3 \to 1/2 + 5 \times 1/2$	5	0.36
$3 \to 6 \times 1/2$	6	0.45
$3 \to -1/2 + 7 \times 1/2$	7	0.36
$3 \to -1 + 8 \times 1/2$	8	0.26
$3 \to -3/2 + 9 \times 1/2$	9	0.14
$3 \to -2 + 10 \times 1/2$	10	0.012

Table 9.2 Fastest decay modes with a given m of the $s = 3$ disclination line

lation of defects with winding numbers higher than 1. The square grid standardly used in simulations reduces the symmetry of the space to a fourfold symmetry only, i.e., $C_\infty \to C_4$. If a growing mode is invariant under C_4 ($m = 4, 8, 12, ...$), it will experience an artificial boost from the grid, such that its growth rate will not vanish with vanishing amplitude! Now, as soon as the spectrum contains a single such mode, it will overwhelm other possibly faster modes, leading to an artificial fourfold decay of the defect. An example of such decay is shown in Fig.s 9.5 and 9.6. To envisage the origin of the boost it is appropriate to ask why there is not any with a non fourfold-symmetric mode. In this case, the rotations of C_4 generate at least two different modes, as opposed to the identity representation in the previous case. These are degenerated with respect to their placement on the grid, since the grid is invariant to C_4. Therefore, in a pure ground state neither must be favored and hence their growth rate must vanish at zero amplitude. Since all defect structures except the ± 1 one possess fourfold-symmetric growing modes, the numerical simulation of the mode dynamics is only possible for the ± 1 defect.

9.1.3 Eigenmodes leading to escape

In an unconfined system, planar defects of integer strengths can escape to the undeformed configuration with a zero deformation free energy (escape in the third dimension) [68,69]. The issues concerning the (meta)stability of defect cores have

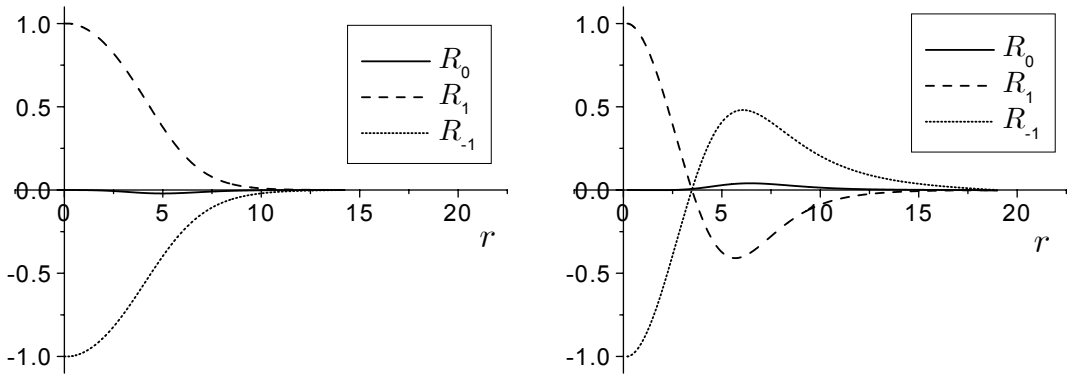

Figure 9.5 Radial eigenfunctions of the growing modes with $m = 4$ for the $s = 2$ defect: (a) $\lambda \approx -0.39$, (b) $\lambda \approx -0.035$

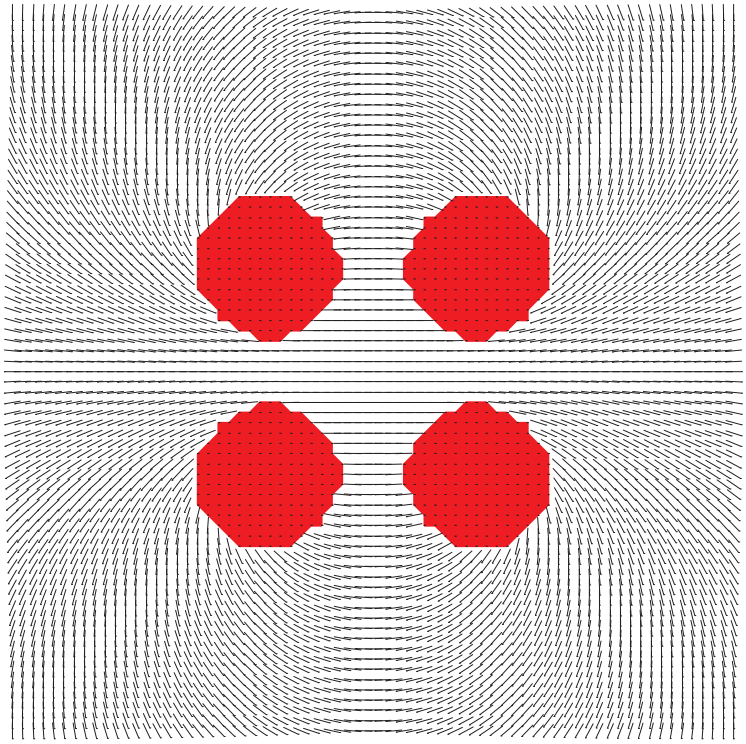

Figure 9.6 Decay of the $s = 2$ defect to four $1/2$ defects, $m = 4$; the corresponding radial eigenfunctions are depicted in Fig. 9.5. The four-fold-symmetric ($m = 4$) modes are numerically boosted due to the fourfold ($m = 4$) symmetry of the computational grid.

been addressed by R. Meyer [69] in 1973. At that time the tensorial defect structure had not been presented yet, so a direct answer could not have been given. Equipped with the present formalism, one should look for another type of possibly growing modes leading to the escape. As here the Q-tensor eigensystem is rotated out of the xy plane, the system (9.13)-(9.14) must be examined this time. In particular, one expects the perturbation x_2 to be crucial, as it corresponds to a rotation of the director out of the plane. The lowest-order expansion of the system (9.22)-(9.23) around the origin is

$$R_{\pm 2} \approx \begin{cases} \pm a_1\, r^{|m-s|} \\ a_2\, r^{|m+s|} \end{cases}, \tag{9.26}$$

the ratio of a_1 and a_2 is determined together with the eigenvalue in the shooting procedure as before. For $m = 0$ the equations (9.22) and (9.23) are decoupled. It is indeed in this case that one finds $\lambda < 0$ and the discrete spectrum for all the modes x_2. The modes x_{-2} are decaying, as are all the other modes with $m \neq 0$.

Noting that $f_2(r \gg \xi) \to 0$ and $f_{-2}(r \gg \xi) \to f_{-2}(\infty) > 0$, the general asymptotic behavior is

$$R_2 \asymp r^{-1/2}\, e^{\pm\sqrt{-\lambda}\, r}, \quad R_{-2} \asymp r^{-1/2}\, e^{\pm\sqrt{f_{-2}(\infty)-\lambda}\, r}, \tag{9.27}$$

i.e., R_2 is localized for $\lambda < 0$. It turns out that here the localized modes are much more extensive than those of the decay.

One may think there is little point in studying the decay if the defects are always unstable to the escape. There exist, however, a large difference in growth rates of the two types of unstable modes, connected with the large difference in localization. In the case of the strength ± 1 defect the decay is approximately 53-times faster than the escape. Whence, provided we prepared the configuration with the strength ± 1, it would always decay before it could even start escaping. Of course, it is just due to the fast decay that the initial configuration is very hard to prepare.

9.1.4 Remarks on the fluctuation problem

The eigenmode problem has been solved in the one elastic constant approximation. Beyond this approximation, one would have to include more elastic terms in the free energy density (9.3). There is only one additional bulk term quadratic in Q and in the first derivative: $(\partial_i \mathsf{Q}_{ik})(\partial_j \mathsf{Q}_{jk})$. It distinguishes between the splay and bend distortions (relevant for the decay) only if the scalar invariants of Q vary, which does take place in our case. To distinguish between the splay and bend in the uniaxial limit with constant degree of order, however, one has to include the third-order term $\mathsf{Q}_{ij}(\partial_i \mathsf{Q}_{kl})(\partial_j \mathsf{Q}_{kl})$. In both cases the generalized cylindrical symmetry of the ground state is lost, making the eigenmode problem two-dimensional, i.e., the variables r and ϕ cannot be separated any longer. It is only in the case of the $+1$ disclination with $\psi_0 = 0$ or $\psi_0 = \pi/2$ (radial and circular disclinations) that the cylindrical symmetry is retained, so that without the third-order term the separation would still be possible. The third-order term, however, brings about mixed derivatives, which inevitably prevent the separation.

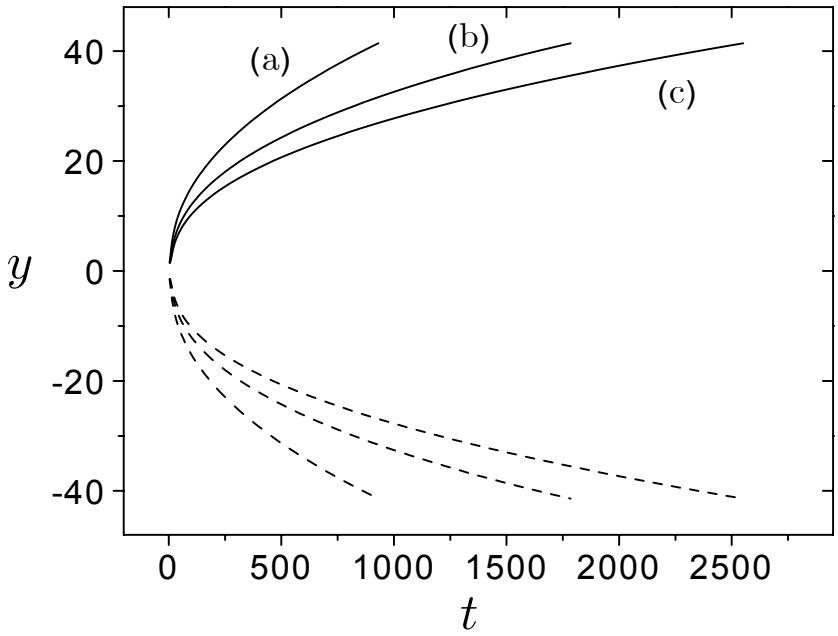

Figure 9.7 Position of the repelling defects as a function of time, after the strength (a) 1 and (b) -1 defects has decayed: (a) 1/2 defects, (b) $-1/2$ defects, and (c) the degenerate case without the flow. Recall that the length unit is $\xi = 2.11$ nm and the time unit is $\tau = 32.6$ ns.

As mentioned, the dependence of the eigenmodes on the coordinate z is simply $\cos(kz)$ or $\sin(kz)$, with k entering Eq. (9.18) to give the eigenvalue. Furthermore, it is also possible to study the disclinations with the half-integer winding numbers, in particular the 1/2 disclination line. To satisfy the continuity of the eigensolutions in this case, in the angular part of the ansatz (9.17) it is required that $m = 1/2, 3/2, 5/2, ...$, while the ansatz (9.16) remains the same. Thus, with the approach taken in this Chapter, one is able to solve the full fluctuation problem of a straight and infinitely long 1/2 disclination line.

9.2 Hydrodynamic speedup

Now let us study the repulsive motion of the two $\pm 1/2$ disclinations, created after the strength ± 1 disclination has decayed. We shall focus on the influence of the hydrodynamic flow. Due to the symmetry of the problem, there is no flow-induced asymmetry (Fig 9.7) like the one encountered in Chapter 7. However, the speedup caused by the flow is larger this time, because both the elastic stress (7.5) and the viscous stress given by the μ_1 term (Eq. (7.6)) drive the defects apart (see the discussion of Chapter 7). The effect depends on the ratio μ_1/β_4, Fig. 9.8.

There is also no subtlety with the initial condition (the final state in this case) like that in Chapter 7. This enables us to study the behavior of the defect velocity at larger separations. Figure 9.9(a) shows the velocity of the defect v as a function of the defect separation r. After the defects have been well isolated from each other,

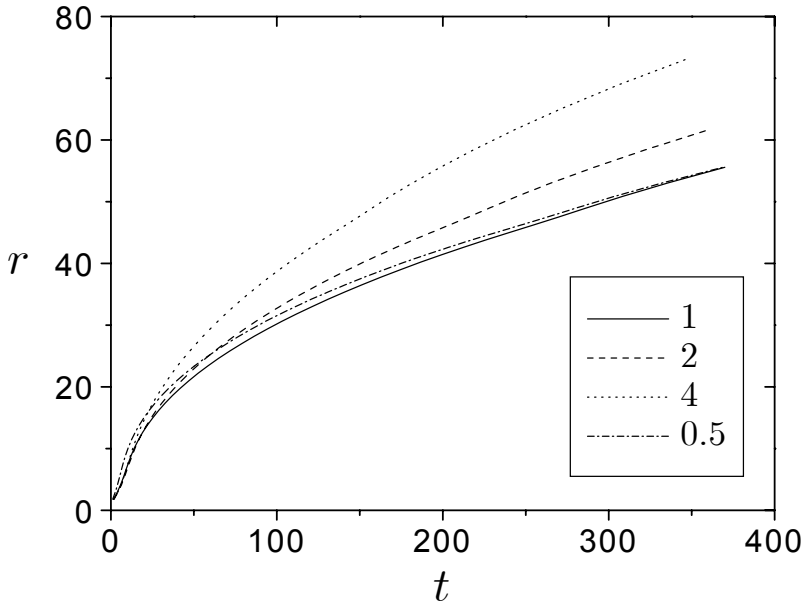

(a)

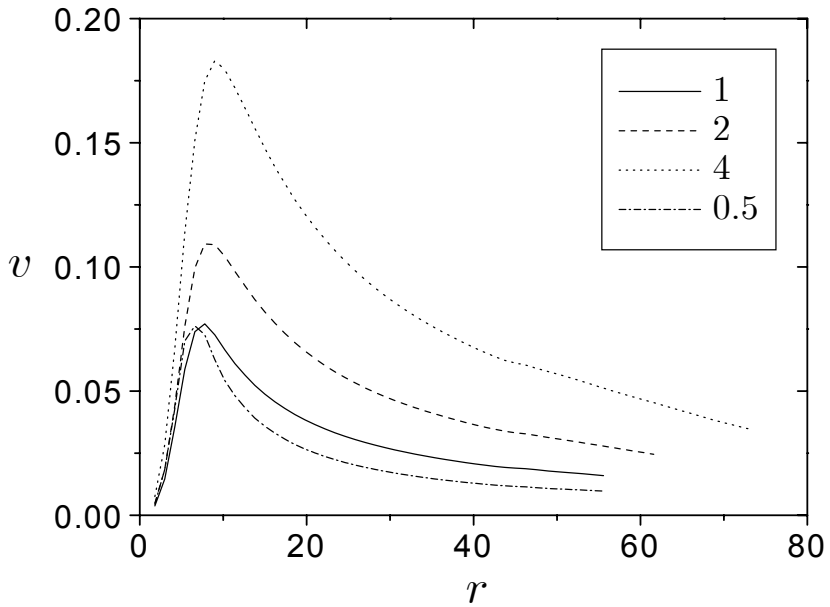

(b)

Figure 9.8 (a) Defect separation r as a function of time and (b) defect velocity v as a function of the separation for different ratios μ_1/β_4. Due to the questionable hydrodynamic situation and ill-defined defect position at small separations, in (b) the curve for the ratio 0.5 is above that for the ratio 1 initially. The kink of the curves in (b) is an artifact of the inhomogeneous grid.

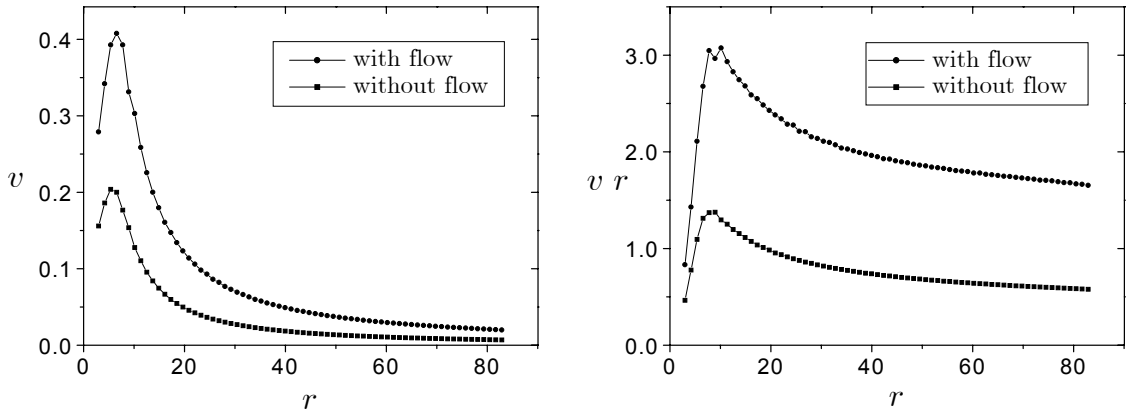

Figure 9.9 (a) Defect velocity v and (b) the quantity vr as functions of the separation r. The behavior at small r is not particularly informative as the defect position is ill-defined there.

the velocity decreases with r. Before that, the velocity cannot be properly defined. Figure 9.9(b) shows the r-dependence of the quantity vr, which at least for the nonhydrodynamic case is constant in the limit $r/\xi \to \infty$ (scale invariance).

Figure 9.10 is particularly significant. It displays the ratio of the advective velocity (transport by the flow) and the total velocity of the defect. One can see that the ratio increases with r, and reaches a value well above 0.5 as hinted by a rough eye-made extrapolation to the data points. This means that at larger separations the contribution of the translational motion (advection) to the defect speed is more important than that of the director reorientation, especially if one recalls that the separations reached in our calculations are still quite small — only $\approx 80\xi$ or 0.17 μm.

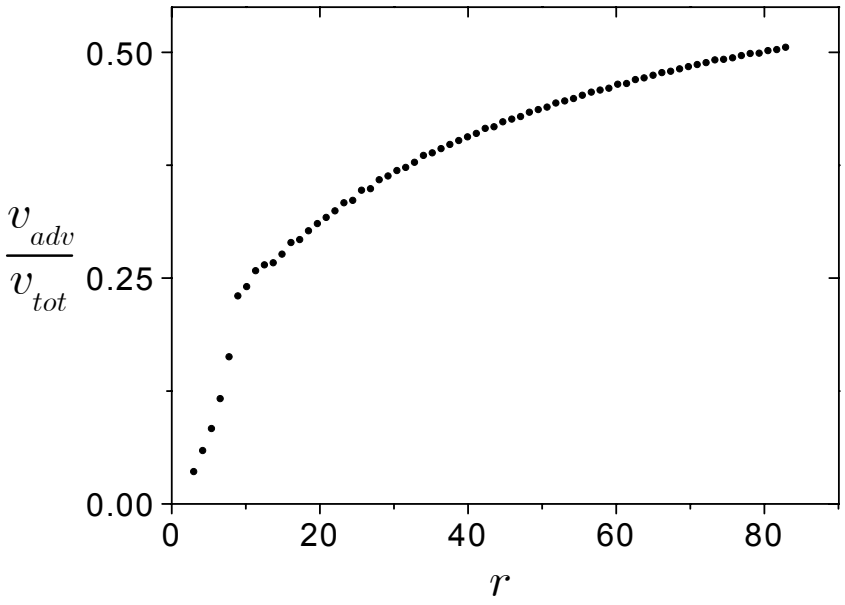

Figure 9.10 Ratio of the advective and total velocities of the defect as a function of the inter defect separation. By a rough extrapolation, the ratio is well above 0.5 at large separations, indicating the importance of the flow transport.

10

Conclusion

It is now time to summarize what has been presented in the Thesis, reviewing the concepts and results and putting them into context of the research going on in the field. The aim of the Thesis has been to study selected problems coupling hydrodynamics and order parameter dynamics in liquid crystals. They were chosen according to theoretical and experimental interest, and, of course, our capability of solving them.

The backflow switching problems of Chapter 4 have been studied in terms of the well-established Ericksen-Leslie theory for the nematic director. Primarily they were intended to serve as an introduction to the research area, setting up the numerical approach to be used in the work to follow. Conceptually, they do not represent any novelty. Regarding their computational complexity, however, they are quite advanced compared to the one-dimensional examples that had been studied previously. More confined geometries increase the number of spatial variables, but at the same time offer more possibility for manipulation with external fields. Having managed to cope with the increasing complexity, we were able to point out special cases, where the hydrodynamic flow causes the perturbation enough to completely alter the time evolution of the system. Effects of this kind had only been studied in context of spinodal instabilities of liquid crystals, mostly in the linearized form, and in various pattern-forming systems involving electro- and thermal convection.

The derivation of the dynamic theory for the complete vector order parameter presented in Chapter 5 features two viewpoints of importance. The vectorial theory is required if one wants to study defects in a medium with the vector order parameter — the SmC system in our case. On the other hand, by demonstrating that the Ericksen-Leslie theory can be naturally extended to yield the vectorial theory, or, in other words, the latter can be consistently reduced to the former, we have shown that the Ericksen-Leslie theory is exactly the reduced version of the vectorial theory, restricted to the unit vector. Despite the Ericksen-Leslie theory has been derived and used for nematics, it does not have any connection with the nematic tensor order parameter.

To study the dynamics of defects in nematics, which has been our primary objective, one has to start over and construct the tensorial theory. It can be reduced to the Ericksen-Leslie theory in the limit of constant scalar invariants of the ten-

sor order parameter. The converse path is not possible, i.e., trying to upgrade the Ericksen-Leslie theory, which is linear in the director, by adding a variation of the scalar order parameter results in a hybrid with severe drawbacks. In Chapter 7, we have solved the hydrodynamic pair-annihilation problem of straight nematic disclination lines using an abridged form of the tensorial theory. We were able to account for the speculated velocity difference of the two disclinations, which arises mainly due to the flow effects. Unfortunately, couple of months before ours the work of another group was published [96], demonstrating essentially identical flow effects. The fact that their treatment is not based on the customary phenomenological description of nematics but rests on a somewhat leaner microscopic model with fewer material parameters has been less important so far. The situation might change in the future.

Despite experimental convenience of the SmC film system, there have been no numerical studies of defect dynamics reported in the literature. A possible reason for the deficiency could be the enormous complexity of the governing equations and the great number of mostly unknown material parameters. In addition, the generalization of the original equations to the variable length of the smectic c-director needed for the description of defects would be a backbreaking task. Instead, in Chapter 8 we have benefited from the observation that under the restricting assumptions the equations can be reduced to the Ericksen-Leslie equations exactly. At this level, the passage to the variable length of the c-director is also quite comfortable. The modelled SmC film system corresponds to the class of the XY-model. Its dynamics is governed by the dynamic equations for the vector order parameter derived in Chapter 5. We have shown that the flow effect accompanying the pair-annihilation of vortices is qualitatively equal to the one in nematics, i.e., the disclination with the positive winding number is faster.

Vortices of strength ± 1 are unstable in the nematic case, i.e., they spontaneously decay to a pair of identical $\pm 1/2$ disclinations, which we first observed numerically. In Chapter 9, this motivated us to study the dynamic behavior of a perturbed strength 1 disclination line. In one elastic constant approximation we were able to solve the complete tensor fluctuation problem for the straight disclination line with a general integer winding number. We found two types of growing fluctuation eigenmodes, leading to the decay to disclinations with lower winding numbers or to the escape in the third dimension, respectively. They are localized and exhibit discrete spectra. In accord with the stronger localization, the characteristic time of the modes leading to the decay is more than an order of magnitude smaller than that of the escaping type, suggesting that the decaying scenario is what takes place, e.g., after a temperature quench, rather than the escaping one. We have also studied the hydrodynamic correction to the growth rate of the fluctuation leading to the decay of the strength 1 disclination, and found it to be under 5%, increasing the growth rate. The validity of this result is questionable due to the incompleteness of the tensorial approach and short (nonhydrodynamic) length and time scales. In Chapter 9 we also studied the influence of the flow on the repulsive motion of the two $1/2$ or $-1/2$ disclinations, created after the strength 1 or -1 disclination has decayed. A strong speed-up has been observed.

If there is one thing one should learn from the Thesis, it is the importance of the hydrodynamic flow accompanying the dynamics of defects in liquid crystals. We have shown that the contribution of the flow transport (advection) to the motion of the defect is quite comparable to the contribution due to the order parameter reorientation. For the specific choice of viscous material parameters, corresponding to the nematic substance MBBA, the advective contribution even dominates at relevant defect separations.

10.1 Future perspectives

There is still a lot of work to do, either improving the methods used, or challenging new problems related to those that have been solved.

In my opinion, by far the most important improvement to be done is to replace the somewhat cumbersome method of solving the Navier-Stokes equation with a more efficient method, e.g., a Fourier-based solver, or a function expansion method. The main difficulty in defect simulations is the large discrepancy between the size of the defect core and the interdefect distance relevant for experiments, which are readily in a ratio of $1/10^5$. The replacement of the Navier-Stokes solver is absolutely inevitable if one wants to reach defect separations of the order of 100 μm, so that numerical results could be directly compared with the measurements.

One of the problems to be attacked in the future is the dynamics of nematic point defects, e.g., the annihilation of a hedgehog-antihedgehog pair, either in a capillary where most of the measurements have been done, or in bulk. This is a 3D problem. One could get rid of the extra spatial coordinate by assuming cylindrical symmetry about the axis joining the defects. However, numerical indices exist that the actual configuration does not possess this symmetry.

Another open problem, which has been already solved to some extent in Chapter 9, are the fluctuations of the strength $\pm 1/2$ nematic disclination line. As suggested by the equations, a part of the fluctuation spectrum corresponds to the simple one-dimensional diffusion spectrum with the dispersion $\lambda = k^2$, where λ is the relaxation rate and $\mathbf{k}$ is the wave vector of the mode, which is parallel to the disclination line in this case. In other words, as far as these fluctuations are considered, the disclination line behaves like a damped massless string subject to line tension. In addition, it would be interesting and quite nontrivial to study the influence of hydrodynamics on the relaxation rates of the fluctuations, particularly those just mentioned. According to what we have learned about the flow effects on defect dynamics we should expect significant corrections, especially for long wavelength fluctuations.

Similar calculations (a bit simpler) as in Chapter 9 can be performed also for the disclinations of the vector order parameter. In these systems, one could thus study the fluctuations of the strength ± 1 disclination and the decay of higher strength

disclinations.

⋆ ⋆ ⋆

Is it in the human nature or just in mine the impression that after the problems have been solved they inescapably start to seem trivial? After a fortnight or so. If I was to start over from scratch again, I would have done many things differently. Much better, I believe. Nevertheless, after all the uncertainty of the early days, months (years?!), I am pretty satisfied with the outcome. And I can hardly consider myself being someone who gets satisfied easily. Still, I would have done many things differently... But if someone had foretold me about the present situation when I was just starting with my research, I would probably never have had the nerve to compete with it. Time is a killer. Especially if one makes effort.

Bibliography

[1] L. Onsager, Ann. N. Y. Acad. Sci. **51**, 627 (1949).

[2] G. Friedel, Ann. Physique **18**, 273 (1922).

[3] W. L. McMillan, Phys. Rev. A **4**, 1238 (1971).

[4] D. Svenšek and S. Žumer, Liq. Cryst. **28**, 1389 (2001).

[5] D. Svenšek and S. Žumer, Continuum Mech. Thermodyn. **14**, 231 (2002).

[6] D. Svenšek and S. Žumer, Phys. Rev. E **66**, 021712 (2002).

[7] D. Svenšek and S. Žumer, accepted for publication in Phys. Rev. Lett.

[8] L. D. Landau, Fiz. Z. Sowjetunion **11**, 26 (1937).

[9] P. G. de Gennes, Mol. Cryst. Liq. Cryst. **12**, 193 (1971).

[10] P. Sheng and E. B. Priestley, *Introduction to Liquid Crystals*, edited by E. B. Priestley, P. J. Wojtowicz, and P. Sheng (Plenum Press, New York, 1974).

[11] J. Goldstone, Nuovo Cimento **19**, 155 (1961).

[12] R. B. Meyer, Phys. Rev. Lett. **22**, 918 (1969).

[13] J. Prost and J. P. Marcerou, J. Phys. France **38**, 315 (1977); J. P. Marcerou and J. Prost, Mol. Cryst. Liq. Cryst. **58**, 259 (1980).

[14] A. K. Sen and D. E. Sullivan, Phys. Rev. A **35**, 1391 (1987).

[15] G. Barbero and G. Durand, *Surface anchoring of nematic liquid crystals*, in *Liquid crystals in complex geometries formed by polymer and porous networks*, edited by G. P. Crawford and S. Žumer (Taylor and Francis, London, 1996).

[16] M. Nobili and G. Durand, Phys. Rev. A **46**, R6174 (1992).

[17] R. Kubo, *Statistical mechanics* (North-Holland Publishing Company, Amsterdam, 1965).

[18] L. O. Onsager, Phys. Rev. **37**, 405 (1931).

[19] L. D. Landau and E. M. Lifshitz, *Statistical Physics, Part 1*, 3rd Edition (Reed Educational and Professional Publishing, Oxford, 1980).

[20] L. D. Landau and I. M. Khalatnikov, Dokl. Akad. nauk SSSR **96**, 469 (1954).

[21] I. Kuščer, A. Kodre, *Matematika v fiziki in tehniki* (DMFA Slovenije, Ljubljana, 1994).

[22] J. L. Ericksen, Arch. ration. Mech. Analysis **4**, 231 (1960).

[23] F. M. Leslie, Quart. J. Mech. appl. Math. **19**, 357 (1966); Arch. ration. Mech. Analysis **28**, 265 (1968).

[24] P. C. Martin, O. Parodi, and P. S. Pershan, Phys. Rev. A **6**, 2401 (1972).

[25] M. G. Clark, F. M. Leslie, Proc. R. Soc. Lond. A. **361**, 463 (1978).

[26] C. Z. van Doorn, J. Physique **36**, C1-261 (1975).
[27] D. W. Berreman, J. Appl. Phys. **46**, 3746 (1975).
[28] D. W. Berreman, J. Appl. Phys. **50**, 3746 (1979).
[29] N. J. Smith, M. D. Tillin, and J. R. Sambles, Phys. Rev. Lett. **88**, 088301 (2002).
[30] F. Brochard, P. Pieranski, and E. Guyon, Phys. Rev. Lett. **26**, 1681 (1972).
[31] P. Pieranski, F. Brochard, and E. Guyon, J. Physique **34**, 35 (1973).
[32] E. F. Carr, Mol. Cryst. Liq. Cryst. **34**, 159 (1977).
[33] E. Guyon, R. Meyer, and J. Salan, Mol. Cryst. Liq. Cryst. **54**, 261 (1979).
[34] A. J. Hurd, S. Fraden, F. Lonberg, and R. B. Meyer, J. Physique **46**, 905 (1985).
[35] K. Migler and R. Meyer, Phys. Rev. Lett. **66**, 1485 (1991).
[36] K. Migler and R. Meyer, Phys. Rev. E **48**, 1218 (1993).
[37] J. Bajc, G. Hillig, and A. Saupe, J. Chem. Phys. **106**, 7372 (1997).
[38] M. Kaiser, W. Pesch, and E. Bodenschatz, Physica D **59**, 320 (1992).
[39] M. Grigutsch, R. Stannarius, Mol. Cryst. Liq. Cryst. A **304**, 455 (1997).
[40] H. R. Brand, C. Fradin, P. L. Finn, W. Pesch, and P. E. Cladis, Phys. Lett. A **235**, 508 (1997).
[41] E. Plaut and W. Pesch, Phys. Rev. Lett. **79**, 2367 (1997).
[42] A. D. Rey and T. Tsuji, Macromol. Theor. Simul. **7**, 623 (1998).
[43] E. Plaut and W. Pesch, Phys. Rev. E **59**, 1747 (1999).
[44] J. J. Feng, J. Tao, and L. G. Leal, J. Fluid Mech. **449**, 179 (2001).
[45] G. Durand, private communication, SILC Mini School, April 2000, Portorož, Slovenija.
[46] C. Oseen, Trans. Faraday Soc. **29**, 883 (1933).
[47] H. Zocher, Trans. Faraday Soc. **29**, 945 (1933).
[48] F. C. Frank, Discuss. Faraday Soc. **25**, 19 (1958).
[49] P. G. de Gennes and J. Prost, *The Physics of Liquid Crystals* (Clarendon Press, Oxford, 1995).
[50] G. Vertogen, W. H. de Jeu, *Thermotropic Liquid Crystals, Fundamentals* (Springer-Verlag, Berlin, 1998).
[51] O. Parodi, J. Phys. France **31**, 581 (1970).
[52] C. A. J. Fletcher, *Computational Techniques for Fluid Dynamics* (Springer Verlag, Berlin, 1988), Vol. II.
[53] A. Kodre, private communication, 1999.
[54] W. H. Press, B. P. Flannery, S. A. Teukolsky, and W. T. Vetterling, *Numerical Recipes* (Cambridge University Press, Cambridge, 1986).
[55] S. Chandrasekhar, *Liquid Crystals* (Cambridge University Press, Cambridge, 1992).
[56] A. J. Bray, in *Soft and Fragile Matter*, Proceedings of the 53rd SUSP, St. Andrews, July 1999, edited by M. E. Cates and M. R. Evans (The Scottish Universities Summer School in Physics, 2000).
[57] J. G. McIntosh, and F. M. Leslie, J. Eng. Math. **37**, 129 (2000).

[58] N. D. Mermin, Rev. Mod. Phys. **51**, 591 (1979).
[59] M. V. Kurik and O. D. Lavrentovich, Usp. Fiz. Nauk **154**, 381 (1988) [Sov. Phys. Usp. **31**, 196 (1988)].
[60] N. Schopohl and T. J. Sluckin, Phys. Rev. Lett. **59**, 2582 (1987).
[61] E. Penzenstadler and H.-R. Trebin, J. Phys. France **50**, 1027 (1989).
[62] A. Sonnet, A. Kilian, and S. Hess, Phys. Rev. E **52**, 718 (1995).
[63] S. Kralj, E. G. Virga, and S. Žumer, Phys. Rev. E **60**, 1858 (1999).
[64] D. Andrienko, M. P. Allen, G. Skačej, and S. Žumer, Phys. Rev. E **65**, 041702 (2002).
[65] P. M. Chaikin and T. C. Lubensky, *Principles of condensed matter physics* (Cambridge University Press, Cambridge, 1997).
[66] L. D. Landau and E. M. Lifshitz, *Theory of Elasticity*, 3rd Edition (Reed Educational and Professional Publishing, Oxford, 1986).
[67] G. P. Crawford, D. Svenšek, and S. Žumer, *Some aspects of polymer-dispersed and polymer-stabilized chiral liquid crystals*, in *Chirality in liquid crystals*, edited by H.-S. Kitzerow and C. Bahr (Springer-Verlag, New York, 2001).
[68] P. Cladis and M. Kléman, J. Phys. France **33**, 591 (1972).
[69] R. B. Meyer, Philos. Mag. **27**, 405 (1973).
[70] W. H. Zurek, Nature **317**, 505 (1985).
[71] H.-R. Trebin, Liq. Cryst. **24**, 127 (1998).
[72] L. M. Pismen, *Vortices in Nonlinear Fields* (Oxford University Press, Oxford, 1999).
[73] I. Chuang, R. Durrer, N. Turok, and B. Yurke, Science **251**, 1336 (1991).
[74] T. W. B. Kibble, Physica C **369**, 87 (2002).
[75] A. Pargellis, N. Turok, and B. Yurke, Phys. Rev. Lett. **67**, 1570 (1991).
[76] K. Minoura, Y. Kimura, K. Ito, and R. Hayakawa, Phys. Rev. E **58**, 643 (1998).
[77] C. Denniston, Phys. Rev. B *54*, 6272 (1996).
[78] G. Guidone Peroli and E. G. Virga, Physica D **111**, 356 (1998).
[79] G. Guidone Peroli and E. G. Virga, Phys. Rev. E **59**, 3027 (1999).
[80] J. Bajc, *Statika in dinamika defektov v ograjenih nematskih tekočekristalnih fazah*, PhD Thesis (Univerza v Ljubljani, 1998).
[81] J. Bajc, G. Guidone Peroli, E. G. Virga, and S. Žumer, Liq. Cryst. **29**, 213 (2002).
[82] A. M. Sonnet and E. G. Virga, Phys. Rev. E **56**, 6834 (1997).
[83] H. Stark and D. Ventzki, Europhys. Lett. **57**, 60 (2002).
[84] A. Kilian and S. Hess, Z. Naturforsch. **44a**, 693 (1989).
[85] E. C. Gartland, Jr., A. M. Sonnet, and E. G. Virga, Continuum Mech. Thermodyn. **14**, 307 (2002).
[86] L. M. Pismen and B. Y. Rubinstein, Phys. Rev. Lett. **69**, 96 (1992).
[87] A. Kilian, Mol. Cryst. Liq. Cryst **222**, 57 (1992).
[88] J. Fukuda, M. Yoneya, and H. Yokoyama, Phys. Rev. E **65**, 041709 (2002).
[89] S. Hess, Z. Naturforsch. **31 a**, 1507 (1976).
[90] P. D. Olmsted and P. Goldbart, Phys. Rev. A **41**, 4578 (1990).

[91] P. D. Olmsted and P. M. Goldbart, Phys. Rev. A **46**, 4966 (1992).
[92] T. Qian and P. Sheng, Phys. Rev. E **58**, 7475 (1998).
[93] J. Fukuda, Eur. Phys. J. B **1**, 173 (1998).
[94] C. Denniston, E. Orlandini, and J. M. Yeomans, Phys. Rev. E **63**, 056702 (2001).
[95] C. Denniston, E. Orlandini, and J. M. Yeomans, Phys. Rev. E **64**, 021701 (2001).
[96] G. Tóth, C. Denniston, and J. M. Yeomans, Phys. Rev. Lett. **88**, 105504 (2002).
[97] P. E. Cladis, W. van Saarloos, P. L. Finn, and A. R. Kortan, Phys. Rev. Lett. **58**, 222 (1986).
[98] A. Bogi, P. Martinot-Lagarde, I. Dozov, and M. Nobili, Phys. Rev. Lett. **89**, 225501 (2002).
[99] S. Kralj and S. Žumer, Phys. Rev. A **45**, 2461 (1992).
[100] H. Pleiner, Phys. Rev. A **37**, 3986 (1988).
[101] B. Yurke, A. N. Pargellis, T. Kovacs, and D. A. Huse, Phys. Rev. E **47**, 1525 (1993).
[102] H. J. Coles, Mol. Cryst. Liq. Cryst. **49**, 67 (1978).
[103] D. R. Link, A. Tewary, G. Natale, V. Ginzburg, J. E. Maclennan, L. Radzihovsky, N. A. Clark, unpublished.
[104] D. R. Link, private communication, September 2000, Erice, Italy.
[105] N. A. Clark, private communication, ILCC, July 2002, Edinburgh, UK.
[106] D. R. Link, L. Radzihovsky, G. Natale, J. E. Maclennan, N. A. Clark, M. Walsh, S. S. Keast, and M. E. Neubert, Phys. Rev. Lett. **84**, 5772 (2000).
[107] A. N. Pargellis, P. Finn, J. W. Goodby, P. Panizza, B. Yurke, and P. E. Cladis, Phys. Rev. A **46**, 7765 (1992).
[108] T. Carlsson, I. W. Stewart, and F. M. Leslie, Liq. Cryst. **9**, 661 (1991).
[109] T. Carlsson, F. M. Leslie, and N. A. Clark, Phys. Rev. E **51**, 4509 (1995).
[110] C. Y. Young, R. Pindak, N. A. Clark, and R. B. Meyer, Phys. Rev. Lett. **40**, 773 (1978).
[111] C. Rosenblatt, R. Pindak, N. A. Clark, and R. B. Meyer, Phys. Rev. Lett. **42**, 1220 (1979).
[112] D. R. Link, J. E. Maclennan, and N. A. Clark, Phys. Rev. Lett. **77**, 2237 (1996).
[113] P. Ziherl and S. Žumer, Liq. Cryst. **21**, 871 (1996).
[114] P. Ziherl and S. Žumer, Phys. Rev. E **54**, 1592 (1996).
[115] E. C. Gartland, Jr. and S. Mkaddem, Phys. Rev. E **59**, 563 (1998).
[116] R. Rosso and E. G. Virga, J. Phys. A: Math. Gen. **29**, 4247 (1996).
[117] I. F. Lyuksyutov, Zh. Eksp. Teor. Fiz. **75**, 358 (1978) [Sov. Phys. JETP **48**, 178 (1978)].
[118] S. Hess, Z. Naturforsch. Teil A **30**, 728 (1975).
[119] V. L. Pokrovskii and E. I. Kats, Zh. Eksp. Teor. Fiz. **73**, 774 (1977) [Sov. Phys. JETP **46**, 405 (1977)].

[120] A. Šarlah, *Effect of the confining substrates on nematic order-fluctuations in liquid crystals*, PhD Thesis (Univerza v Ljubljani, 2001).
[121] A. Kodre, private communication, 2002.
[122] H. R. Brand, private communication, 2002.
[123] H. Pleiner, M. Liu, and H. R. Brand, Rheol. Acta **41**, 375 (2002).

Izjava

V disertaciji sem predstavil rezultate lastnega znanstvenoraziskovalnega dela.

Ljubljana, marec 2003 Daniel Svenšek

ERRATUM

While Eqs. (5.9) and (5.17) (pp. 57 and 60) themselves are intact, they do not represent the diagonalized quadratics f^{el} and $T\dot{s}^i$ as referred to in the text, but merely express them as the sums of square terms. Thus, Eqs. (5.9) and (5.17) do not stipulate the positivity of the coefficients, as falsely stated in the text. The quadratics can be diagonalized in principle. However, the diagonalized forms are too convoluted to be useful.